OCTOBER 2008

DEVELOPMENT AND TESTING OF A SEMI-DISTRIBUTED WATERSHED MODEL: CASE STUDIES EXPLORING THE IMPACT OF CLIMATE VARIABILITY AND CHANGE IN THE RíO SALADO

WRRI Technical Completion Report No. 345

Carlos A. Aragón
Enrique R. Vivoni

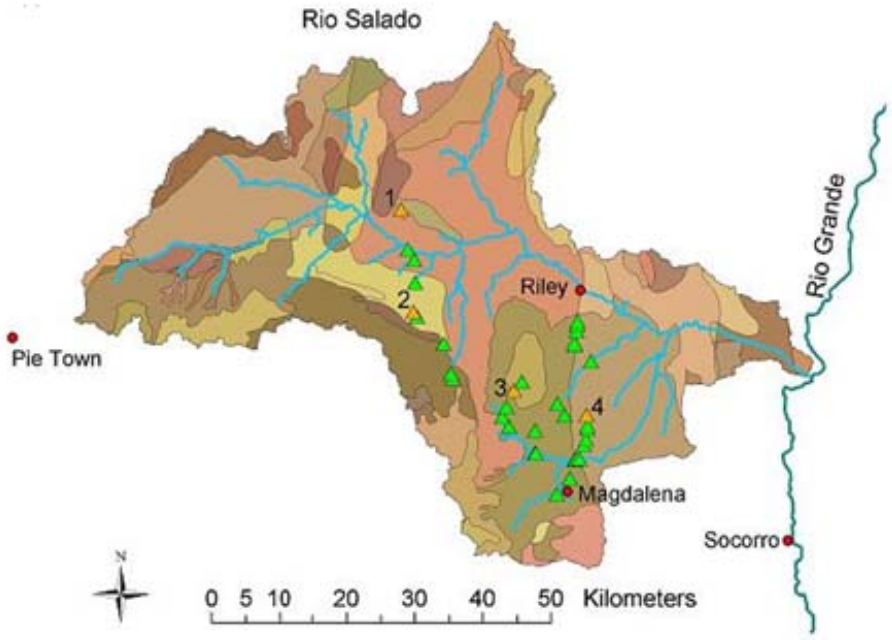

NEW MEXICO WATER RESOURCES RESEARCH INSTITUTE
New Mexico State University
MSC 3167
Box 30001
Las Cruces, New Mexico 88003-0001
Telephone (575) 646-4337 FAX (575) 646-6418
email: nmwrri@wrri.nmsu.edu

DEVELOPMENT AND TESTING OF A SEMI-DISTRIBUTED WATERSHED MODEL: CASE STUDIES EXPLORING THE IMPACT OF CLIMATE VARIABILITY AND CHANGE IN THE RÍO SALADO

By

Carlos A. Aragón, Graduate Assistant
and
Enrique R. Vivoni, Associate Professor
New Mexico Institute of Mining and Technology
Socorro, New Mexico

TECHINICAL COMPLETION REPORT
Account Number 109469B

June 2008

New Mexico Water Resources Research Institute
in cooperation with the
New Mexico Institute of Mining and Technology
and
Sandia National Laboratories

The research on which this report is based was financed in part by the U.S. Geological Survey, through the New Mexico Water Resources Research Institute.

DISCLAIMER

The purpose of the Water Resources Research Institute (WRRI) technical reports is to provide a timely outlet for research results obtained on projects supported in whole or in part by the institute. Through these reports the WRRI promotes the free exchange of information and ideas and hopes to stimulate thoughtful discussions and actions that may lead to resolution of water problems. The WRRI, through peer review of draft reports, attempts to substantiate the accuracy of information contained within its reports, but the views expressed are those of the authors and do not necessarily reflect those of the WRRI or its reviewers. Contents of this publication do not necessarily reflect the views and policies of the Department of the Interior, nor does the mention of trade names or commercial products constitute their endorsement by the United States government.

ACKNOWLEDGEMENTS

We would like to acknowledge the efforts of the following individuals: Vincent Tidwell, Len Malczynski, and Geoffery Klise from Sandia National Laboratories; Ricardo Mantilla, New Mexico Institute of Mining and Technology. We also thank additional funding from the New Mexico Alliance for Graduate Education and the Professoriate (NM AGEP), the New Mexico Water Resources Research Institute and Sandia National Laboratories. The material presented here drawn in large part from the Master of Science thesis of Carlos A. Aragón, completed June 2008 at the New Mexico Institute of Mining and Technology (Aragón, 2008).

ABSTRACT

Water supply problems in the Middle Río Grande are increasing as New Mexico's population grows and new demands are placed on finite amounts. Policy and decision makers require tools, such as hydrologic models, to assist in the management of water resources. To exacerbate the problem, anticipated variations induced by global warming will have an uncertain impact on water resources. In this work, we develop and test a semi-distributed watershed model for simulating hydrologic conditions in semiarid river basins. The model is applied to the Río Salado and tested at the point, regional and basin-scales using a range of different atmospheric forcings and a set of plausible climate change scenarios. The model performed well at simulating point-scale soil moisture and gave plausible results for other hydrological variables at the scale of different Hydrologic Response Units (HRUs). Reproducing historical streamflow in the Río Salado with the model was difficult due to an underestimation of high elevation precipitation in the basin. Nevertheless, forcing the model with stochastically-generated, coarse precipitation fields showed improved results during long-term simulations. More importantly, the climate change scenarios demonstrate the usefulness of the semi-distributed watershed model as a tool for assessing hydrologic impacts of seasonal precipitation and temperature changes.

Keywords: climate change, hydrologic response unit, modeling, precipitation, semiarid, streamflow, stochastic, system dynamics, watershed

TABLE OF CONTENTS

LIST OF FIGURES

LIST OF TABLES

JUSTIFICATION OF WORK PERFORMED

The last decade has been marked by serious disputes over water resources. There are many factors that lead to and amplify water related conflicts making it an extremely difficult problem. Improved living conditions around the world have increased the demand for potable water supplies. Some urban communities are developing new methods for reusing wastewater, however, agricultural uses remain the largest consumer of water (Archibold, 2008). While technologies exist to improve irrigation efficiency, they are often too expensive to be employed by most small farmers, especially in developing countries, and in some cases these technologies can increase water shortages by eliminating recharge (Yardley, 2007). As the world population continues to increase and more people migrate from rural areas to larger cities conflicts over water allocation can become more intense. Additionally, recent climate change predictions suggest that changes in precipitation distribution (location, frequency and duration) will further tax the resources of water managers, making it more difficult to provide a consistent supply of water.

The conflict over water has become an international problem, as trans-boundary watersheds lead to disputes among neighboring countries over the allocation of this precious resource. Soon these disagreements may lead to wars as already limited resources are further diminished (Toepfer, 1999). As a consequence, the development of sensible water use plans that are able to maintain the delicate balance between all interested parties (e.g. industrial, municipal, agricultural, and natural ecosystems), presents a challenge to both scientists and policy makers (Cox, 2004, Falkenmark and Rockstrom, 2004, YDP/Cienega Workgroup, 2005, POST, 2006).

An accurate estimate of the available water resources (surface water and ground water) is necessary to correctly plan sustainable usage (Ward et al., 2006). While purely stochastic or

empirical studies, which provide streamflow predictions based on simple relationships, are easy to implement, they fail to account for the physical processes necessary for runoff production (Singer, 2004). Improvements in the understanding of physical hydrological processes, as well as increases in the availability of computational resources, have resulted in the growing popularity of hydrological models as a tool for addressing this problem. However, when attempting to predict the amount and frequency of streamflow volumes over large areas, care must be taken to use a model that correctly represents hydrological processes at varying scales.

Throughout the southwestern United States, aquifers that have long fed the growth of major cities are being reduced to alarmingly low levels. As a result, it often becomes necessary to use surface water to enhance these rapidly diminishing resources. Achieving estimates of these resources is hindered by the fact that most watersheds remain uninstrumented. The vast quantity of ungauged basins and the infrequency of streamflow within them make instrumentation an unrealistic and costly process. The goal of this project is to create a semi-distributed watershed model to predict hydrological processes in ungauged basins that incorporates the following objectives. The model must be able to account for differences in vegetation and soil properties in semiarid regions. The model must be able to process large tributary basins quickly to allow for simulations to be run "real time" to assist in the decision-making process. Such a model has been created using the Powersim system dynamics software package (www.powersim.com) and is applied to the Río Salado, a semiarid basin in New Mexico that is an important tributary to the Río Grande. This exercise provides us with an example of the models performance in an ungauged basin, building confidence in the use of the watershed model in similar areas around the world.

The lack of high quality datasets is a problem often faced when using a hydrological model. To bypass this issue, most physical rainfall-runoff models use analytical equations to produce runoff from measured rainfall data (Beven, 2000). Often reasonable results are achieved when these point scale equations are applied to large watersheds (Burnash et al., 1973, USACE, 1994). Nijssen and Lettenmaier (1997) even created a continent scale model that incorporates these physical rainfall-runoff equations. We have chosen to describe the watershed as a collection of Hydrologic Response Units (HRUs) in order to approximate the physical processes in a semi-distributed manner. Each HRU is comprised of a unique soil and vegetation combination that responds similarly to precipitation forcing (Arnold et al., 2005). The use of HRUs reduces the number of individual units that must be modeled by lumping multiple small areas with similar properties together into a single uniform unit.

As previously stated, the model has been tested in the Río Salado, a currently ungauged semiarid basin. The Río Salado was selected because of the availability of a historical dataset nearly forty years in length, which ended in 1984. Currently, only large flood events are recorded at the basin outlet, and these are estimated by manual measurements. We will compare our model results to the historical measurements to evaluate the performance of the model in a semiarid region. Once we have gained confidence in the models abilities, we will be able to use it as a tool to assess potential changes in the responses of semiarid ungauged basins to climate variability and change.

Through this work we aim to present the application of the watershed model at the HRU scale, using an event-based precipitation forcing scheme. The model will be created in the Powersim software environment to facilitate decision-making processes. The model will be tested at multiple scales (point, HRU, basin) to build confidence in the ability of the model to represent

hydrological processes. Finally, climate variability and climate change scenarios will be examined to demonstrate the robustness of the model.

The remainder of this report will be divided into three additional chapters. In the METHODS chapter we describe the study area and provide a walk through of the hydrological processes and associated equations that are included in the watershed model. The RESULTS chapter describes application of the model at different scales and presents results that illustrate the capabilities of the model and its response to variations in climate forcing. The final chapter, SUMMARY, CONCLUSIONS AND RECOMMENDATIONS, provides a brief summary of the report, states the major conclusions that were reached, and offers recommendations for future exploration of this subject. The majority of this report is based on the Master of Science thesis of Carlos A. Aragón (Aragón, 2008) at the New Mexico Institute of Mining and Technology.

METHODS

Introduction

In this chapter, we introduce the Rio Salado and describe how the model domain was created for the study region. We then discuss in detail how different hydrological processes are treated in the watershed model, describing the underlying theory and presenting the set of equations that have been implemented. These processes include rainfall generation, interception by vegetation, infiltration into the soil, evapotranspiration, and the generation and routing of runoff. We illustrate the model physics with HRU scale examples over a limited set of conditions. Finally, we summarize the model development and its components, providing a reference for the presentation of model testing and sensitivity studies in the results chapter.

Watershed delineation and domain representation

The Río Salado, located in central New Mexico, is part of the Middle Rio Grande drainage basin, and extends into Catron, Cibola, and Socorro counties (Figure 1.a). The basin was selected for this study due to its historical stream gauge located near its confluence with the Río Grande, its semiarid nature and its significant size (3,610 km^2). The maximum elevation in the Río Salado is 3060 m in the Magdalena Mountains and drops to 1430 m near the outlet to the Río Grande. The stream network in the basin consists of a wide braided channel near the outlet and narrow, highly incised channels in the headwaters. Stephens et al. (1988) stated that the mean annual discharge for the Río Salado is approximately 0.4 m^3/s, with over 86% of the total runoff occurring during the summer monsoon. While the Río Salado does not contribute large volumes of water to the Río Grande, it does contribute a great deal of sediment (Simcox, 1983). The stream channel is made up of mostly sandy soils with occasional interbeds of gravels, cobbles, and shale and clay

layers (Stephens et al., 1988). The saturated hydraulic conductivity of the streambed has been estimated to be on the order of 10^{-2} cm/s. (Byers and Stephens, 1983; Stephens and Knowlton, 1984).

The basin extent for the Río Salado is delineated from U.S. Geological Survey 30-meter digital elevation data. (Figure 1.b) shows the Río Salado watershed and stream network overlaying the 30-meter Digital Elevation Model (DEM) of the Middle Rio Grande. The process of deriving a stream network and basin boundary from the DEM begins with the creation of a flow direction map. The direction of flow is determined using a D8 single flow direction algorithm, which is widely accepted in the literature (Marks et al., 1984; Band, 1986; Jenson and Domingue, 1988; Morris and Heerdegen, 1988; Tarboton et al., 1988; Jenson, 1991; Tarboton, 1997). The original D8 algorithm developed by O'Callaghan and Mark (1984) moves water from a cell to one of the eight surrounding cells depending on the steepest descent (Figure 2.a). The next step in watershed delineation is to determine the accumulation of flow, or the number of upstream cells that feed into each cell (Figure 2.b). The upstream area is often used to determine the channel network using a constant area threshold (O'Callaghan and Mark, 1984; Jenson and Domingue, 1988; Morris and Heerdegen, 1988; Tarboton et al., 1991; Tarboton et al., 1992). In the Río Salado, the National Hydrography Dataset (NHD) blue lines have a drainage density of 1.1 (1/km). We found that a stream threshold of 0.5 km^2 matched the NHD drainage density well, while minimizing the introduction of new first order streams. For visualization purposes, a threshold of 40,000 upstream cells or 36 km^2 was used to delineate the stream network in the Río Salado (Figure 1).

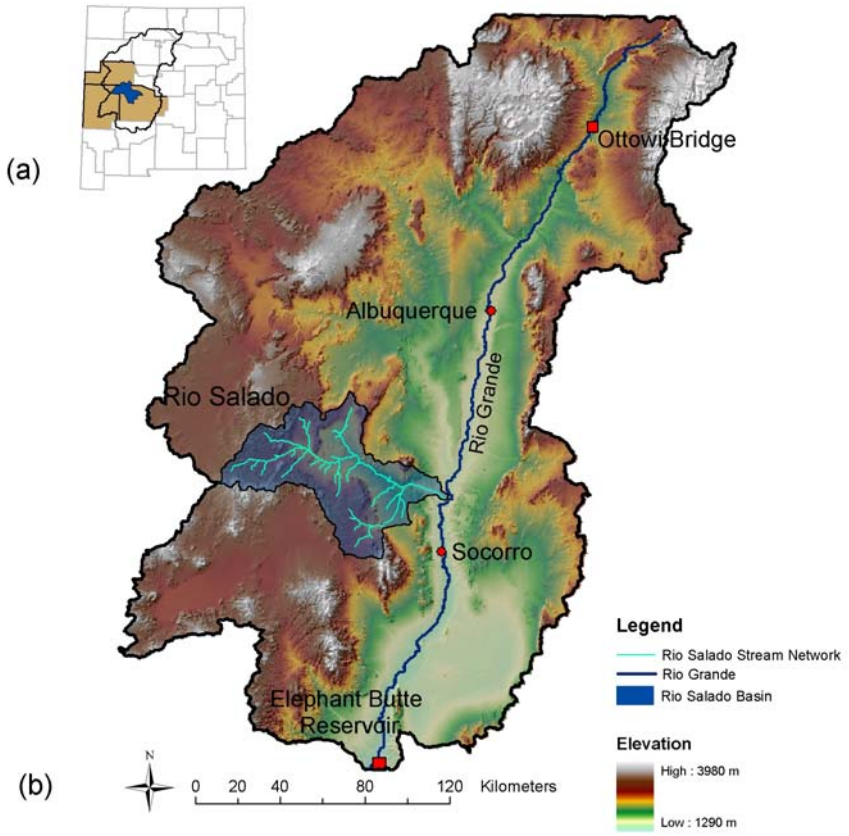

FIGURE 1: (a) Río Salado reference map, showing New Mexico state boundary, county boundaries, and the highlighted counties of Catron, Cibola, and Socorro. (b) 30-meter Digital Elevation Model of Middle Río Grande basin, with Río Salado watershed in dark blue and stream network in cyan. The cities of Albuquerque and Socorro, for spatial reference, are shown as red dots, Ottowi Bridge and Elephant Butte Reservoir are shown as red squares.

DEM Elevation Values

(a)

2336	2338	2340	2342	2348
2337	2341	2344	2347	2347
2340	2341	2351	2358	2361
2344	2340	2351	2361	2368
2350	2344	2351	2360	2369

Flow Direction

(b)

Outlet	16	16	16	16
64	32	32	32	32
64	32	8	32	32
64	32	16	16	32
128	64	32	32	16

Flow Accumulation

(c)

24	9	5	2	0
12	0	2	1	0
10	0	0	1	0
0	8	3	0	0
0	0	0	1	0

Flow Path

(d)

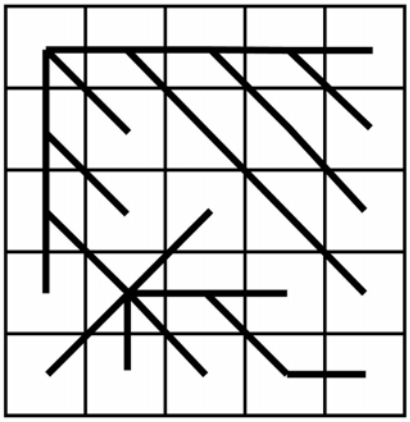

FIGURE 2: (a) Elevation values from the DEM for each cell from Bear Mountains located NW of Magdalena, NM. (b) Flow direction determined by following D8 assignments: 1=E, 2=SE, 4=S, 8=SW, 16=W, 32=NW, 64=N, 128=NE. (c) Flow accumulation grid calculated from the number of upstream cells along flow path. Cells with 0 values have local 30 m by 30 m pixel as contributing area. (d) Flow path based on flow directions. (O'Callaghan and Mark, 1984)

Figure 3 shows the products of the delineation steps, including the stream network and basin boundary. For the purpose of this modeling effort, the model domain defined by the basin boundary is divided into Hydrological Response Units or HRUs. An HRU is defined as a contiguous (map, land, surface) unit with unique soil and vegetation class combination, each of which are treated as homogeneous within the HRU (e.g. Hay et al., 2006). The HRU concept is often used in models with large grid cells when a finer discretization of the model domain is desired (e.g. Arnold, 1998; Liang et al., 1994). The Variable Infiltration Capacity (VIC) model provides an example of how HRUs can be used to address sub-grid variability of land surface characteristics (Liang et al., 1994). In their 2006 study, Hay et al. determined that their results using polygon-based HRUs are as good as results achieved using raster grids of finer resolution Hay et al. (2006) forced the USGS Precipitation Runoff Modeling System (PRMS) with output from the MM5 weather forecasting model. Comparable performance of the HRU and grid-based models in simulating stream flow discharge was determined using the Nash-Sutcliffe goodness of fit (Nash and Sutcliffe, 1970) and the root mean square error (RMSE).

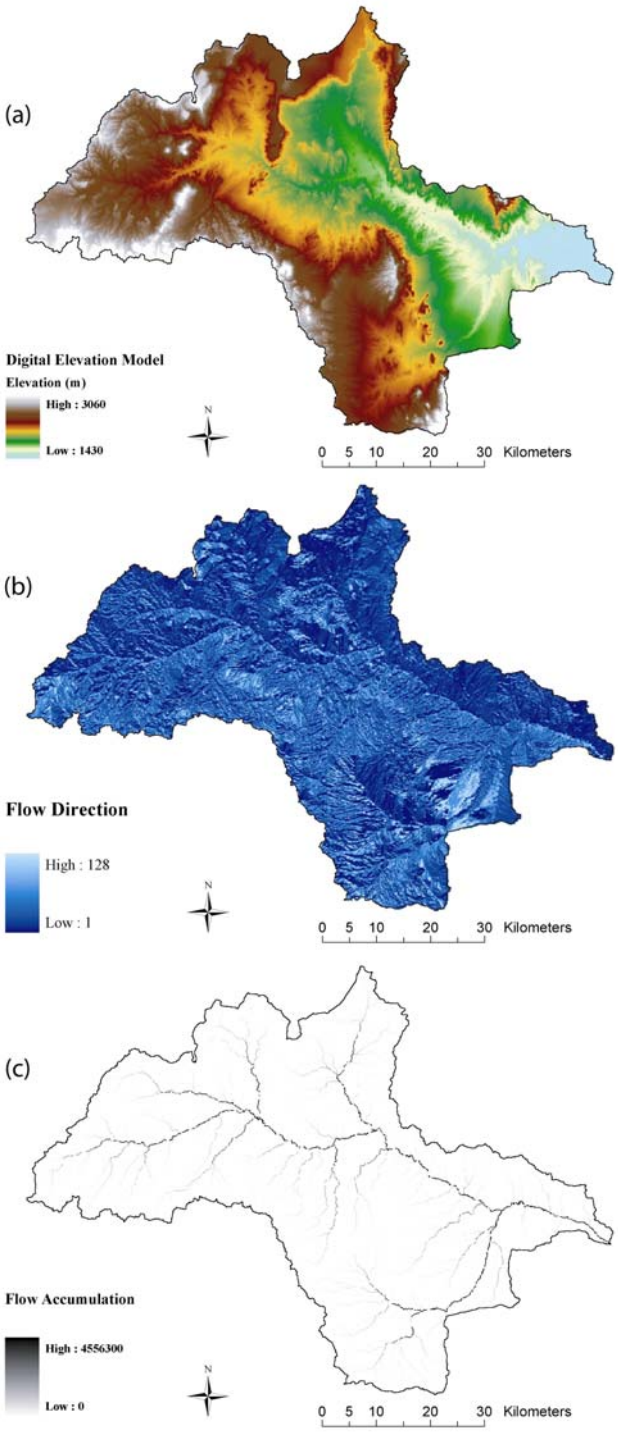

FIGURE 3: (a) 30-meter Digital Elevation Map of Río Salado watershed, elevation ranges from 1430 to 3060 meters. (b) Flow direction map showing direction of steepest descent for each cell in the DEM. (c) Flow accumulation map displaying the number of upstream cells for each location in the basin, used to delineate the stream network.

Hydrologic response units are also useful when computational efficiency is important in a hydrological model. For example, a grid-based simulation in the Río Salado would require calculations be performed on over 4 million grid cells at 30-m resolution, whereas only 68 HRUs are required for the same domain. Gurtz et al. (1999) and others have found similar comparisons in other regions. However, the computational efficiency is gained at the expense of losing information, such as the topographic distribution. Another weakness of the HRU concept is that uniform parameters are applied to each unit, introducing uncertainties in parameter estimates due to potential sub-HRU variability (Gurtz et al., 1999; Liang et al., 1994). In the process of aggregation, detailed information on soil and land cover may also be lost. Finally, HRUs typically do not interact with each other, but directly route produced runoff to the basin outlet (Arnold, 1998). The lack of lateral connectivity is enforced to simplify model representations and facilitate rapid computations over large regions.

The HRU concept is adapted in this study to capture the internal landscape variability present in a large, complex, and semiarid watershed. Intersecting coarse-resolution soil class and land cover maps resulted in the creation of an HRU map for the Río Salado basin. The State Soil Geographic (STATSGO) database for New Mexico and the General Vegetation Map of New Mexico were used to create the HRUs in this model application. The number of HRUs is dependent on the original resolution and variability of the two parent maps. To reduce the computational burden of the model, the soils map was reclassified and then dissolved, a GIS process that combines adjacent features that share similar properties (Figure 4). This process captured the major soil regions in the Río Salado and minimized the need for extensive parameter estimation. For example, if the following three units were adjacent on the map, a gravely sand, fine sand, and very fine sand, the resulting soil unit would be classified as simply a

sand unit. Similarly, the coarse-resolution General Vegetation Map of New Mexico was used instead of the high-resolution (30-m) National Land Cover Database (NLCD) map to minimize the number of HRUs in the domain. Reclassification was also performed on the General Vegetation Map to reduce the number of HRUs that would be produced when combining the parent maps (Figure 5). Since each HRU has distinct soil and vegetation characteristics, we make the assumption that the landscape properties (e.g., soil hydraulic conductivity, porosity, rooting depth, and leaf area index (LAI)) within each HRU are uniform. This assumption is appropriate when HRUs are of a scale at which hydrologic processes can be treated as homogeneous (Singh, 1995). Our desire to decrease the computational burden of the watershed model led us to use the coarser scale definition of an HRU in this study. This was particularly needed to allow long-term simulations of the large tributary basin to be run quickly on a personal computer, for the purpose of use in a decision support system. Figure 6 shows the creation of the HRU map for the Río Salado, with the final HRU map containing 68 HRUs of various sizes. Using HRUs in the Río Salado allows for the capture of properties from four major land cover types (Figure 6.a) and eight major soil classes (Figure 6.b). In general, the basin land surface is dominated by shrubland underlain by clay loam soil (19%), and grassland underlain by sandy loam soil (9.5%).

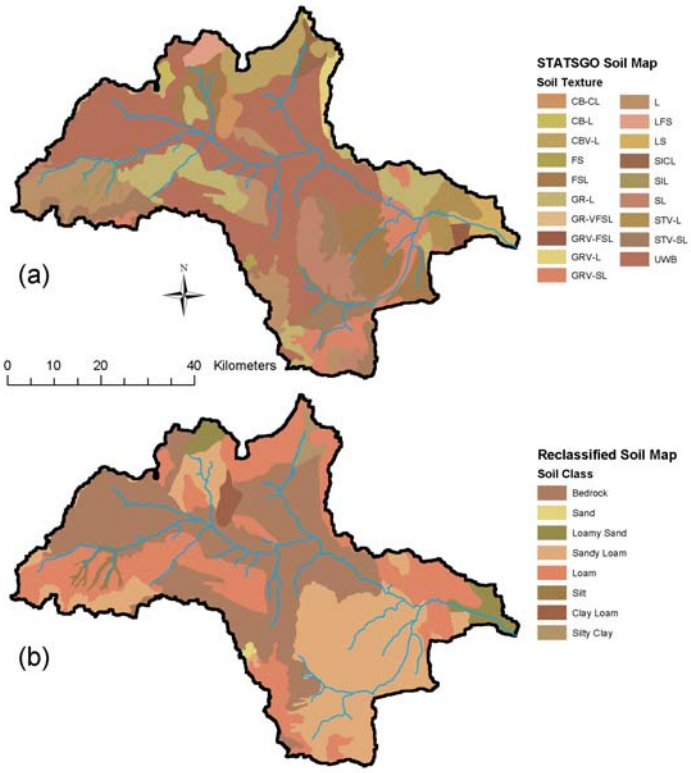

(c)

Soil Class	Percent of area
Bedrock	38.43
Sand	0.22
Loamy sand	3.08
Sandy loam	28.67
Loam	27.46
Silt loam	1.01
Clay loam	1.03
Silty clay loam	0.10

FIGURE 4: Reclassification of (a) STATSGO soil texture map to (b) a coarser soil class map, and (c) the percentages of area for each new soil class in the Río Salado.

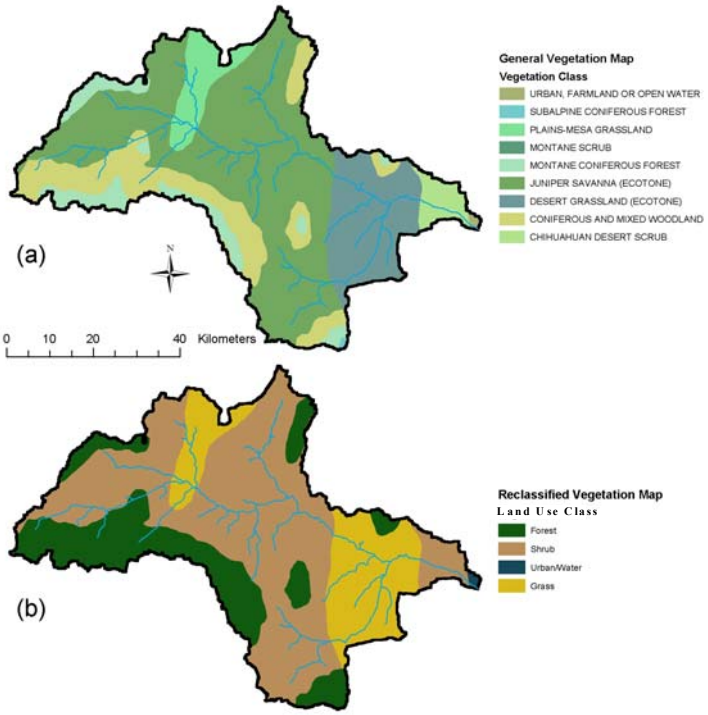

(c)

Land Use Class	Percent of area
Forest	23.73
Grass	23.83
Shrub	55.44
Urban/Water	0.002

FIGURE 5: Reclassification of (a) the General Vegetation Map of New Mexico to (b) a coarser vegetation class map, and (c) the percentages of area for each new land use class in the Río Salado.

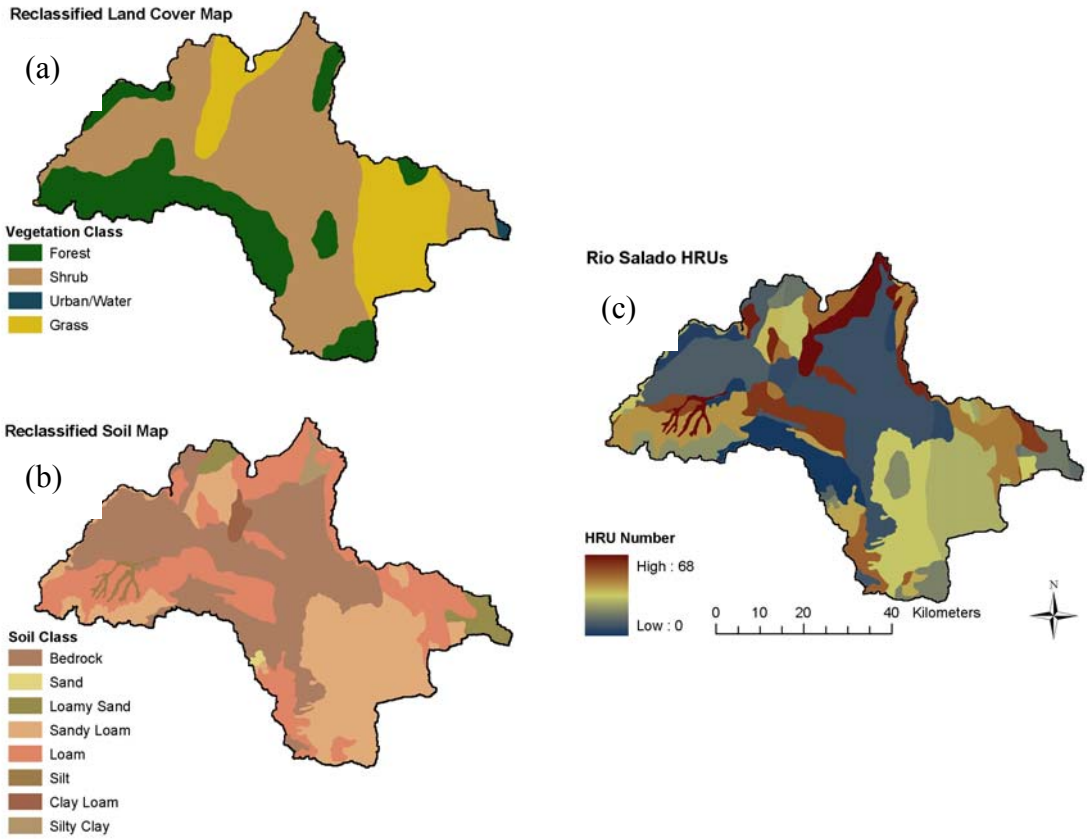

FIGURE 6: Reclassified (a) vegetation and (b) soil maps are combined to produce (c) the final HRU map. Properties from respective classes are associated with each HRU.

Figure 7 shows the distribution of HRU areas within the Rio Salado, the majority of the HRUs are small in size, each with an area less than 1% (e.g. <0.01) of the total Río Salado watershed. However, when the seven largest HRUs are combined, ~10% of total number of HRUs, these cover nearly 65% of the total basin area. This inequality in HRU sizes led us to a perform field validation exercise to examine the approach of using large uniform HRUs to represent the landscape. The entire set of verification locations are shown as 28 green triangles in Figure 8.a, while the four yellow triangles are the sites pictured in Figure 8.b. The site visits showed that the coarse land cover description from the general vegetation map was generally, but not always, representative of the actual environment. In the majority of cases, the descriptions are suitable, such as those pictured in Figure 8.b.2 and Figure 8.b.4, where a shrubland and grassland sites are

found, respectively. However, Figure 8.b.1 is labeled as shrubland on the vegetation map, but there is almost no vegetation cover, while Figure 8.b.3 appears more like grassland with scattered trees (e.g. savanna) than closed canopy forest. Since few locations were very different from their land cover descriptions, we felt confident in the use of the coarse vegetation map in creating the HRUs used by the model.

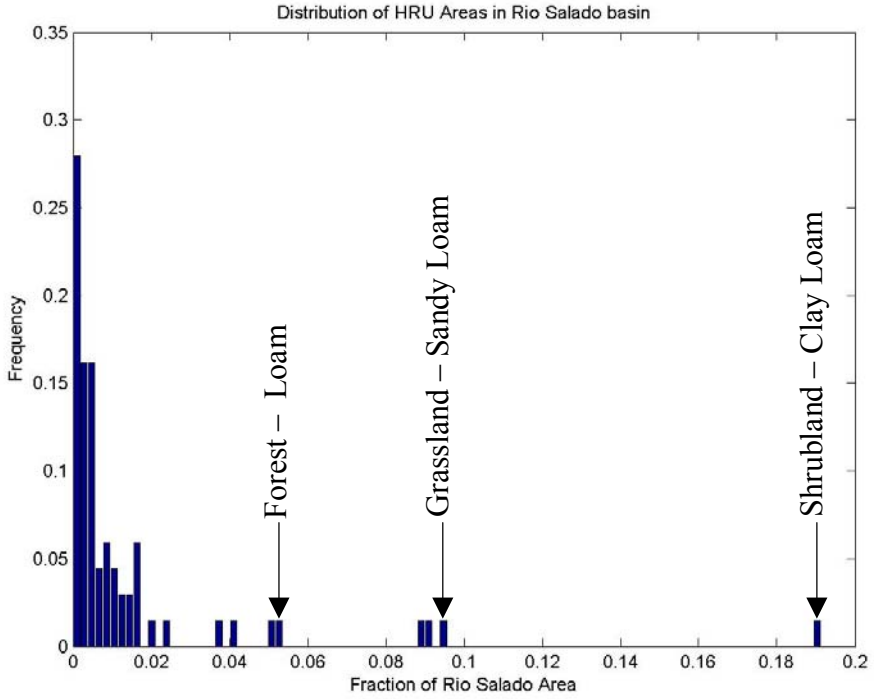

FIGURE 7: Frequency histogram of the HRU areas in the Río Salado basin.

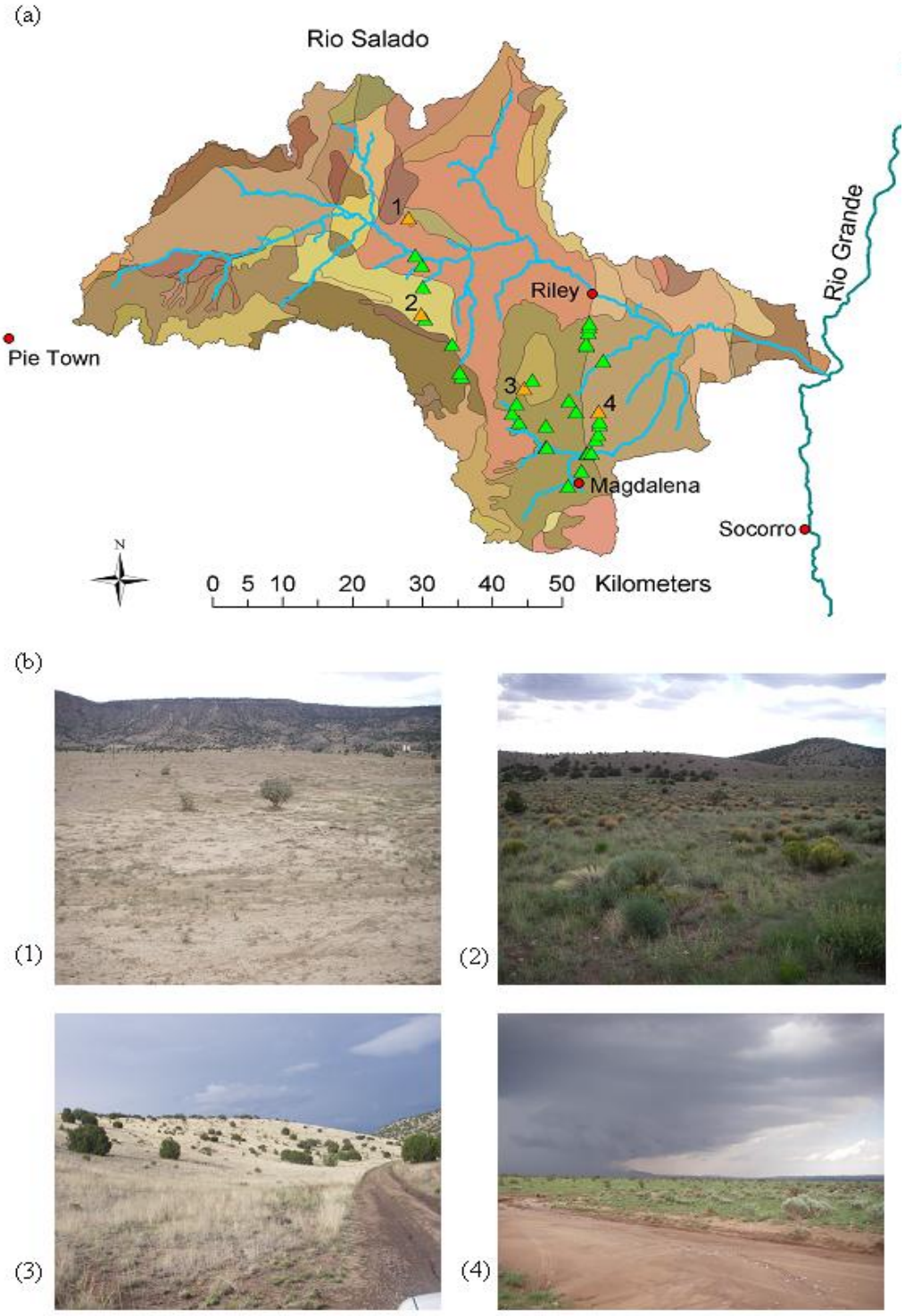

FIGURE 8: (a) Rio Salado HRU map with photo validation sites (triangles). (b) Photographic examples of HRU vegetation: (1) and (2) are shrubland sites, (3) is a forest, and (4) is a grassland location.

In summary, the Río Salado watershed was delineated from the USGS 30-m DEM. Next, the watershed boundary was further divided into uniform soil and vegetation units called HRUs, used to supply land surface characteristics to the watershed model. Finally, field visits were performed to verify the accuracy of the land cover descriptions used to determine the HRUs, allowing for the rainfall and other hydrological processes described in the next sections to be applied uniformly to each HRU.

Rainfall time-series generation using a stochastic approach

Due to the scarcity of long-term rainfall observations, watershed models often create synthetic rainfall time series to use as model forcing. Synthetic rainfall generation techniques provide a means of estimating rainfall characteristics (depth, duration, arrival time) in areas that lack rain gauges or other observation data for extended periods. In this study, a stochastic rainfall model based on the work by Eagleson (1978) is used as part of the Rio Salado watershed model to create a time series of rainfall input. The rainfall model has been widely used in earlier studies in hydrology and geomorphology (e.g., Rodríguez-Iturbe and Eagleson, 1987; Tucker and Bras, 2000). Figure 9 shows how continuous precipitation time series are converted into discrete storm and inter-storm events, modeled as rectangular pulses (Eagleson, 1978). It should be noted that only non-zero intensity events are used to calculate storm intensity and duration values, while the zero intensity events make up the inter-storm period. The rectangular pulse model is an example of a Poisson rainfall model that provides a simple and general method of simulating the randomness of discrete storm events with inter-storm durations that are large when compared to the storm duration (Eagleson, 1978). An exponential distribution is often used to simulate the time between rainfall events as it fits the distribution of the actual data from surrounding gauges (Haan, 1977). We are also using the exponential distribution to simulate the amount of rain in

each event, since most rainfall events are small in both intensity and duration, while very large storms are rare.

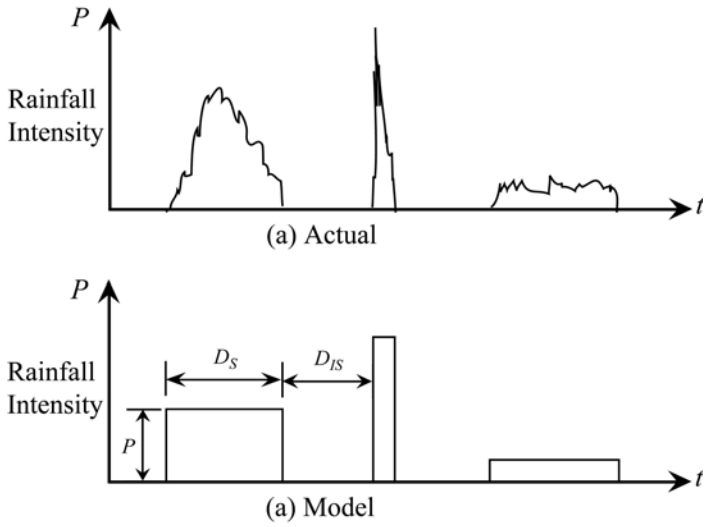

FIGURE 9: Schematic illustration of Poisson rectangular pulse model (after Eagleson, 1978).

The stochastic model samples separate exponential distributions of the storm intensity (P), storm duration (D_S) and inter-storm duration (D_{IS}) as follows:

$$f(P) = \frac{1}{\overline{P}} e^{\left(-\frac{P}{\overline{P}}\right)}, \quad (1)$$

$$f(D_S) = \frac{1}{\overline{D_S}} e^{\left(-\frac{D_S}{\overline{D_S}}\right)}, \text{ and} \quad (2)$$

$$f(D_{IS}) = \frac{1}{\overline{D_{IS}}} e^{\left(-\frac{D_{IS}}{\overline{D_{IS}}}\right)}, \quad (3)$$

where $\overline{P}$, $\overline{D_S}$, and $\overline{D_{IS}}$ represent the mean values, in units of mm/hr for precipitation intensity, and days for durations. Using parameters derived from historical datasets reduces the degrees of freedom in the model compared to the approach of treating rainfall as a free parameter that can

be adjusted to produce a desired output (Tucker and Bras, 2000). Thus, the stochastic approach attempts to mimic local conditions using the available historical rainfall data.

The ability to create synthetic rainfall time series is extremely useful in the Rio Salado, since data is only available for one rain gauge within the extent of the basin. Rather than using this single gauge to apply uniform rainfall over the entire watershed, synthetically generated rainfall can provide each HRU with a time rainfall series, conditioned on nearby, long-term historical records. This procedure introduces randomness to the precipitation forcing and increases the spatial variability of the model input, while maintaining some spatial correlation for adjoining HRUs. Synthetic datasets allow the model to be forced with one of five unique rainfall time series derived from a set of rain gauges that border the watershed. The five gauges that were used to condition the stochastic model are named Augustine, Brushy Mountain, Datil, Laguna, and Socorro, their locations are shown in Figure 13. Table 1 provides a list of the rain gauge characteristics such as record length and rain gauge resolution. Each gauge provides hourly rainfall measurements with time series lengths varying from 4 to 30 years. The Augustine, Laguna, and Socorro gauges are National Climatic Data Center Cooperative (NCDC-COOP) stations, while the Brushy Mountain and Datil gauges are Remote Automated Weather Stations (RAWS) stations. The NCDC-COOP stations are standard National Weather Service, 8 in., Fisher-Porter weighing rain gauges, while the RAWS gauges are 8 in. Forest Technology Systems tipping bucket rain gauges. Some of the datasets are of limited lengths and may not be completely representative of the historical rainfall behavior at their respective locations.

Rain gauge	Augustine	Brushy Mountain	Datil	Laguna	Socorro
Record length	1948 to 2007	1992 to 2007	2003 to 2007	1946 to 2006	1948 to 2006
Minimum resolution	0.01 in	0.01 in	0.01 in	0.01 in	0.01 in
Long Lat Elevation (m)	-107.617 34.083 2133.6	-107.848 34.719 2670.7	-107.766 34.289 2316.5	-107.367 35.033 1773.3	-106.883 34.083 1397.5
Data set source	NCDC	WRCC	WRCC	NCDC	NCDC

TABLE 1: Characteristics of rain gauges surrounding Rio Salado collected from National Climatic Data Center (NCDC) and Western Regional Climate Center (WRCC).

The Socorro rain gauge provides an example of how a historical record of hourly rainfall measurements can be used to determine the parameters of the stochastic model. The Socorro rain gauge has an hourly dataset that spans from 1948 to present. Prior to 1978, the rain gauge consisted of a 12 in. dual traverse rain gauge with a paper chart, which required frequent changing. This was replaced by the current Fisher-Porter rain gauge in late 1978, however this resulted in a reduction of accuracy from 0.01 in. to 0.1 in. (J. Alfieri, personal communication, 2007). Changing gauge resolution caused an underestimation of the frequency of small rainfall events, recording them only when the cumulative rainfall volume surpassed the 0.1 in. threshold. As a result of higher rain gauge precision, the 30-year period from 1948 to 1978 is used to establish the required parameters at the Socorro gauge. The mean values of each parameter (P, D_S, D_{IS}) are extracted from this dataset to determine if the rainfall observations fit the exponential distributions defined above. A simple arithmetic mean is used to compute the mean value for each variable:

$$\bar{x} = \frac{1}{n}\sum_{i=1}^{n} x_i \,, \tag{4}$$

where $\bar{x}$ is the mean value, x_i is the individual record, and n is the number of samples in the time series.

Having estimated the mean value for each parameter, (Equation 1) is used to plot the distribution of rainfall depths for the entire period. Figure 10 shows the probability distribution function (PDF) of the rainfall data for the Socorro rain gauge, compared to an exponential distribution using the mean value. The extensive period of record for the Socorro rain gauge shows a good visual fit to the exponential distribution, suggesting that the exponential distribution reasonably captures the observed variations in rainfall. However, the exponential distribution underestimates the frequency of very low-intensity events by a factor of 2 and at times overestimates the moderate events. A visual comparison of the data from the Datil rain gauge Figure 11, which has a much smaller sampling period (2003-2007), suggests that the exponential distribution is also an accurate distribution for the short duration records in the study area.

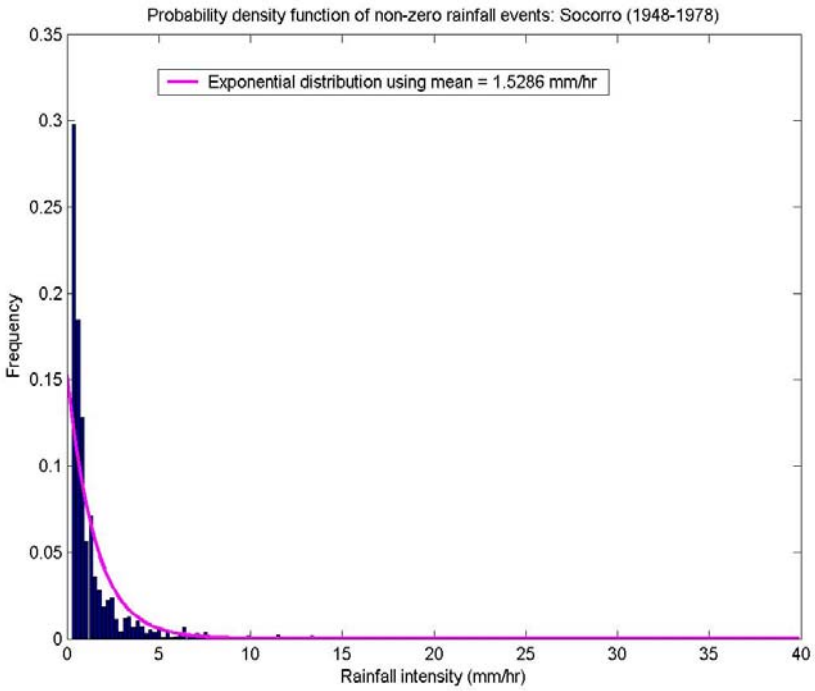

FIGURE 10: Probability density function of rainfall intensity for the Socorro rain gauge, along with the exponential distribution generated using mean values estimated from the historical record (1948 – 1978).

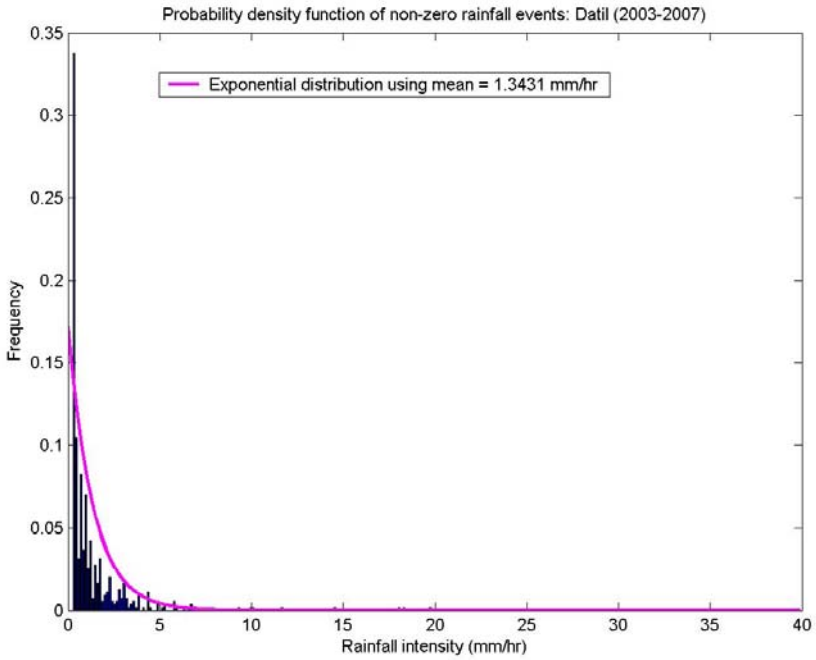

FIGURE 11: Probability density function of rainfall intensity for the Datil rain gauge, along with the exponential distribution generated using mean values estimated from the historical record (2003 – 2007).

In order to evaluate how well the probability distribution function of the rainfall data fits to an exponential distribution based on the mean value of the historical data, the two functions are plotted on a semi-log plot (Figure 12). The PDF has a value of 1/N (single event) in each bin for high intensity rainfall events. These infrequent events cause the tail of the distribution to flatten out in semi-log space toward a value of log(F) = -4. Figure 12 shows that the frequency of the non-zero events below 10 mm/hr is almost linear ($R^2 = 0.7658$). This implies that sampling rainfall intensities from exponential distribution will provide a good estimate of small volume events, however, it will underestimate the occurrence of larger events, which typically occur in the summer for this region.

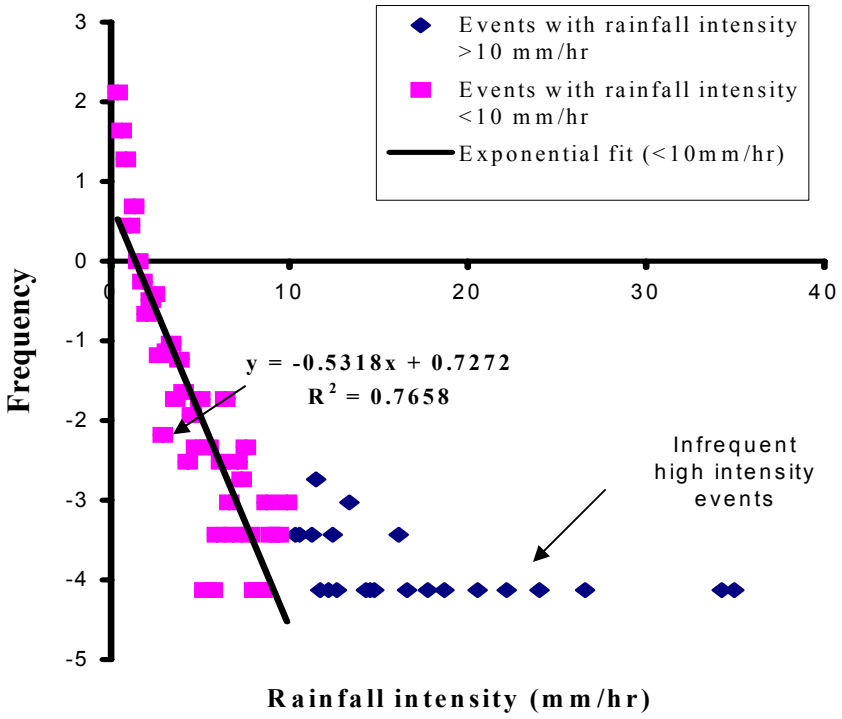

FIGURE 12: Semi-log plot of PDF of non-zero rainfall events, showing that events with intensity of less than 10 mm/hr fit well with an exponential distribution.

The assignment of each HRU to a particular rain gauge is determined by creating Thiessen polygons (nearest neighbor) around each rain gauge location. The Thiessen polygon approach to the distribution of rainfall is frequently used, including for comparisons of distributed and HRU-based models (El- Nasr et al., 2005). The majority of the watershed is located within the boundaries of the polygons for the Augustine (24.3%), Datil (37.3%), and Socorro (22.2%) rain gauges, with a small percentage associated with the Brushy Mountain (11.0%) and Laguna (5.2%) sites. Figure 13 shows the distribution of HRUs with their assigned rain gauges. HRUs that are overlain by more than one gauge are given the parameters of the rain gauge associated to the polygon with the largest percentage of the HRU area within its boundaries.

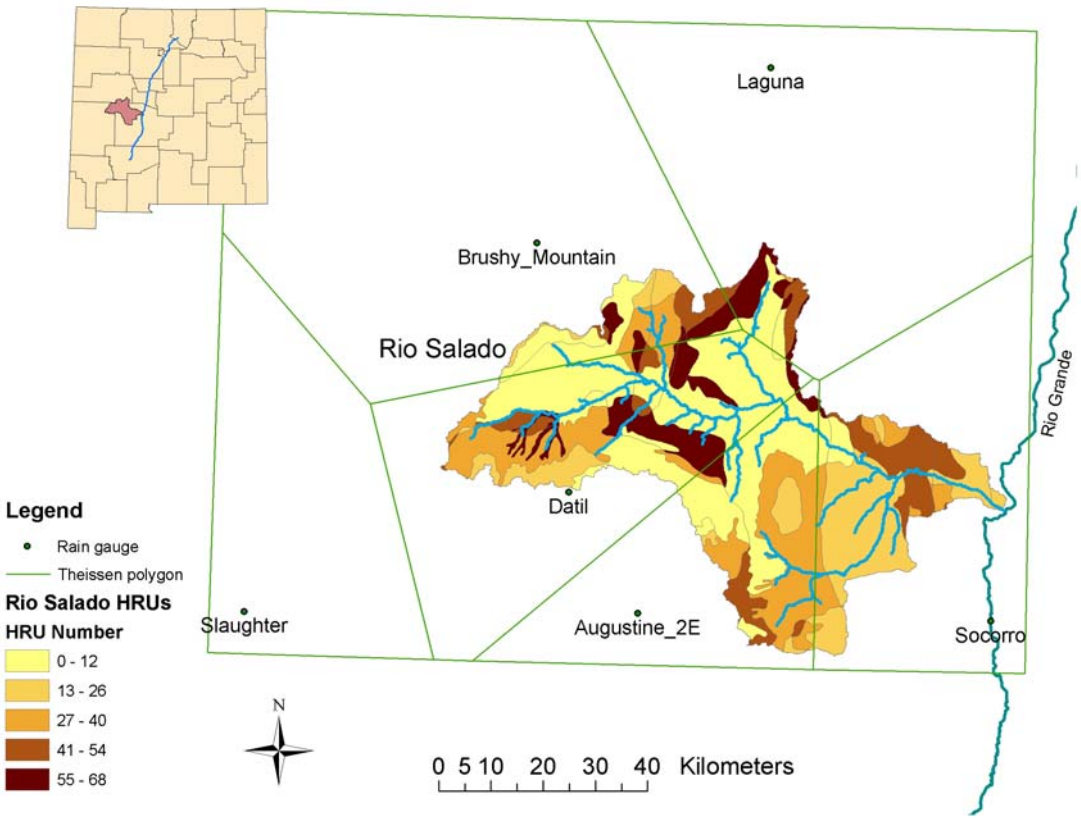

FIGURE 13: Thiessen polygons of rain gauges surrounding the Rio Salado basin.

Individual HRUs are forced with a stochastic rainfall time series for each month based on the rain gauge they are linked to. The parameters used to generate these time series are assigned to the HRU based on the Thiessen polygon association described above. A comparison of the mean stochastic parameters for each gauge can be seen in Figure 14. Strong seasonality in storm intensity and frequency (inter-storm length) is apparent in all five rain gauges. The seasonality is best observed when comparing the winter months (Dec. to Feb.) with the late summer months (Jul. to Sep.). While the mean value for rainfall intensity at the Brushy Mountain gauge does seem to be anomalous in the month of March, the data fits well with the other gauges the rest of the year. Tables 2, 3, and 4 present the numerical values of the mean stochastic parameters for each rain gauge, for reference purposes, as well as to highlight the differences between summer and winter values.

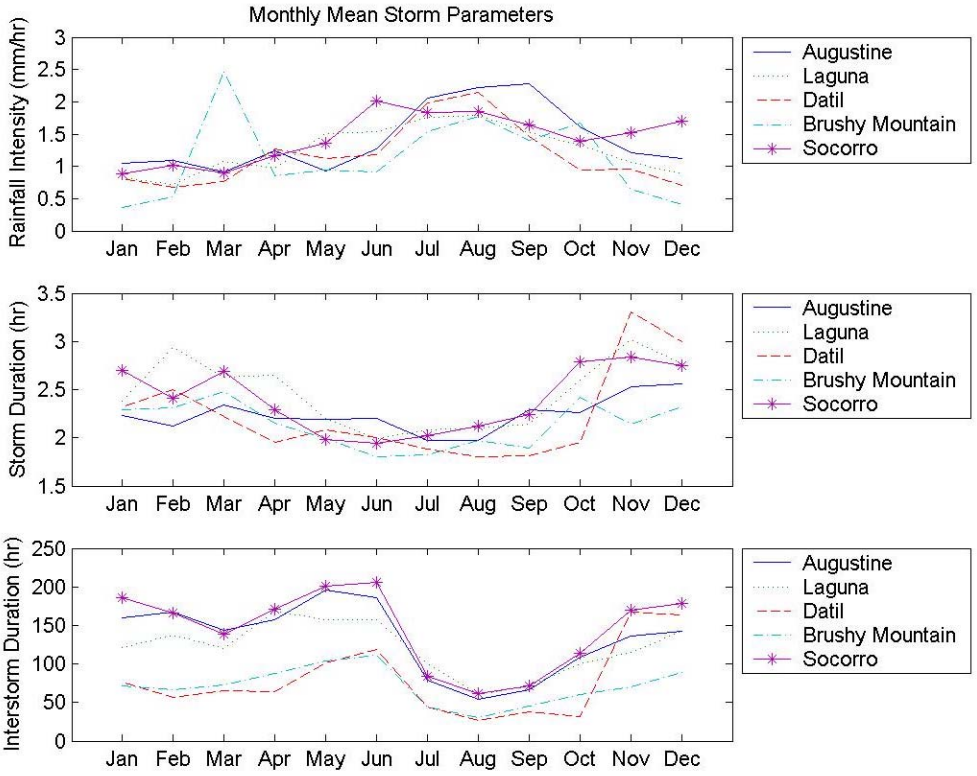

FIGURE 14: Comparison of the monthly mean values of estimated parameters from the historical record used for the generation of stochastic rainfall time series at rain gauges surrounding the Río Salado basin.

The rainfall time series that are produced by the stochastic model are dependent on the parameter values used. Figure 15 shows the effects of different forcing parameters on the generation of storm events. As shown by the highlighted values in Tables 2-4, the July storms should occur nearly twice as often and are twice as intense as the January storms. The marked increase in larger rainfall events can be seen visually by comparing Figures 15a,b to Figures 15c,d with the second pair showing a greater frequency of large rainfall events. The effects of a long inter-storm duration are best seen in the decrease in the number of rainfall events in Figure 15a for January at the Augustine rain gauge. The rain gauge at Datil receives more rainfall than the Augustine gauge when using the July means due to a decrease in the inter-storm duration. In order to better visualize the difference between rainfall time series, Figure 16 shows the Cumulative Distribution Function (CDF) of rainfall depth, for the selected months and rain gauges. The CDF shows that large rainfall events are more likely to occur when the July parameters are used for both gauges, due to the increase in the mean rainfall intensity for July events when compared to January events. Therefore, this suggests that rainfall is more dependent on seasonal changes as compared to spatial variations across the region.

Monthly Mean Storm Intensity (mm/hr)					
Gauge	**Augustine** ***P***	**Laguna** ***P***	**Datil** ***P***	**Brushy Mountain** ***P***	**Socorro** ***P***
Jan	1.05	0.82	0.81	0.37	0.88
Feb	1.10	0.72	0.68	0.53	1.01
Mar	0.92	1.08	0.76	2.48	0.89
Apr	1.24	0.98	1.27	0.85	1.17
May	0.93	1.51	1.13	0.94	1.37
Jun	1.27	1.54	1.18	0.92	2.01
Jul	2.05	1.76	1.98	1.54	1.83
Aug	2.23	1.79	2.15	1.78	1.86
Sep	2.28	1.53	1.46	1.41	1.64
Oct	1.61	1.33	0.94	1.67	1.39
Nov	1.22	1.07	0.96	0.65	1.53
Dec	1.13	0.89	0.70	0.40	1.70

TABLE 2: Comparison of monthly mean values of storm intensity (P). Highlighted values show differences between summer and winter events.

Monthly Mean Storm Duration (hr)					
Gauge	**Augustine** D_S	**Laguna** D_S	**Datil** D_S	**Brushy Mountain** D_S	**Socorro** D_S
Jan	2.23	2.38	2.32	2.29	2.70
Feb	2.12	2.94	2.50	2.31	2.41
Mar	2.34	2.63	2.23	2.48	2.69
Apr	2.21	2.65	1.95	2.15	2.29
May	2.19	2.21	2.08	1.99	1.99
Jun	2.20	1.99	2.00	1.80	1.94
Jul	1.98	2.08	1.89	1.82	2.03
Aug	1.97	2.10	1.80	1.98	2.12
Sep	2.29	2.14	1.82	1.89	2.24
Oct	2.26	2.60	1.95	2.42	2.79
Nov	2.53	3.02	3.31	2.14	2.84
Dec	2.56	2.77	3.00	2.32	2.74

TABLE 3: Comparison of monthly mean values of storm duration (D_S). Highlighted values show differences between summer and winter events.

Monthly Mean Inter-Storm Duration (hr)					
Gauge	**Augustine** D_{IS}	**Laguna** D_{IS}	**Datil** D_{IS}	**Brushy Mountain** D_{IS}	**Socorro** D_{IS}
Jan	159.99	121.31	76.24	71.84	185.52
Feb	167.82	137.65	56.15	66.97	166.18
Mar	144.00	119.77	65.61	72.17	138.19
Apr	157.09	168.02	63.68	87.37	171.06
May	195.88	157.66	100.83	103.56	201.46
Jun	186.46	157.38	118.33	110.96	205.35
Jul	78.81	99.64	43.99	44.60	84.05
Aug	53.55	60.59	27.15	30.36	61.29
Sep	66.49	71.05	37.91	45.73	71.46
Oct	108.54	100.15	32.32	60.84	113.87
Nov	136.40	115.51	166.88	70.56	169.22
Dec	142.87	142.71	163.00	89.44	177.92

TABLE 4: Comparison of monthly mean values of inter-storm duration (D_{IS}). Highlighted values show differences between summer and winter events.

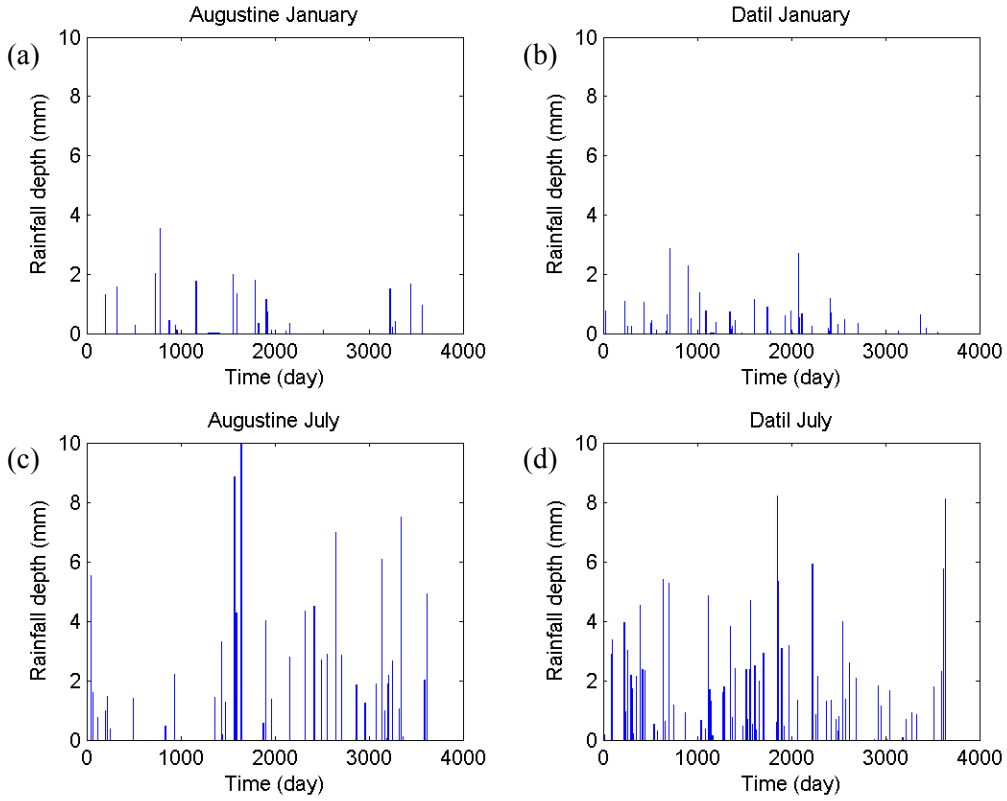

FIGURE 15: Ten-year simulation of stochastic rainfall time series using monthly mean values (a) Augustine rain gauge with January parameters, (b) Datil rain gauge with January parameters, (c) Augustine rain gauge with July parameters, and (d) Datil rain gauge with July parameters.

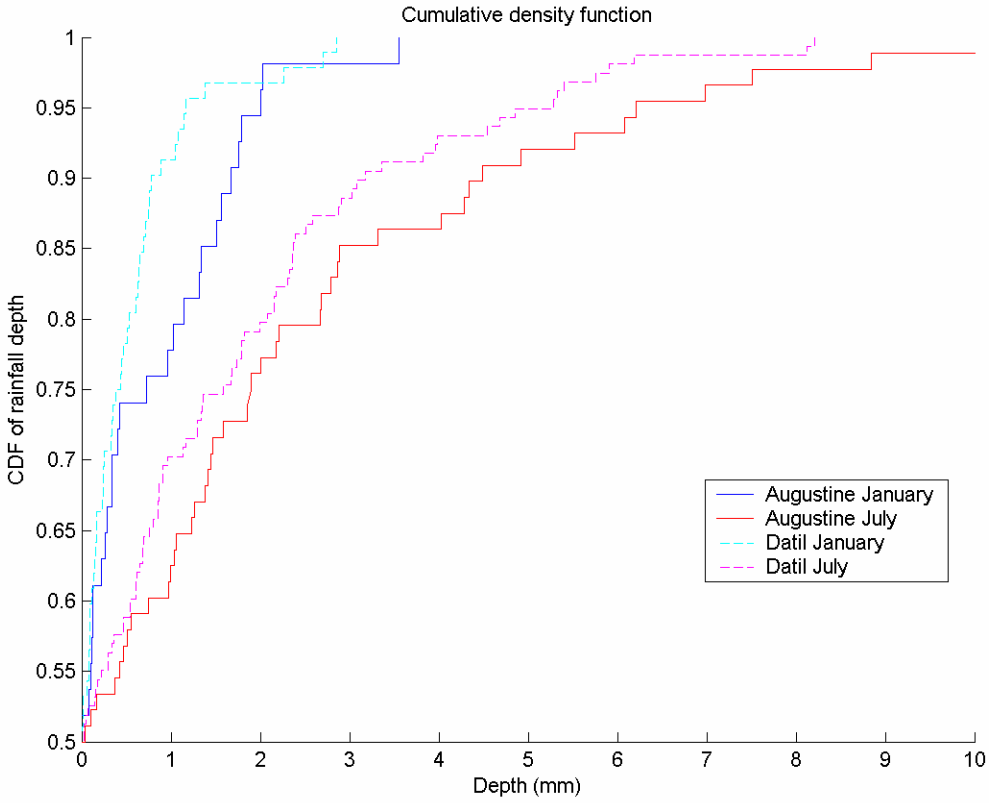

FIGURE 2.16: Cumulative density function of stochastic rainfall time series at Augustine (solid line) and Datil (dotted line) rain gauges, using monthly mean values for January (blue) and July (red).

In order to verify that the higher elevation Datil and Brushy Mountain gauges receive more precipitation than the other three gauges, we compared the measured gauge data to a spatially-distributed product known as Parameter-elevation Regressions on Independent Slopes Model (PRISM) data. PRISIM provides a measure of spatial variability in precipitation caused by orographic effects through its elevation-based regression model. Figure 17 shows a map of the mean 30-yr annual precipitation data from PRISM clipped to the rain gauge thiessen polygons for each gauge in the Rio Salado region. According to the PRISM data the Datil and Brushy Mountain gauges both receive about 100 mm/yr more precipitation that the Augustine gauge and nearly 200mm/yr more than the Socorro or Laguna gauges. This confirms that the Datil and Brushy Mountain gauges receive larger amounts of rainfall and that excluding these gauges from

a model simulation would lead to underestimations of precipitation. Clearly, the PRISM data show spatial variations in precipitation due to elevation differences that cannot be captured through Thiessen polygon interpolations. Using the two high elevation rain gauges, however, will reduce the underestimation for the simulations presented here.

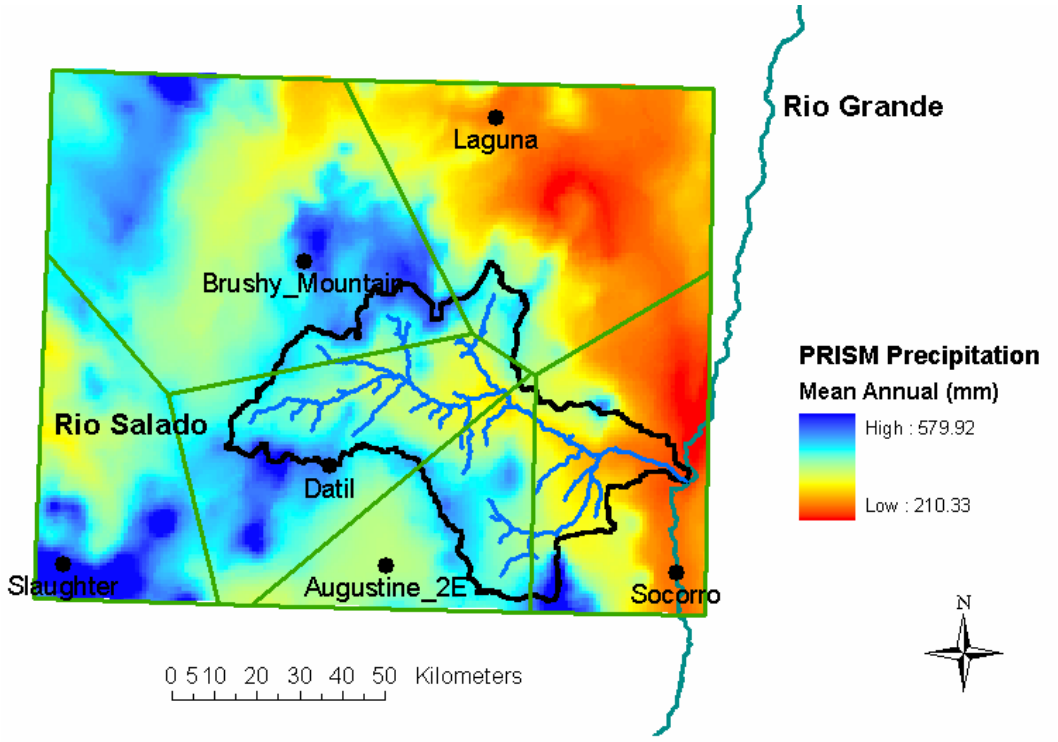

FIGURE 17: 30-yr mean annual PRISM precipitation data clipped to thiessen polygons of rain gauges surrounding the Rio Salado basin. "PRISM Group, Oregon State University, http://www.prismclimate.org, created 4 Feb 2004."

In summary, we have shown that rainfall events are effectively generated using a stochastic method with an exponential distribution, which provides a good fit to actual rain gauge data. The generated rainfall time series are linked to HRUs associated with each rain gauge in the area using a Thiessen polygon method. The rainfall parameters determined from historical records are shown to produce storm events that are plausible for the semiarid environment in the Río Salado. Finally, the spatial variability of precipitation was examined using PRISM data.

Hydrological processes in the watershed model

This section describes the hydrological processes that are represented in the HRU-based watershed model of semiarid basins. The processes begin with the partitioning of precipitation into rainfall and snow, and proceed to interception of precipitation by the vegetation canopy. Water that is able to bypass the canopy and reach the land surface then either infiltrates into the soil column or becomes runoff that is routed to the basin outlet. Losses to evapotranspiration affect each portion of the hydrologic system, which is treated as a set of water balance equations. A final summary will complete the description of the hydrological processes implemented in the HRU-based watershed model.

Snow accumulation and melt

Snow accumulation in the snow pack is treated as a simple water balance, where the change in storage in the snow pack (ΔS_{Snow}) over time is the difference between the volume of new snow that falls (V_{NS}) and the volume of melt from the snow pack (V_M).

$$\frac{\Delta S_{Snow}}{\Delta t} = \frac{V_{NS} - V_M}{\Delta t}, \qquad (5)$$

To determine the volume of snow that falls on each HRU, a temperature-based allocation method was used to partition a portion of the precipitation as snowfall (Federer, 2003). In the same way that random precipitation events are generated, the minimum and maximum temperatures for each event are taken from an exponential distribution.

$$f(T) = \frac{1}{\overline{T}} e^{\left(-\frac{T}{\overline{T}}\right)}, \qquad (6)$$

where $\overline{T}$ represents the mean temperature value for each month of the historical dataset. Average monthly temperature values (minimum, maximum, mean values in each month) in degrees C for each HRU are taken from monthly dataset summaries associated with each rain gauge. Figure 18

shows how the average monthly maximum and minimum temperature varies throughout a year, for a representative HRU. When the maximum temperature for an event drops below a threshold value T_b = -0.5 ^{o}C, all of the precipitation will fall in the form of snow (Federer, 2003). Similarly, if the minimum temperature rises above the same threshold, rain is the exclusive form of precipitation. In the case when the air temperature is between the maximum and minimum for the event, precipitation is partitioned between rainfall and snowfall as:

$$S_f = \frac{T_b - T_{min}}{T_{max} - T_{min}}, \tag{7}$$

$$S_f = 1, \text{ if } T_{max} \le T_b, \text{ and} \tag{8}$$

$$S_f = 0, \text{ if } T_{min} \ge T_b, \tag{9}$$

where S_f is the fraction of precipitation that falls as snow, and T_{max} and T_{min} are sampled from an exponential distribution for each event in the manner described above for the storm parameters, based on historical monthly temperature observations.

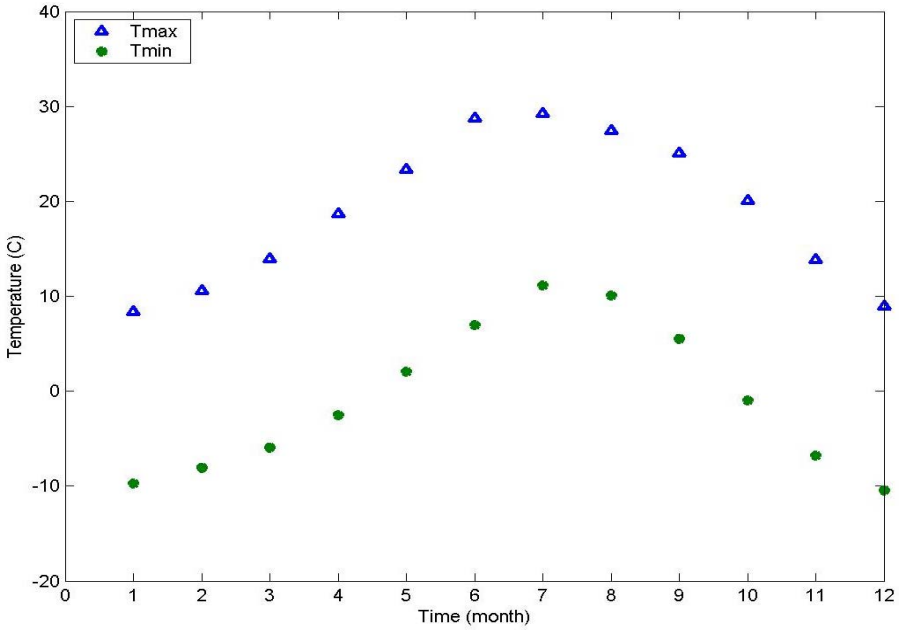

FIGURE 18: Plot of average monthly temperature data (maximum and minimum) for HRU #20 (Forest, Sandy Loam).

Melting of the snow is based on the degree-day method developed by Martinec et al. (1983) as:

$$V_M = M_f (T_i - T_b), \qquad (10)$$

where V_M is the melt volume (m^3), M_f is an empirical melt factor $M_f = 0.011\ \rho_s$ ($m^3/^oC$), T_b is the threshold temperature (^oC), T_i is the index air temperature (^oC) set to the average of the stochastically generated maximum and minimum air temperatures for each event, and ρ_s is the snow density (100 kg/m^3) (Dingman, 2002). The snow dynamics for a representative period (March), including the accumulation and melting of a snow pack, based on the input of precipitation for each event, are shown in Figure 19.a. Figure 19.b shows the air temperature time series for the same month. Note how the low temperatures between hour 320 and 726 allows the snow pack to persist and increase with new snowfall inputs. Additionally, the high maximum temperature at the end of the month results in a melting of the snow pack. Future work may include an improved snow model, which accounts for a multiple-layer snow pack and canopy interception of snow.

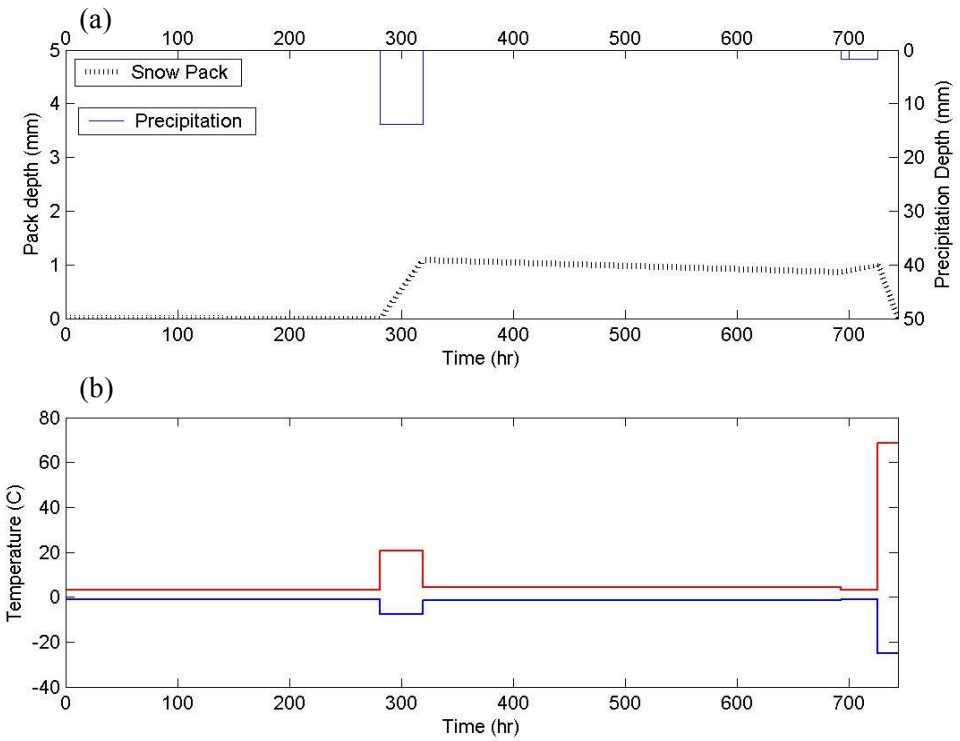

FIGURE 19: Plot of snow dynamics for a representative March, for HRU #2 (Forest, Bedrock). (a) Shows snow pack depth (mm), dotted line, and precipitation depth in (mm), solid line, and (b) and maximum and minimum air temperature for each event (C).

Canopy Interception

Rainfall interception by the vegetation canopy is also treated as a water balance, where the change in storage in the canopy (ΔS_C) over time is the difference between canopy inputs (intercepted water, V_{Int}) and canopy outputs (evaporation, V_{CE}, and drainage, V_D):

$$\frac{\Delta S_C}{\Delta t} = \frac{V_{Int} - (V_{CE} + V_D)}{\Delta t}. \qquad (11)$$

Figure 20 shows the canopy interception processes. Since interception of rainfall requires a canopy, the vegetated area within an HRU (m^2) must be calculated as:

$$A_{veg} = p_{veg} A, \qquad (12)$$

where p_{veg} is the fraction of the HRU that contains vegetation [0 to 1] and A is the total area (m^2) of the HRU. Once the vegetated portion of the HRU has been assigned, the maximum interception capacity of the canopy (I_{CMax}), or the depth of water (mm) that the canopy can hold, is calculated as:

$$I_{CMax} = I_{CL} LAI \,, \tag{13}$$

where LAI is the leaf area index (cm^2/cm^2) and I_{CL} is the leaf interception capacity (mm) for a particular vegetation type. To determine the amount of rainfall captured by the canopy, the rate at which rainfall is intercepted by leaves (I_R) in the canopy (mm/hr), is treated as a linear function of LAI, as:

$$I_R = F_{IntL} RLAI \,, \tag{14}$$

where F_{IntL} is the fraction of rainfall intercepted by leaves, assumed to be $0.1p_{veg}$, and R is the rainfall rate (mm/hr) (Federer, 2003).

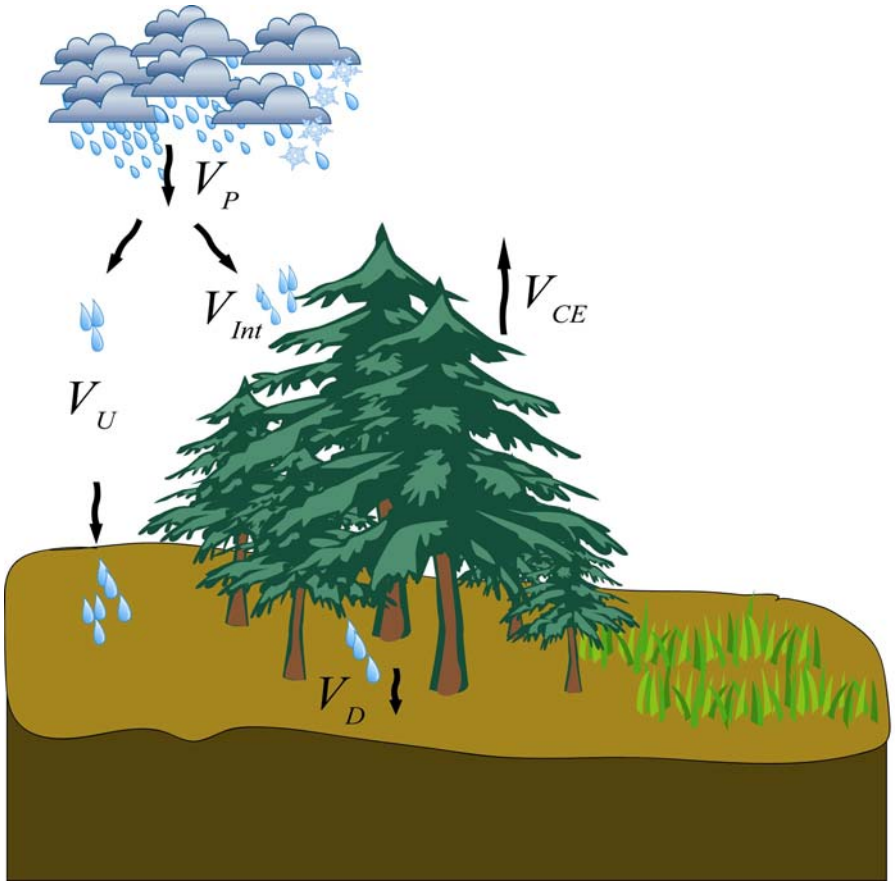

FIGURE 20: Precipitation (V_P) is divided into intercepted (V_{Int}) and un-intercepted (V_U) volumes. The intercepted water that fills the canopy storage space is eventually lost to evaporation (V_{CE}), water that bypasses the canopy as drainage (V_D) then reaches the soil surface.

The total volume of water intercepted during a storm event (V_{Int}) is computed as:

$$V_{Int} = I_R A_{veg} D \,, \tag{15}$$

where D is the duration of the rainfall event (hr). The intercepted volume V_{Int} (m^3) is added to water currently stored in the canopy up to the maximum canopy storage volume (V_{CS}) (m^3) defined as:

$$V_{CS} = I_{CMax} A_{veg} \,, \tag{16}$$

where I_{CMax} is the maximum interception capacity (mm), which is the leaf interception capacity (I_{CL}) multiplied by the leaf area index (LAI). I_{CL} has been estimated to be about 1 mm for pine forests (Rutter et al., 1971). The average of the available values of I_{CL}, provided in a table by Breuer et al. (2003), for each vegetation type is used in the model. Once the canopy is completely full, any further input of water to the canopy is released to the ground surface as drainage (V_D). The un-intercepted volume of water (V_U) or free throughfall, falls over non-vegetated areas and immediately reaches the ground. V_U is the difference between the total precipitation volume (V_P) and the intercepted volume (V_{Int}) calculated as:

$$V_U = V_P - V_{Int} \,. \tag{17}$$

Table 5 shows the values of interception parameters for each vegetation class used in the Río Salado. Figure 21 shows model output of each of the interception processes for a forest canopy for the typical rainfall input during the months of July and August. In Figure 21.b, the canopy storage volume responds quickly to inputs from precipitation (Figure 21.a) and losses from evaporation (Figure 21.c). The water stored in the canopy persists over multiple events until the rate of evaporation is large enough to dry it completely. The lack of drainage from the canopy (Figure 21.d) is a result of the canopy not being filled to capacity at any time during this period.

	Vegetation Percent (p_{veg}) (%)	Leaf Interception capacity (I_{CL}) (mm)	Fraction intercepted by leaves (F_{IntL})	Interception Fraction ($F_{IntL}LAI$)	Rooting Depth (cm)	LAI
Forest	60	4.5	.06	0.18-0.36	150	3-6
Shrub	30	1.1	.03	0.48-.09	150	1.6-3
Grass	50	1.9	.05	0.065-0.15	150	1.3-3
Urban/ Water	0	0	0	0	0	0

TABLE 5: Mean parameter values based on vegetation class (Breuer et al., 2003, Federer, 1996, Wigmosta et al., 1994, Gutierrez et al., 2006).

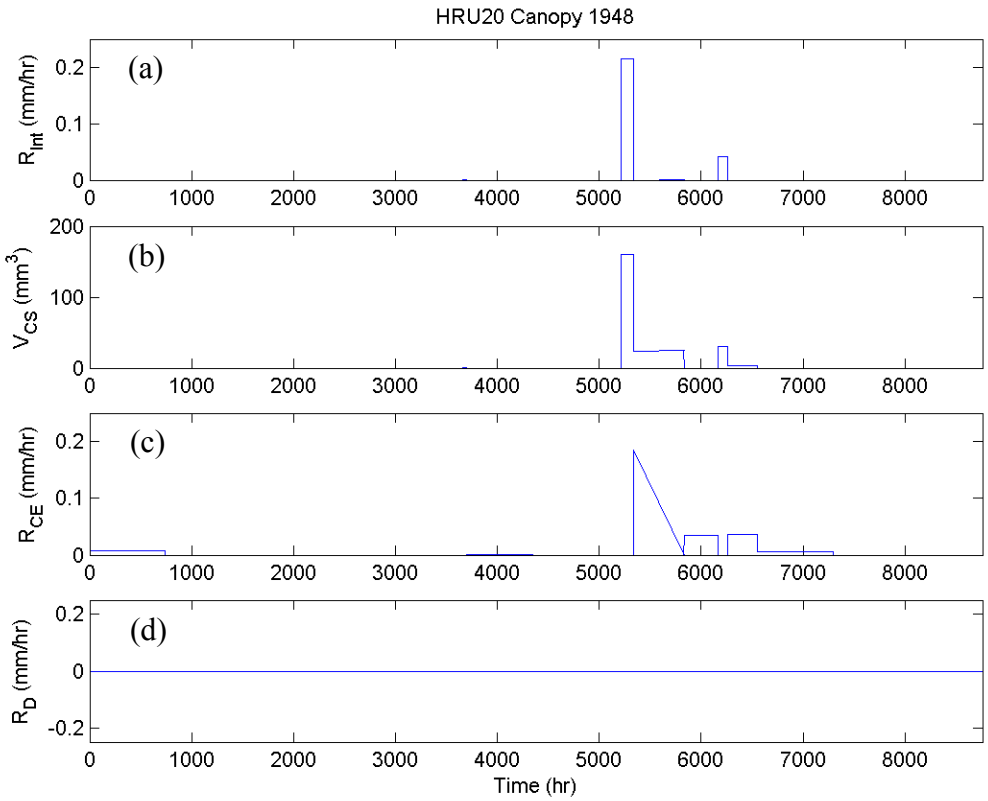

FIGURE 21: Event-scale canopy output from HRU #20 for a representative year. (a) Rate of interception by the canopy (mm/hr). (b) Volume of water stored in the canopy (mm^3). (c) Rate of evaporation from the canopy (mm/hr). (d) Rate of drainage from the canopy (mm/hr).

Vadose zone processes

Water inputs in the form of free throughfall, drainage, and snowmelt, which reach the soil surface, are allocated depending on the state of the hydrologic system. The water balance at the land surface is modeled after the Three-Layer Variable Infiltration Capacity (VIC-3L) model of Liang et al. (1994, 1996). VIC-3L divides a watershed into land cover units based on vegetation type and calculates runoff using a three-layer infiltration model. For the purpose of this modeling study, the VIC-3L model was applied to each HRU in the Río Salado basin. The components of the water balance equations for each soil layer are shown in Figure 22. Water that reaches the land surface of an HRU is able to infiltrate into all three layer of the soil, filling the column from top to bottom.

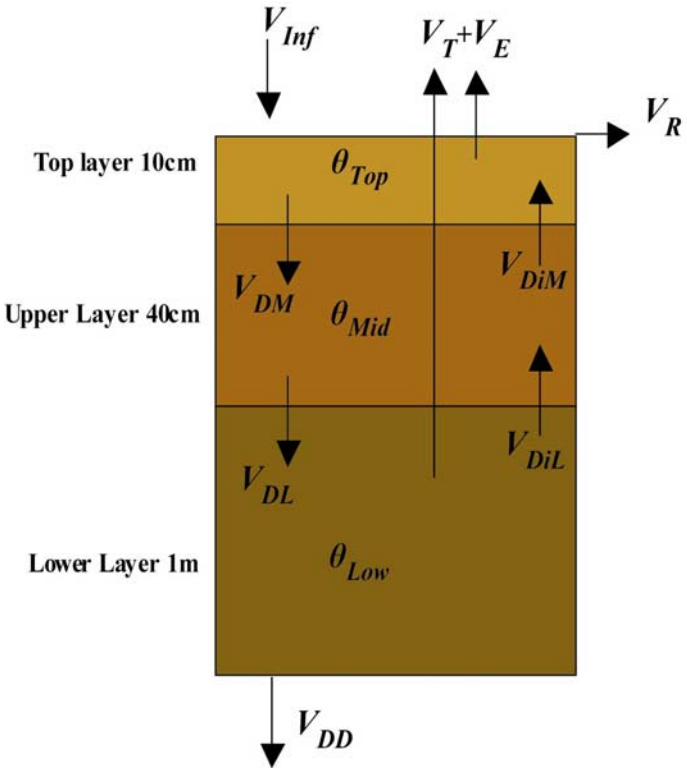

FIGURE 22: Three-layer soil column depicting flows between layers, adapted from the VIC-3L model (Liang et al., 1994, 1996). Layer thicknesses are indicated on the left hand side.

The generation of runoff for each HRU begins with the calculation of infiltration-excess runoff. If the rate that the available water infiltrates is greater than the saturated hydraulic conductivity of the soil (K_S), then infiltration-excess runoff (R_I) will occur. The rate at which infiltration-excess runoff is produced is determined by:

$$\begin{aligned} R_I &= I_{RS} - K_S \\ for\ \ I_{RS} &\geq K_S, \end{aligned} \tag{18}$$

where I_{RS} is the infiltration rate of the top layer in cm/hr and K_S is the saturated hydraulic conductivity of the soil in cm/hr. Next the VIC method is used to produce saturation-excess runoff.

The VIC method assumes that the degree of saturation over the HRU area varies spatially (Liang, 1994). To accomplish this, the water in each layer is redistributed, so that a portion of the HRU area is completely saturated, while the remaining area remains at some lower degree of saturation. The consumed infiltration capacity (i_o) of the soil column (m^3) is calculated using the variable infiltration capacity curve described as:

$$\left(1 - \frac{i_o}{i_m}\right) = \left(1 - A_{sf}\right)^{\frac{1}{b}}, \tag{19}$$

where i_o is the consumed infiltration capacity (mm), i_m is the maximum infiltration capacity (mm), A_{sf} is the fraction of the area that is saturated, and b is the saturation shape parameter (-). This equation can be solved for the infiltration capacity, i_o, or the saturated fraction, A_{sf}, as:

$$i_o = i_m \left[1 - \left(1 - A_{sf}\right)^{\frac{1}{b}}\right], \text{ or} \tag{20}$$

$$A_{sf} = 1 - \left(1 - \frac{i_o}{i_m}\right)^b. \tag{21}$$

To find the maximum infiltration capacity, i_m, we use the following expression:

$$V_m = \int_0^{i_m} \left(1 - \frac{i}{i_m}\right)^b di \ , \tag{22}$$

where V_m is the maximum water volume in the top two layers of the soil column, defined as $A\phi z_u$, where z_u is the depth of the top two layers.(see Appendix 1 for a full derivation) Using a u substitution of $u = 1 - \frac{i}{i_m}$ we arrive at:

$$V_m = i_m \int_0^{i_m} (u)^b du \ , \tag{23}$$

Integrating, resubstituting and evaluating at the limits $i = 0$ to $i = i_m$, we calculate the maximum infiltration capacity:

$$i_m = V_m (1 + b) . \tag{24}$$

Solving Equation 22 with the limits of $i = 0$ to $i = i_o$, results in the consumed infiltration capacity (i_o):

$$i_o = V_m (1 + b) \left[1 - \left(1 - \frac{V_o}{V_m} \right)^{\frac{1}{1+b}} \right], \tag{25}$$

where V_o is the current volume of water in the soil column. Subtracting i_o from i_m, we get the current infiltration capacity (i_c):

$$i_c = \left[1 - \left(1 - \frac{V_o}{V_m} \right)^{\frac{1}{1+b}} \right]. \tag{26}$$

Representing the water volumes as a difference in volumetric water contents ($V_m = (\phi - \theta_r)$, $V_o = (\theta_i - \theta_r)$), results in an expression for the current infiltration capacity in terms of soil moisture:

$$i_c = \left\{ 1 - \left[1 - \frac{\theta_i - \theta_r}{\phi - \theta_r} \right]^{\frac{1}{1+b}} \right\}, \qquad (27)$$

where ϕ is the soil porosity, θ_i is the current soil moisture (volumetric water content, m^3/m^3) and θ_r is the residual soil moisture (m^3/m^3).

As shown in Figure 23, the amount of saturation-excess runoff that is produced by an HRU, controlled by the infiltration capacity, is dependent on the amount of the HRU area that is currently saturated (A_{sf}) (Equation 21). As water is added to the soil column, increasing the current volume V_o, a new amount of consumed infiltration capacity (i_o) is calculated using Equation 25, moving i_o toward i_m. The remaining infiltration capacity is the unshaded region under the curve. Figure 23 also shows that an increase in the saturated area (A_s) will result in an increase i_o or a decrease in the infiltration capacity of the soil (Equation 20). Figure 24 shows the control of the parameter b on the shape of the infiltration capacity curve for different values (b = 0.6, 1, 1.4). b describes the distribution of storage capacity in an HRU and is set to 1.4 for this study following Liang et al., (2001). Since the VIC method accounts for the spatial variability in soil moisture, a more realistic estimate of the amount of water produced by saturation-excess runoff (R_S) is obtained using an HRU-averaged value (Liang et al., 2001). As a result, the watershed model used in this study includes both major mechanisms for runoff generation to more accurately depict the potential runoff processes in semiarid regions.

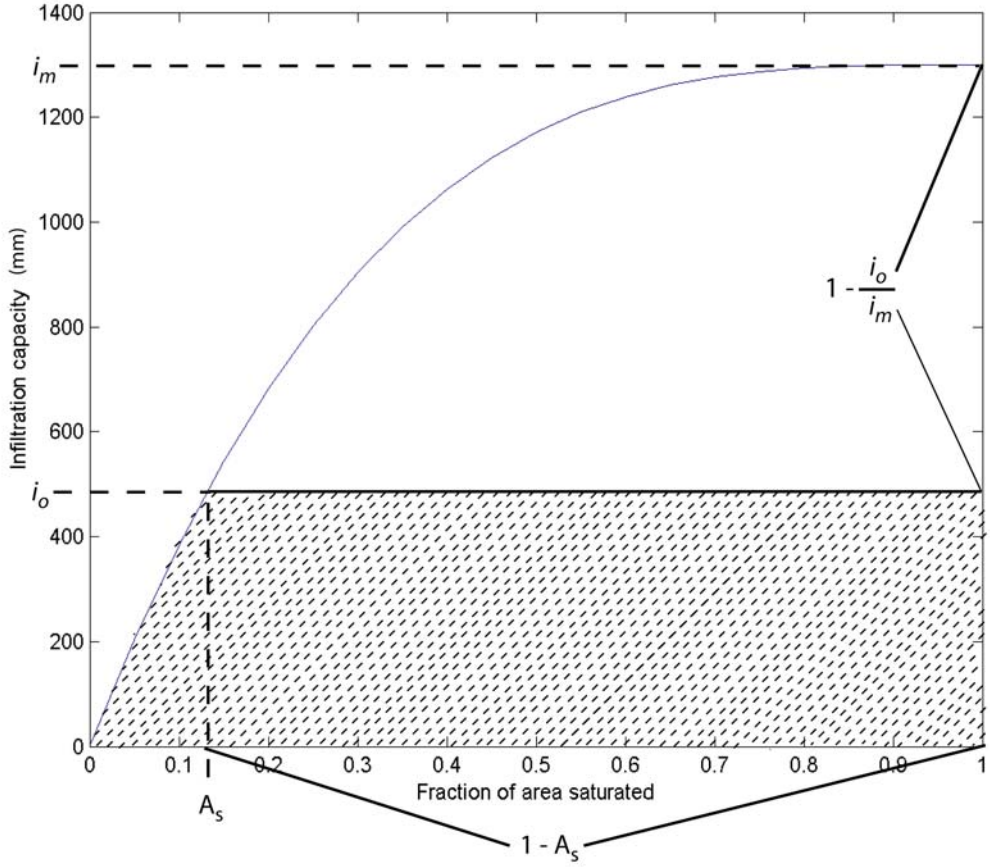

FIGURE 23: Schematic of infiltration capacity curve: i_m is the maximum infiltration capacity (mm), i_o is the current infiltration capacity (mm), and A_s is the fraction of the area that is saturated (m^2).

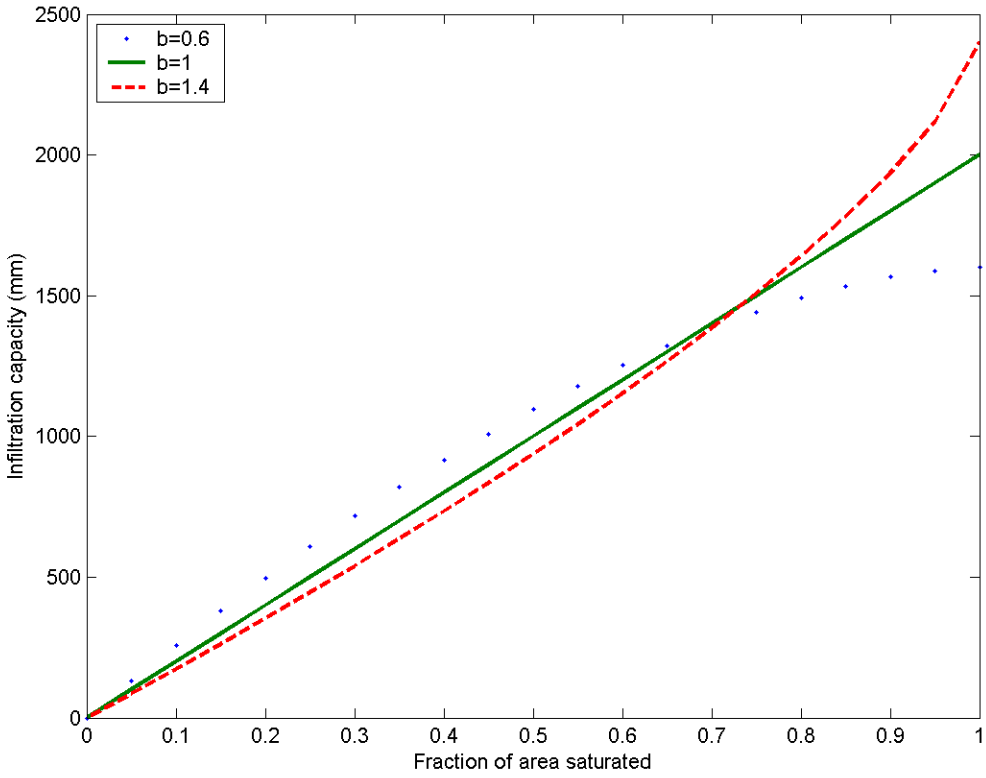

FIGURE 24: Plot showing the effect of *b* on the infiltration capacity of the soil column. Each line represents the same control volume.

In each HRU, a single soil column is divided into three layers with soil layer depths adopted from the VIC-3L model (Liang et al., 1996), which are assumed to be uniform over all HRUs. Table 6 shows the soil parameters for each soil class. Direct evaporation from the soil can occur from the top layer (10 cm) and the middle layer (40 cm). The lower layer (1 m) accounts for long-term storage of water and provides drainage to the regional aquifer. Each layer loses water to transpiration depending on the degree of saturation of the layer, the plant root distribution, and the threshold that each vegetation type transpires at.

	K_s (cm/hr)	B_P	ϕ	θ_r
Bed Rock	0.05	0.05	0.10	0.01
Sand	23.56	0.69	0.42	0.02
Loamy sand	5.98	0.55	0.40	0.04
Sandy loam	2.18	0.38	0.41	0.04
Loam	1.32	0.25	0.43	0.03
Silt loam	0.68	0.23	0.49	0.02
Clay loam	0.20	0.24	0.39	0.08
Silty clay loam	0.20	0.18	0.43	0.04

TABLE 6: Parameter values based on soil class (Rawls et al., 1993).

Movement of water between layers is calculated using a modified form of the Brooks-Corey equation (see Appendix 2 for a full derivation):

$$Q = AK_\theta, \tag{28}$$

where Q is the flow rate between layers (m^3/hr), A is the HRU area (m^2), and K_θ is unsaturated hydraulic conductivity defined as:

$$K_\theta = Bz\left(\theta_{final} - \theta_r\right)^{\frac{2}{b}+3}, \tag{29}$$

where θ_{final} is the adjusted water content at the end of a storm or interstorm period defined as:

$$\theta_{final} = \theta_r + \left\{\left[\left(\theta_i - \theta_r\right)^{(1-m_2)}\right] - \left(1-m_2\right)B\left(\Delta t\right)\right\}^{\frac{1}{(1-m_2)}}, \tag{30}$$

and B is defined as:

$$B = \frac{K_S}{z\left[(\phi - \theta_r)^{m_2}\right]}, \tag{31}$$

where K_S is the saturated hydraulic conductivity (cm/hr), θ_i is the current volumetric water content (m^3/m^3), ϕ is the porosity of the soil, z is the depth below the ground surface, Δt is the duration of the event, θ_r is the residual water content (m^3/m^3), and m_2 is defined as:

$$m_2 = \frac{2}{B_P} + 3, \tag{32}$$

where B_P is the pore size distribution index (Liang et al., 1994). For each layer, the current volumetric water content θ_i, is calculated as:

$$\theta_i = \frac{V_i}{V_T}, \tag{33}$$

where V_i is the current volume of water in the layer, and V_T is the maximum possible volume of water for the layer, defined as:

$$V_{max} = A\phi z_i, \tag{34}$$

where A is the HRU area, ϕ is the soil porosity, and z_i is the depth of the soil layer.

The water balance equation for the top layer is:

$$\frac{\Delta V_{Top}}{\Delta t} = \frac{(V_{Inf} + V_{DiM}) - (V_{E_T} + V_{T_T} + V_{DM} + V_R)}{\Delta t}, \tag{35}$$

where V_{Inf} is the volume of water that infiltrates into the top layer, V_{DiM} is the volume that diffuses into the top layer from the middle layer, V_{E_T} is the volume lost from the top layer to evaporation, V_{T_T} is the volume lost from the top layer to transpiration, V_{DM} is the volume that drains from the top layer to the middle layer, and V_R is the volume of runoff produced by each HRU (sum of R_S and R_I). All volumes are expressed in m^3.

The water balance equation for the middle layer is:

$$\frac{\Delta V_{Mid}}{\Delta t} = \frac{(V_{DM} + V_{DiL}) - (V_{T_M} + V_{DL})}{\Delta t}, \tag{36}$$

where V_{DiL} is the volume that diffuses into the middle layer from the lower layer, V_{T_M} is the volume lost from the middle layer to transpiration, and V_{DL} is the volume that drains from the middle layer to the lower layer.

The water balance equation for the lower layer is:

$$\frac{\Delta V_{Low}}{\Delta t} = \frac{V_{DL} - (V_{T_L} + V_{DD})}{\Delta t}, \tag{37}$$

where V_{T_L} is the volume lost from the lower layer to transpiration, and V_{DD} is the volume that drains from the lower layer to the regional aquifer.

As the top soil layer fills, water can either drain to the lower layers, evaporate directly from the top layer of soil, or be transpired by vegetation. Figure 25 provides a visual example of the response of the three soil layers to precipitation forcing. The top layer (Figure 25.b) shows rapid filling in line with the precipitation inputs as well as rapid drying caused by evapotranspiration, and drainage to the layers below. The middle layer (Figure 25.c) is muted in comparison to the top layer, the increases are coincident with the precipitation forcing but the moisture is able to persist beyond the initial input event. The lower layer (Figure 25.d) shows an even less pronounced response to precipitation and maintains its level of saturation over many events, resulting in long term drainage into the regional aquifer at a very low rate (Figure 25.e).

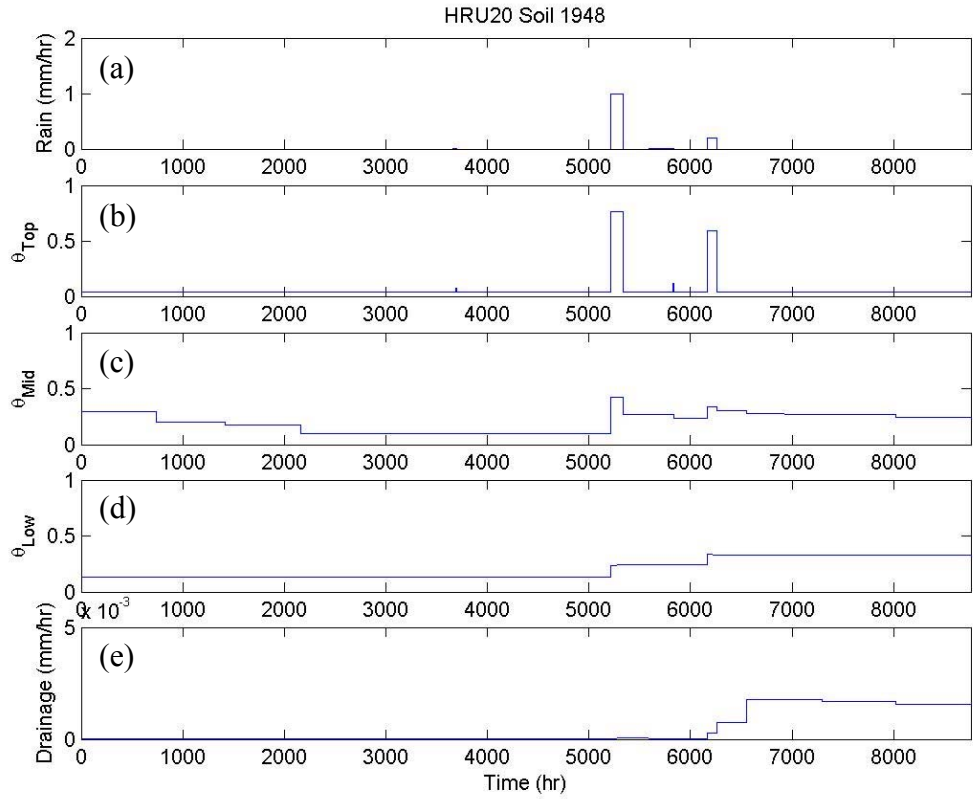

FIGURE 25: Model output of event scale soil moisture for each layer in HRU #20 for the year 1948. (a) Rainfall rate (mm/hr). (b) Volumetric water content of the top layer (m^3/m^3). (c) Volumetric water content of the middle layer (m^3/m^3). (d) Volumetric water content of the lower layer (m^3/m^3). (e) Drainage from the lower layer to the regional aquifer (mm/hr), note that the scale of the y-axis for the drainage is 0-5x10^{-3} mm/hr.

Evapotranspiration processes

Several methods exist for estimating the amount of water that is lost to evapotranspiration (ET), the combination of soil evaporation and plant transpiration. However, most methods such as the Penman-Monteith and Priestley-Taylor approaches require a great deal of atmospheric data (e.g. air temperature, vapor pressure, wind speed, and radiation). To simplify the model and reduce the data requirements, the temperature-based Hargreaves evapotranspiration model was implemented. This method provides a reasonable estimate of the potential evapotranspiration (E_H) for each HRU (Shuttleworth, 1993). The Hargreaves equation is defined as:

$$E_H = 0.0023\left[S_o\left(T+17.8\right)\right]T_R^{\frac{1}{2}}, \qquad (38)$$

where E_H is based on the amount of incoming solar radiation (S_o) (mm/day) and monthly air temperature values (Hargreaves 1975; Hargreaves et al., 1985; Hargreaves et al., 2003). For the purpose of this study temperatures used in calculating the potential ET are sampled monthly from an exponential distribution. Thus T is the mean air temperature (^oC), and T_R is the difference between the monthly minimum and monthly maximum air temperatures (^oC) defined as:

$$T_R = T_{max} - T_{min}. \tag{39}$$

The amount of incoming solar radiation that reaches the land surface and is thus available for evaporation is estimated using the method described by Shuttleworth (1993):

$$S_o = 15.392\left\{d_r\left[\omega_S \sin(\phi)\sin(\delta) + \cos(\phi)\cos(\delta)\sin(\omega_S)\right]\right\}, \tag{40}$$

where d_r is the relative distance between the Earth and the Sun, ω_S is the sunset hour angle (radians), ϕ is the latitude of the study area (radians), δ is the solar declination angle (radians). The following equations describe the computation of the solar radiation factors:

$$d_r = 1 + 0.033\cos\left(\frac{2\pi}{365}J\right), \tag{41}$$

$$\omega_S = \arccos(-\tan(\phi)\tan(\delta)), \quad \text{and} \tag{42}$$

$$\delta = 0.4093\sin\left(\frac{2\pi}{365}J - 1.405\right), \tag{43}$$

where and J is the Julian day. We set J to the 15th day of each month to simulate the average monthly ET.

The actual ET for each HRU is limited by the water available in the soil and by the ability of the vegetation to remove that water from the lower soil layers. Actual evaporation from the top layer (E_a) occurs at a reduced rate for unsaturated soils as:

$$E_a = ET_p A_s + ET_p \left(A - A_s\right)\left(\frac{\theta_i - \theta_r}{\theta_s - \theta_r}\right), \tag{44}$$

where ET_p is the Hargreaves potential ET (E_H), A is the total HRU area, A_s is the saturated area, θ_i is the current water content, θ_r is the residual water content, and θ_s is the water content at which the soil is considered saturated. Following the method of Salvucci (1997), the value of E_a is reduced to E_R when the interstorm period is greater than two days, shown by:

$$E_R = \frac{\left(E_a + ET_2\right)}{2} \quad , \quad if \quad T > 48hrs \tag{45}$$

where ET_2 is defined as:

$$ET_2 = 0.811 E_a \left(\frac{48}{T}\right). \tag{46}$$

where E_a is the ET without the two day reduction, and T is the current interstorm duration. This reduction is implemented because, as the soil dries, E_a is controlled by the rate at which the soil can conduct water to the surface.

The volume that is transpired from the lower layers is controlled by the rooting depth of the plants and the degree of saturation in the soil. To further simulate the effects of dry soils, the transpiration rate is also reduced for long interstorm periods (>2 days). The seasonal changes in monthly potential ET generated using the parameters from the Augustine gauge, showing high potential ET in the summer and lower potential ET in the winter, are shown in Figure 26. A comparison of the potential and actual ET for HRU #20, calculated using stochastic temperature values for each event, can be seen in Figure 27. A lack of available water in the soil causes the actual ET for each event to be much smaller than the potential ET. ET calculations are only performed during the interstorm periods.

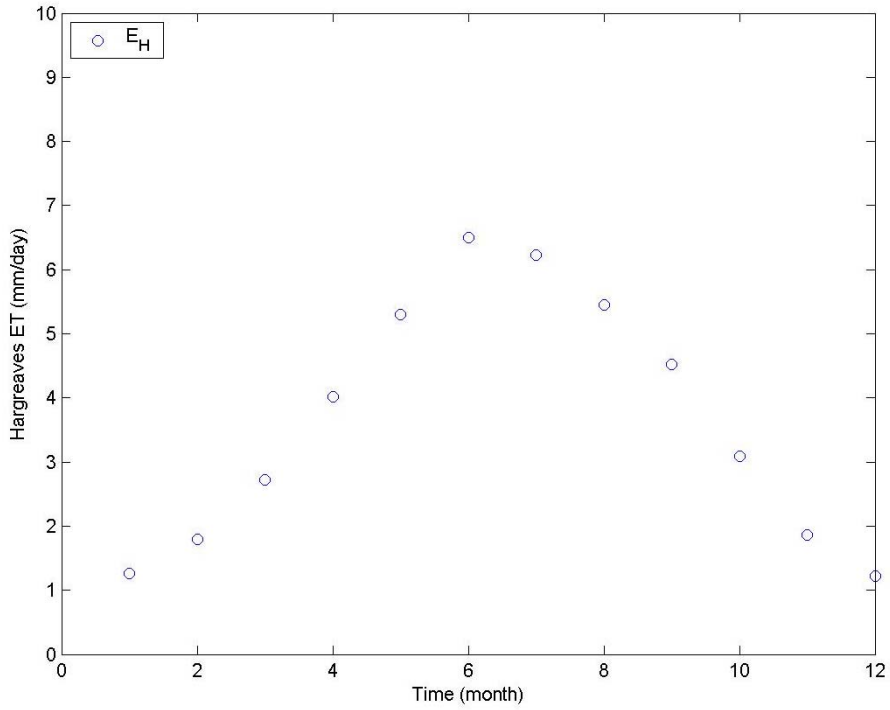

FIGURE 26: Monthly potential ET for Augustine gauge.

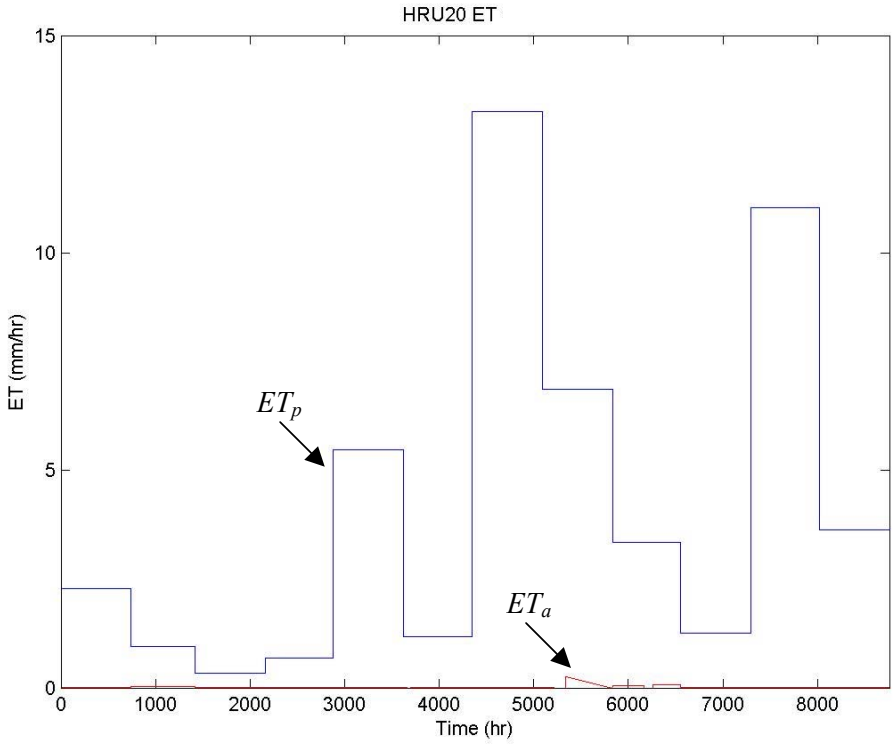

FIGURE 27: Comparison of potential ET (black) and actual ET (red) for HRU #20 for a representative year.

Routing processes

Water is routed to the basin outlet using simple hydrologic routing along the different flow-paths computed from the DEM (Figure 28). To reduce computations, the average flow distance for each HRU is used to route the water. The residence time of water in the channel (t_c) is defined as:

$$t_c = \left(\frac{L_{Out}}{V} \right) \tag{47}$$

where L_{Out} is the average distance to the outlet for each HRU, and V is the average flow velocity, set to 0.5 m/s for this study. This mimics the average residence time in the surface streams that link each HRU to the basin outlet. The channel bed is treated as a soil with variable properties and the volume of water lost within the channel (V_{Loss}) is calculated as:

$$V_{Loss} = K_S t_C L_{Out} c_W \, , \tag{48}$$

where K_S is the saturated hydraulic conductivity, and c_W is the average channel width, set to 5 m. This simple calculation assumes independent flow paths from each HRU to the outlet. Realistically the flow paths from different HRUs merge along the main stem of the Río Salado. This simplification may lead to overestimates of channel losses, but allows channel routing to be handled in a parsimonious fashion for the semi distributed watershed model. Figure 29 shows the distribution of residence times for runoff routed from every HRU in the Río Salado to the basin outlet. It is important to note that all of the water will exit the basin in under 90 hours (3.75 days), indicating that monthly total runoff volumes may account for multiple events. The variability of the routing times shown in Figure 29 causes the model to behave more realistically at sub-monthly time scales than if all HRUs delivered runoff to the basin outlet at the same time.

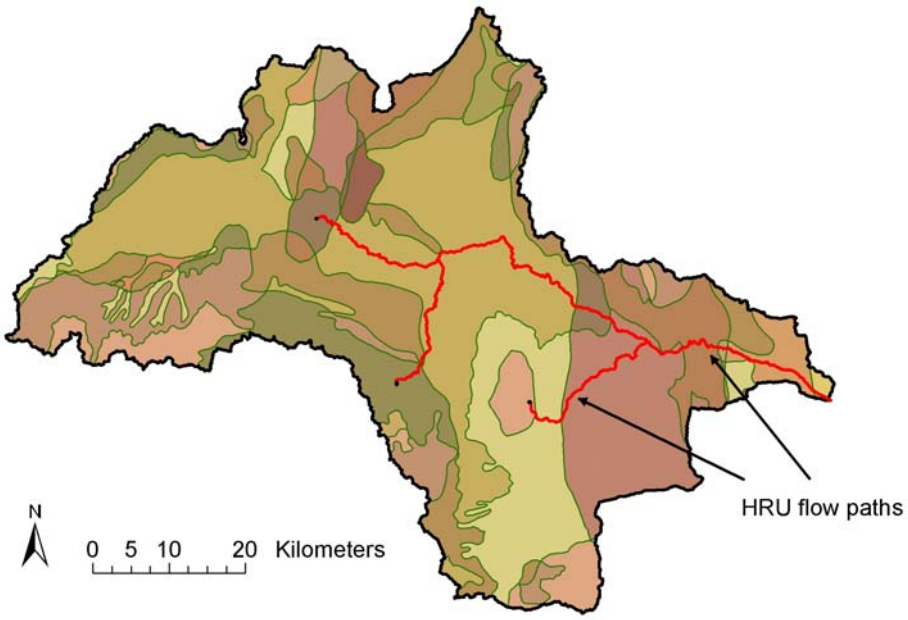

FIGURE 28: Examples of possible flow paths for three different HRUs in the Río Salado basin.

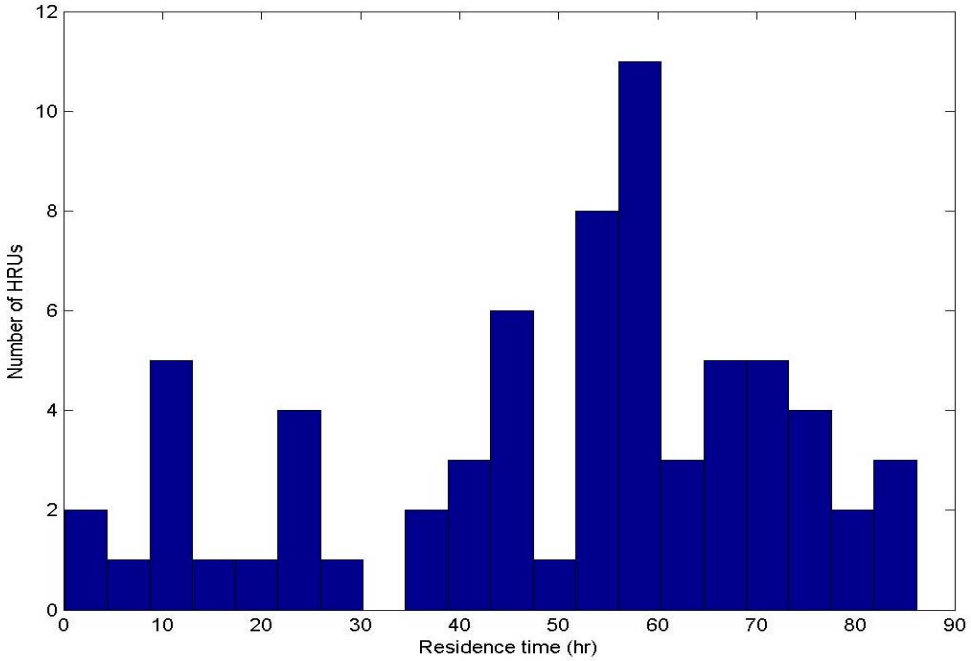

FIGURE 29: Histogram of residence times for HRUs in the Río Salado basin.

Summary

This concludes the description of the model development, which has included a detailed explanation of the hydrologic processes used in the watershed model. The description has focused on the aspects of the water balance necessary to transform precipitation into runoff (e.g. interception, evapotranspiration, and infiltration). The following chapter will present the model results at different spatial and temporal scales, compare the model results to historical observations, and test the sensitivity of the model to changes in both climate forcing and parameter values.

RESULTS

Introduction

In this chapter we describe the watershed model results at different spatial and temporal scales for applications in central New Mexico. We begin by comparing modeled soil moisture values for the top two soil layers to measurements from the Deep Well site in the Sevilleta National Wildlife Refuge to build confidence in the model physics. In the following section, we examine storm event scale results for individual HRUs, in order to compare the effects of soil and vegetation properties on runoff generation during wet and dry periods. Subsequently, we increase the spatial scale to encompass the entire Río Salado basin at the monthly timescale over a long (~60-yr) sequence of different years. At the monthly scale, we compare modeled basin runoff to the historical streamflow measurements at the Río Salado gauge. In the final section, the sensitivity of the watershed model to different climate forcing is tested. This is carried out using a range of different stochastic precipitation scenarios in order to capture the potential effects of climate variations on the semiarid basin response.

Comparison of model simulations at the point scale

To build confidence in the abilities of the watershed model, we first examine the model behavior at the point scale. This is accomplished by comparing observed data from three soil pits at the Deep Well site in the Sevilleta National Wildlife Refuge (Moore, TDR-1996-2001). Soil and vegetation properties for the Deep Well site are derived from the site description included with the Time-Domain Reflectometry (TDR) and meteorological (MET) datasets. Deep Well is treated as a sandy soil for the first 10 cm and as a sandy-loam soil for the remaining 1.4 meters, and is overlain by a mixture of shrubs and grasses. We do not attempt to explicitly capture the

potential impact of the calcium carbonate (caliche) layer on the soil hydraulic properties at the site. The focus of the point scale study is to inspect the simulated values of soil water content for the top and middle layers in the model and compare it to conditions observed in the field, averaged over the three soil pits.

We used the average soil moisture values from three different sensors installed at similar depths, but placed 1 to 5 meters apart, to account for potential variations at the point scale among the sampling sites (e.g. microtopography or vegetation differences between sites). For the purpose of the point scale tests, the interception of water by plants was not considered since the Deep Well site is a sparse grassland/shrubland site with open bare soil patches. Additionally, the depth of the middle layer in the model was modified to 10-40 cm from 10-50 cm to improve the correspondence with the observation depths.

The wettest (1997 with 325 mm of total rainfall) and driest (2001 with 214 mm of total rainfall) years of the record were selected from a six-year dataset at the Deep Well site collected by the Sevilleta Long-Term Ecological Research program (Moore, MET-1996-2001). In order to account for initialization effects, the model was run for a 10-year spin-up created by duplicating each of the selected historical years. The first ten years are used to bring the model to a quasi-steady state in terms of the soil moisture values for the three layers, and the water content results from the eleventh year (after the model spin-up time) are compared to the Deep Well data. We use these same two years (1997 and 2001) for subsequent runs performed at the HRU scale.

Figure 30 shows that the modeled water content of the top layer (0-10 cm) falls within two standard deviations of the mean values calculated over the three sensors in the Deep Well dataset. The model performs well in simulating soil moisture in both the wet and dry years with a

few differences that may be caused by variations in soil properties between the sampling locations and the model. We are encouraged by the model's capability for capturing both the timing and magnitude of the soil moisture pulses, and believe that event-based time step in our model results in the differences that occur while drying. Comparisons of the middle layer (10-40 cm), shown in Figure 31, exhibit a similar behavior as the top layer, albeit with a less flashy response to precipitation inputs. The initial conditions induced by the spin up period provide a better fit for the 1997 dataset as compared to the 2001 dataset. However, in the latter part of each year, as more precipitation is input, the model is able to match the measured conditions. In each year, there are instances where the model simulates the actual soil water content within two standard deviations.

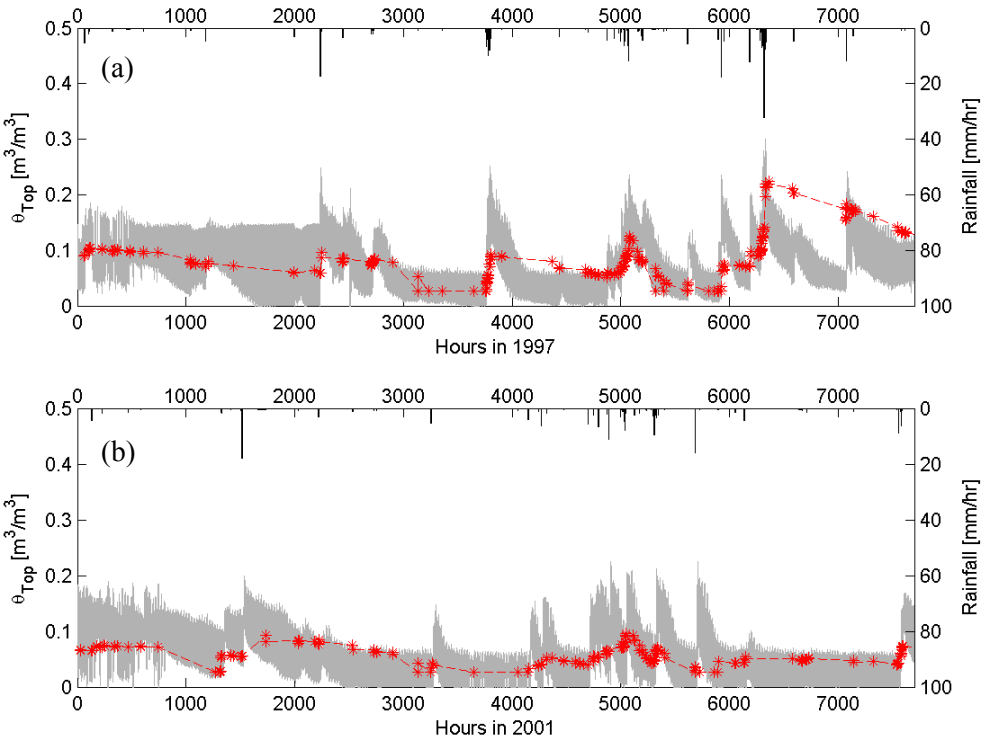

FIGURE 30: Comparison of volumetric water content for the top soil layer (0-10 cm). Model results are shown in red, with the gray shaded area representing the actual data from the Deep Well site (at 5 cm depth), depicted as ±2 standard deviations. Results are shown for a (a) wet year (1997) and (b) dry year (2001).

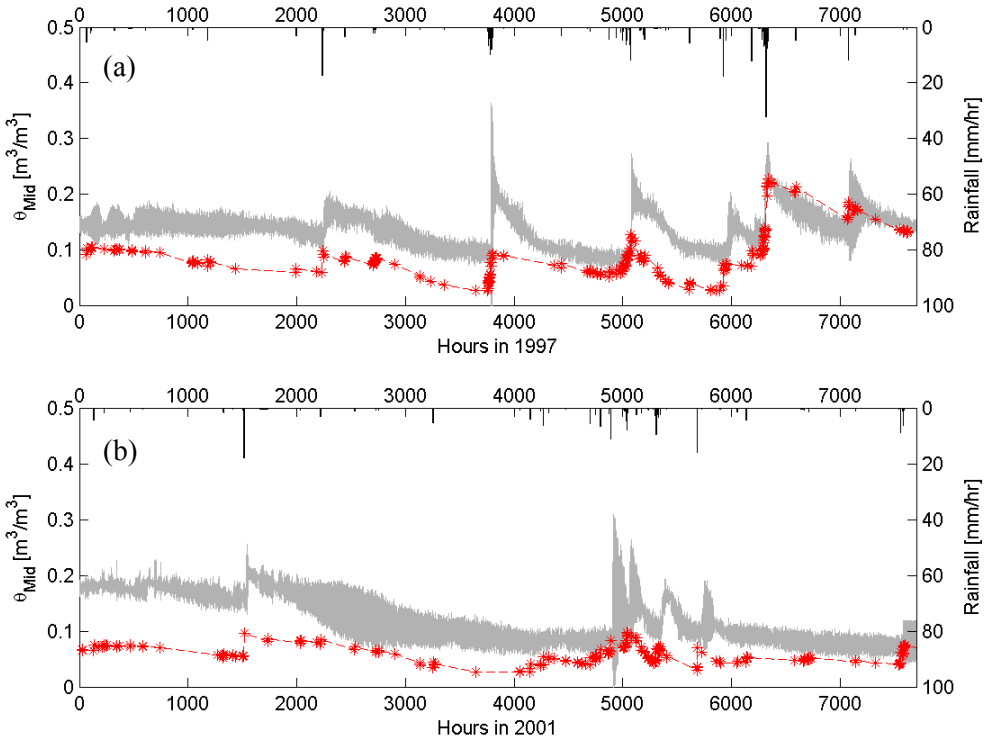

FIGURE 31: Comparison of volumetric water content for the middle soil layer (10-40 cm) from field observations and model simulations. Model results are shown in red, with the gray shaded area representing the actual data from the Deep Well site (at 20 cm depth), depicted as ±2 standard deviations. Results are shown for a (a) wet year (1997) and (b) dry year (2001).

Additionally, the model structure required to improve the basin-scale results, including evaporation from the middle layer, may cause excessive drying at the point scale for the middle layer. The mean volumetric water content values for 1997 and 2001, observed and modeled, are shown in Table 7 for each layer. A comparison of the lower layer was not included because there are no actual measurements at a depth that corresponded with the lower layer.

Year	θ_{top} modeled	θ_{top} observed	θ_{mid} modeled	θ_{mid} observed
1997	0.09	0.14	0.09	0.12
2001	0.05	0.13	0.06	0.10

TABLE 7: Mean volumetric soil moisture values, modeled and observed, for years 1997 and 2001.

Comparison of model simulations at the HRU scale

This section examines how soil and vegetation properties control the hydrologic dynamics of the canopy layer and soil column. Two representative HRUs in the Río Salado were selected (Forest–Sand and Grass-Clay loam), based on the large differences in the combined soil and vegetation parameter values associated with each. The differences in hydrologic dynamics for each HRU over the wet (1997) and dry (2001) years demonstrate the importance of vegetation and soil parameters in controlling the response to precipitation forcing.

We begin our comparison of the HRU hydrologic response by inspecting the canopy dynamics of a forest and a grassland over the same two time periods used for the point scale comparison. The forest canopy (Figure 32, left column) is able to capture a large amount of the rainfall, as shown by the high interception rates in Figure 32.b, which have the same temporal distribution as the rainfall events. This leads to high water, storage in the canopy with a maximum storage depth of approximately 20 mm shown in Figure 32.c lasting 54 hrs, from hours 6312 to 6366. The canopy evaporation removes all the available water from storage leaving the canopy dry at the end of long interstorm events. The lack of drainage from the canopy (Figure 32.d) is due to the large canopy interception capacity depth (I_{CMax}) of the forest (27 mm), which allows the forest to capture and store all but the largest rainfall events in the record. It is important to note that free throughfall, defined as water that bypasses the canopy and goes directly to the ground surface (not shown), is the difference between the rainfall and interception rates.

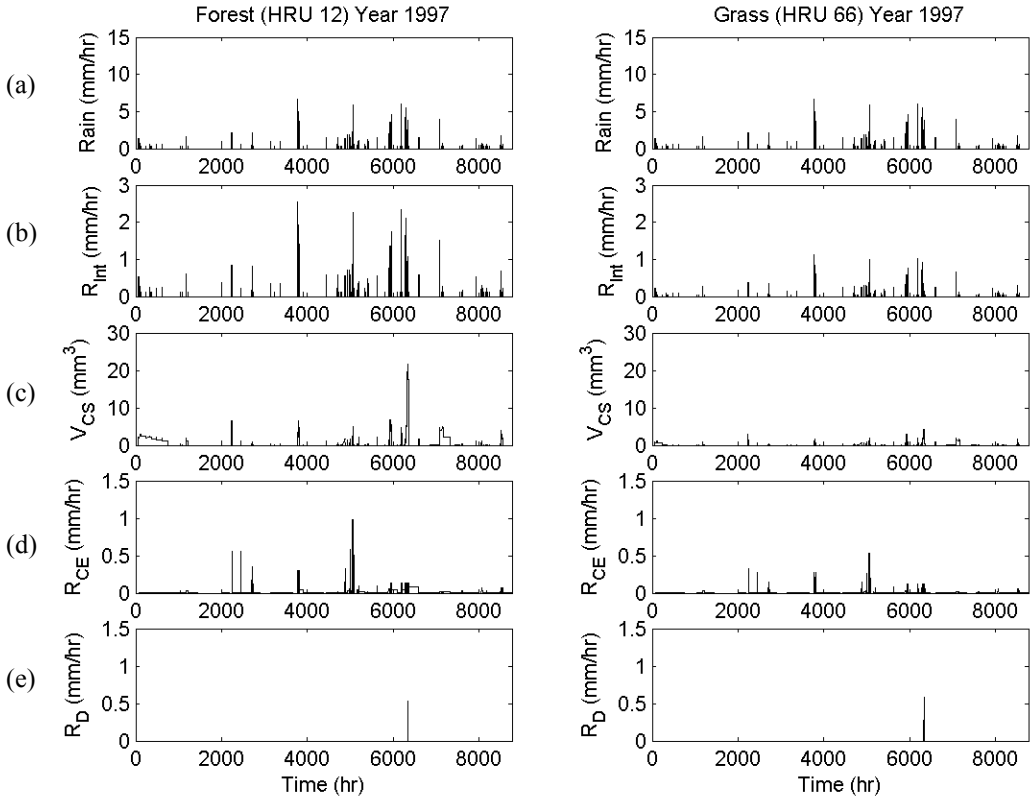

FIGURE 32: Comparison of canopy interception dynamics for a forest (HRU 12) and grassland (HRU 66) for 1997, the wettest year of the dataset. (a) Rainfall time series, (b) Canopy interception rates (R_{Int}), (c) Canopy storage (V_{CS}), (d) Evaporation rates from the canopy (R_{CE}), and (e) Drainage from the canopy to the ground surface (R_D).

Similar dynamics are observed for the grass HRU (Figure 32, right column). Interception again follows the pattern of the rainfall events although at lower rates (Figure 32.b). Less water is captured by the grass, causing the depth of water stored in the canopy to be lower than in the forest (Figure 32.c). As in the case of the forest, any water put into storage is lost to canopy evaporation (Figure 32.d), and there is drainage near hour 6000 as the canopy storage volume of the grass (5.7 mm) is exceeded. The results presented in Figure 32 imply that the model is able to capture the anticipated differences in interception dynamics for varying land cover types.

Figure 33 examines forest and grassland canopy dynamics over the span of a dry year (2001). In contrast to the nearly three months of low intensity storms (~5 mm/hr) in 1997, the rainfall time

series in 2001 is dominated by a pronounced monsoon season (July/August) with maximum rainfall rates exceeding 10 mm/hr. Only small amounts of rainfall are observed during the rest of the year (Figure 33.a). The interception in the canopy for the dry year behaves in the same fashion as for the wet year, capturing a percentage of the rainfall and storing it in the canopy (Figure 33.b). It is interesting to note that even in the very large intensity storm near hour 5000, the canopy is not filled to capacity. This is primarily due to the short duration of the storm (1 hour) and the long inter-storm periods before and after the event (12 hours and 119 hours, respectively). Figures 33.d and Figure 33.e indicate that all of the water that is intercepted is eventually lost to evaporation and that no drainage from the canopy occurs. This clearly shows that the model captures the differences in canopy dynamics of the forest and grassland.

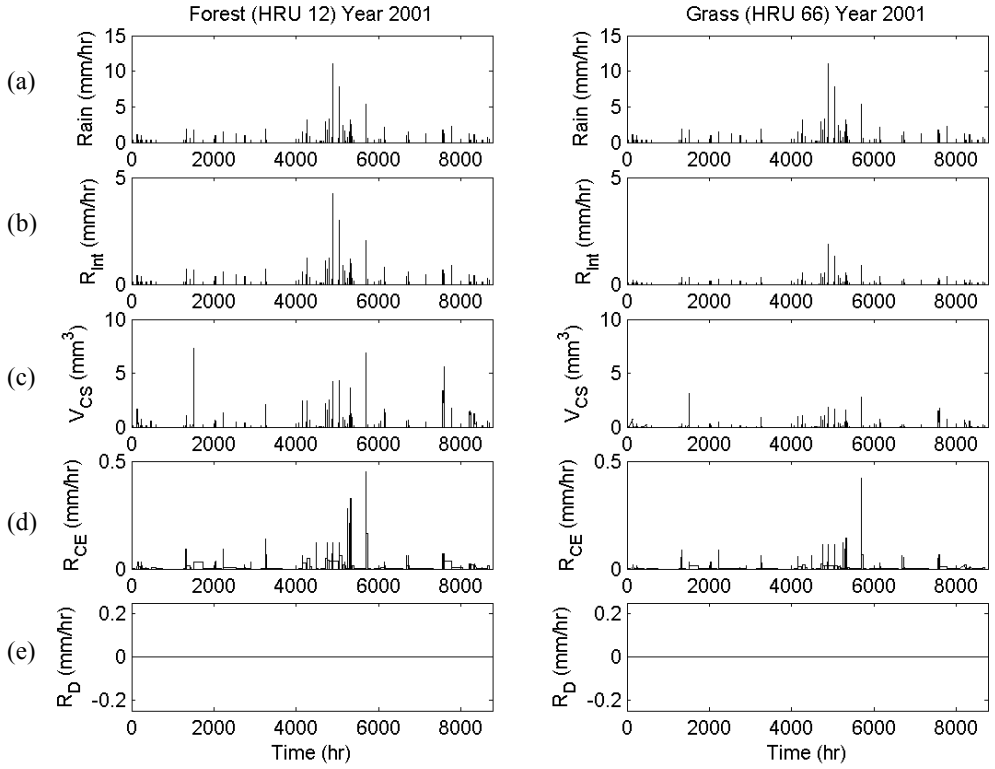

FIGURE 33: Comparison of canopy interception dynamics for a forest (HRU 12) and grassland (HRU 66) for 2001, the driest year of the dataset. (a) Rainfall time series, (b) Canopy interception rates (R_{Int}), (c) Canopy storage (V_{CS}), (d) Evaporation rates from the canopy (R_{CE}), and (e) Drainage from the canopy to the ground surface (R_D).

To illustrate the effect of soil and vegetation properties on the HRU dynamics, we inspect the soil moisture conditions in the three-layer soil column used in the watershed model. As stated previously, we are examining two HRUs found in the Río Salado: (1) a forested, sandy soil and (2) a grass covered, clay loam soil. The rainfall time series for each year are shown to provide a reference for the timing of storm and interstorm events. Recall that free throughfall (un-intercepted rainfall), drainage from the canopy, and snow melt waters are applied to the soil surface. We begin with a discussion of the sandy soil dynamics (Figure 34, left column) and subsequently compare these to the clay loam soil dynamics (Figure 34, right column). The high hydraulic conductivity (23.56 cm/hr) of the sandy soil enables the top layer (0-10 cm) to fill and drain quickly in response to inputs from storm events (Figure 34.b). The middle layer shows a more muted response to rainfall inputs and is able to store water through long interstorm periods, as seen after the concentrated events after hour 6000. The middle layer is more isolated from the atmosphere, and loses water slower due to drainage to the lower layer and through evaporation and transpiration losses (Figure 34.c). The lower layer, shown in Figure 34.d, is influenced slightly by the precipitation that reaches the ground surface, and remains very close to the residual water content value of 0.03 m^3/m^3. While the water content of the lower layer is primarily controlled by drainage to the regional aquifer, the drainage rate is very small (Figure 34.e). The water content of the lower layer is also dependent on the antecedent moisture conditions from the preceding year. The clay loam soil (Figure 34, right column) exhibits significantly different soil-moisture dynamics in response to the rainfall inputs. Note that this soil type receives slightly greater water inputs, as the interception rate of the grassland is lower than that of the forest. The lower hydraulic conductivity of the clay loam (0.20 cm/hr) reduces the soils ability to move water to the lower layers causing increases in the water content of the top

layer (Figure 34.b). Due to its hydraulic properties, the clay loam is more sensitive to the initial conditions of the model, causing the middle and lower layers to remain wetter than the sandy soil (Figure 34.c,d). Drainage occurs from the lower layer in the clay loam soil at a higher rate than in the sand due to the wetter conditions of the soil (Figure 34.e). Having described the soil dynamics of the wet year (1997), we now proceed to examine the behavior of these soils during the drier and more monsoonal year (2001).

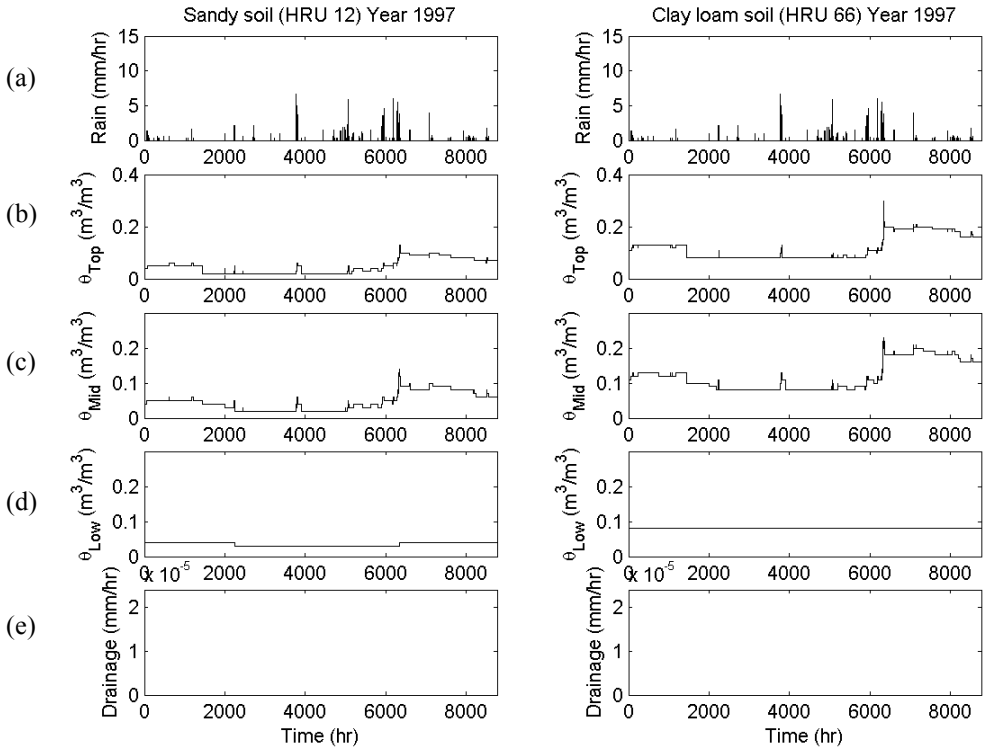

FIGURE 34: Comparison of soil moisture dynamics for a sandy soil (HRU 12) and a clay loam soil (HRU 66) for 1997, the wettest year of the dataset. (a) Rainfall time series. Volumetric water contents of the (b) top layer (θ_{Top}) (10 cm), (c) middle layer (θ_{Mid}) (40 cm), and (d) lower layer (θ_{Low}) (100 cm), as well as (e) the drainage to the regional aquifer.

When comparing the soil column response for each HRU, one notices similarities among the different years. For example, the sandy soil exhibits a quick response to precipitation inputs in the top layer and increasingly muted responses deeper into the soil column (Figure 35, left column). The lower layers of the clay loam are insulated from the effects of precipitation and

evapotranspiration, due to the low conductivity of the soil (Figure 35, right column). The high initial water content of the lower layer controls the state of the middle and lower layers in the clay loam. Next we will examine components of the water balance at the HRU scale to provide a link to the basin scale results that will be presented in the following section.

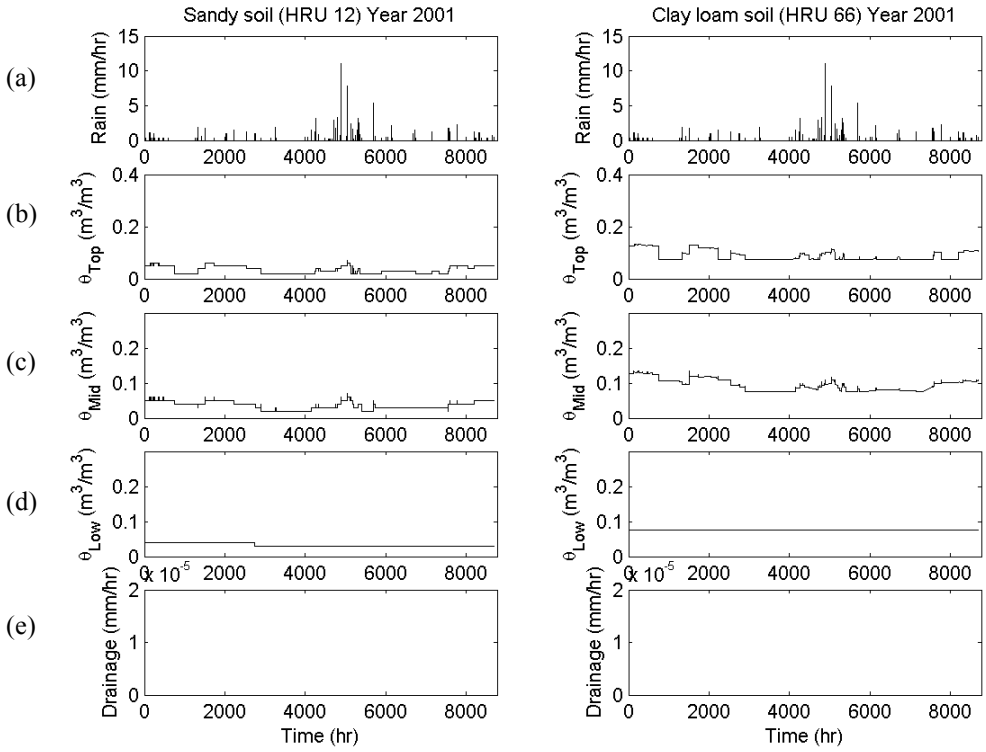

FIGURE 35: Comparison of soil moisture dynamics for a sandy soil (HRU 12) and a clay loam soil (HRU 66) for 2001, the driest year of the dataset. (a) Rainfall time series. Volumetric water contents of the (b) top layer (θ_{Top}) (10 cm), (c) middle layer (θ_{Mid}) (40 cm), and (d) lower layer (θ_{Low}) (100 cm), as well as (e) drainage to the regional aquifer.

We begin our discussion of the water balance by examining the two HRUs for the wet year (1997) in Figure 36. The volume of water lost to ET in the sandy soil is generally greater than in the clay loam soil (Figure 36.b). This is due to the clay loam's increased ability to retain water (e.g. higher residual water content and wilting point water content). However, the pattern of the ET during the year is similar for both HRUs. The high hydraulic conductivity of the sandy soil results in negligible runoff, while the clay loam produces runoff on several occasions throughout

the year, typically during the summer (Figure 36.c). Figures 36.d and 36.e illustrate that all of the runoff for clay loam soil is in the form of infiltration-excess runoff as the soils do not remain saturated long enough to generate saturation-excess runoff. Note that infiltration-excess runoff only occurs during periods of high rainfall intensity.

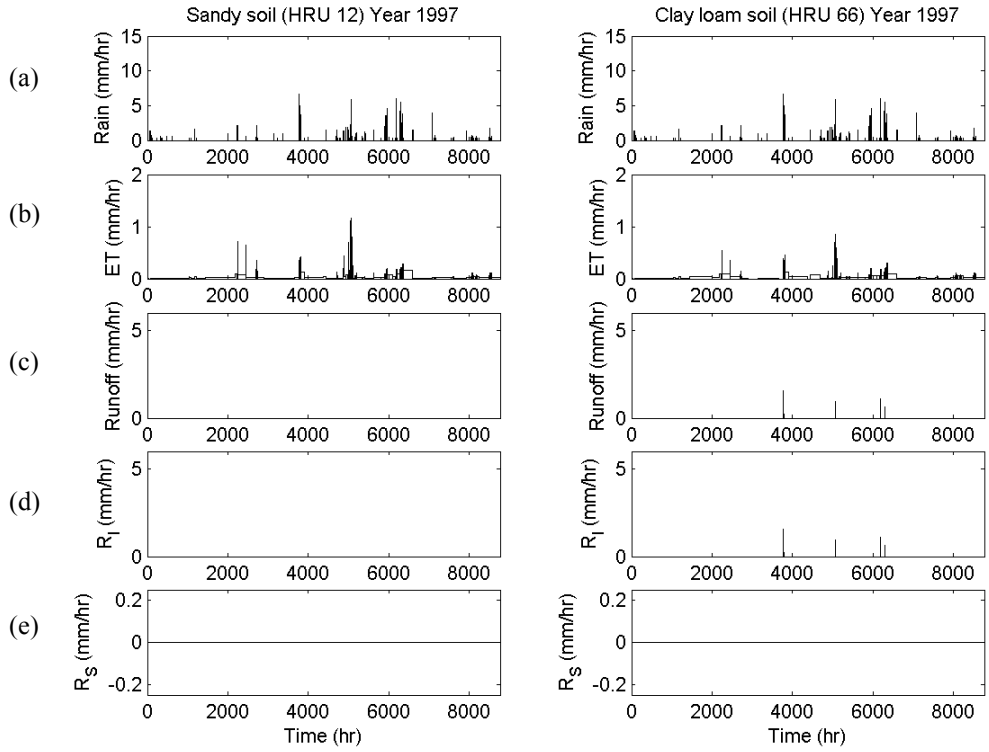

FIGURE 36: Comparison of water balance dynamics for a sandy soil (HRU 12) and a clay loam soil (HRU 66) for 1997. Depicting volumetric time series of (a) rainfall, (b) evapotranspiration, (c) total runoff, (d) infiltration-excess runoff (R_I), and (e) saturation-excess runoff (R_S).

Figure 37 presents the water balance dynamics for the two HRUs during the dry year (2001). Again, the volume of water lost to ET in the sandy soil is greater than in the clay loam soil (Figure 37.b), and the temporal patterns remain similar in the two HRUs Note how the stronger seasonality in rainfall during 2001 (as compared to 1997) induces a seasonal pattern in ET with higher values during the summer monsoon period. Runoff is produced only in the clay loam soil, and it remains in the form of infiltration-excess runoff (Figures 37.d). Clearly, the runoff

production occurred in the summer period and was more intense in 2001 (dry year) as compared to 1996 (wet year). This illustrates how the watershed model as applied to the HRU scale captures the nonlinear behavior in the rainfall runoff transformation.

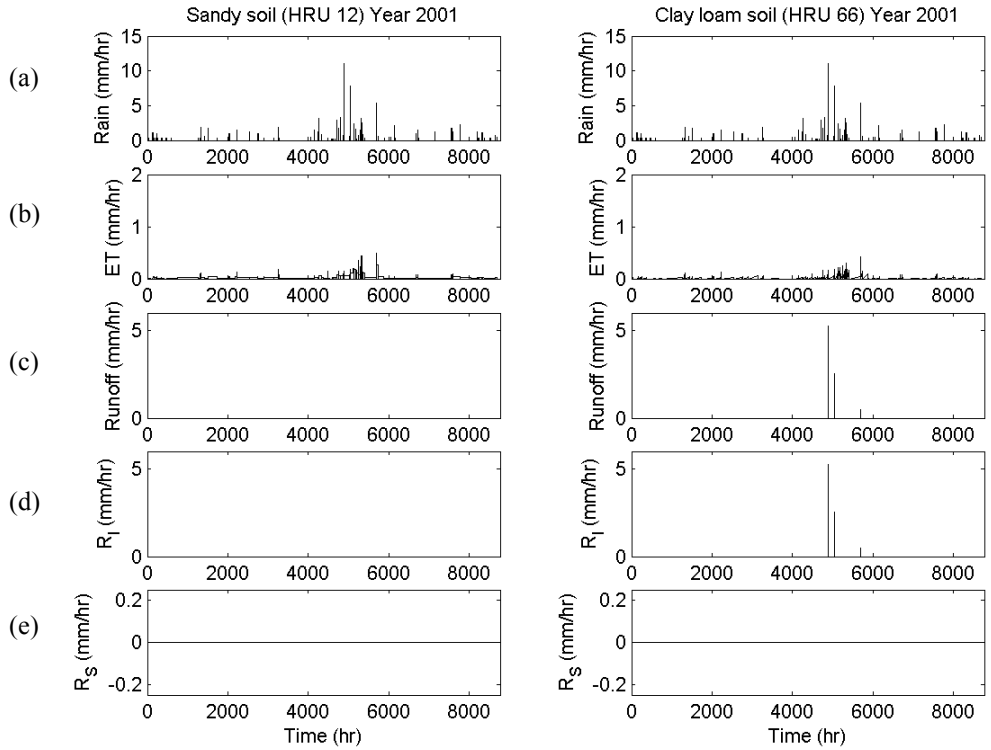

FIGURE 37: Comparison of water balance dynamics for a sandy soil (HRU 12) and a clay loam soil (HRU 66) for 2001. Depicting volumetric time series of (a) rainfall, (b) evapotranspiration, (c) total runoff, (d) infiltration-excess runoff (R_I), and (e) saturation-excess runoff (R_S).

This concludes the HRU scale results and shows that the model is able to capture differences in output caused by soil and vegetation properties at varying time intervals (e.g. dry and wet years). In the next section, we will compare model results at the basin scale to historical data from the Río Salado stream gauge located near the outlet.

Comparison of model simulations at the basin scale to historical data

In this section, we compare the model simulations at the basin scale to stream gauge measurements at the outlet of the Río Salado over the period 1949-1978. This period was

selected based upon the availability of streamflow measurements (1948-1984) and the limitations of the precision of rain gauge forcing after 1978. We begin with a comparison of the total streamflow volume (km^3) at the basin outlet for the period of record using different rain gauge data. Next, we inspect the total streamflow volume for each year in the time series to examine the inter-annual variability induced by precipitation. Finally, we inspect the mean monthly streamflow volumes in order to compare observed and simulated seasonal patterns in the regional basin response (e.g. summer monsoon streamflow versus winter runoff events).

To compare total streamflow volumes in the record, the Río Salado basin was forced with spatially uniform rainfall from three different rain gauges (Augustine, Laguna, Socorro). These rain gauges were selected since the individual record lengths overlapped with the historical streamflow observations. No other rainfall observations are available from this historical period, limiting our ability to provide distributed rainfall forcing in the watershed model. The rainfall amounts at these sites should underestimate the total rainfall in the basin, as they are located in the lower elevations of the region. For example, Figure 14 indicates that while the mean rainfall intensities for the Brushy Mountain and Datil rain gauges, located at higher elevations, are similar to the other gauges, the interstorm periods are significantly shorter. This suggests that the lack of data from the rain gauges located in the basin headwaters (Brushy Mountain and Datil) will lead to an underestimation of rainfall inputs during the historical period when forcing the model with data from Augustine, Laguna or Socorro.

Figure 38 shows the total streamflow volume obtained from simulations using each rain gauge forcing uniformly over the entire basin. Clearly, running the model using the three rain gauges results in an underestimation of the total streamflow volume produced in the basin when

compared to historical data. We believe this is primarily due to an underestimation of rainfall in the upper parts of the basin, where we lack observation data. In order to achieve a cumulative streamflow volume of 12.96 km^3 observed in the historical data, while maintaining an annual runoff ratio of 15% (a reasonable approximation for semiarid environments), a cumulative precipitation volume equal to 86.39 km^3 is needed. The total volume of precipitation captured at the Augustine, Laguna or Socorro rain gauges over the study period (1949-1978) are 21.60 km^3, 21.18 km^3, and 21.24 km^3, respectively and assumed uniform over the basin. This reinforces the idea that these lower elevation rain gauges underestimate the volume of precipitation falling on the Río Salado basin by 75.0%, 75.5% and 75.4%, respectively. This leads us to believe that a large percentage of the precipitation within the Río Salado falls in the upper elevation headwaters. Because of the lack of data from these locations we are unable to precisely compare the model results to the historical data. Introducing channel transmission losses further reduces the modeled streamflow volumes reaching the basin outlet. The modeled streamflow after imposing transmission losses from a loamy sand bed is approximately 30% of the total streamflow volume.

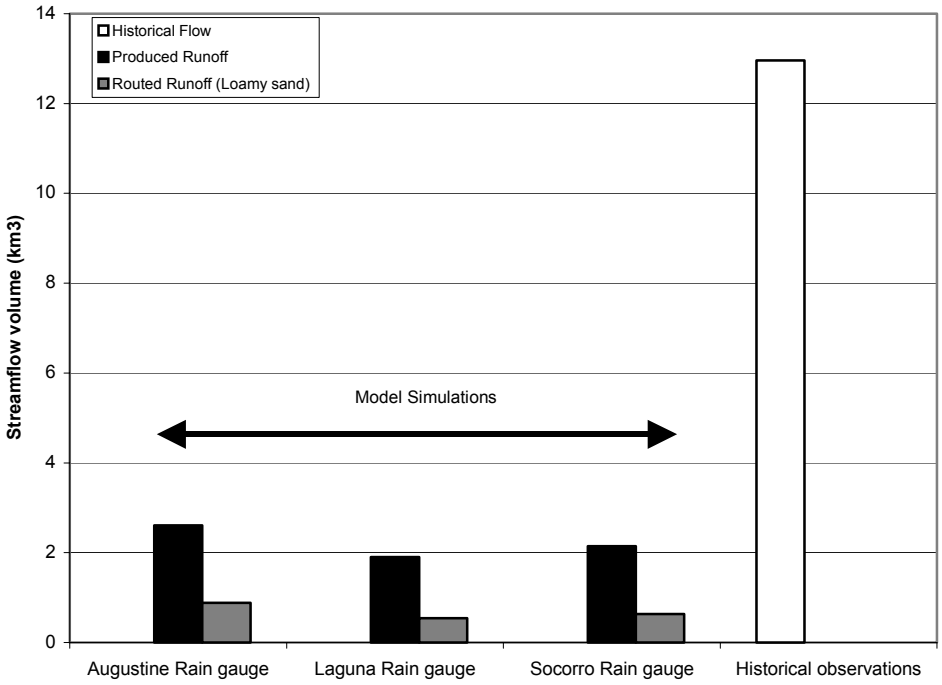

FIGURE 38: Cumulative streamflow volumes for the Río Salado basin from the historical stream gauge observations and model simulations generated using uniform rainfall forcing from the various rain gauges over the period 1949-1978. Produced runoff indicates total streamflow without considering transmission losses in the Río Salado. Routed runoff represents streamflow volumes after applying the channel losses for a loamy sand bed.

Inter-annual variability of tributary runoff is important for determining water resource availability in main stem rivers of the Southwestern United States (Grimm et al., 1997, Molles and Dahm, 1992). Periods with multiple high-flow years allow for the storage of water in reservoirs, such as Elephant Butte, while extended low-flow periods may signify regional drought conditions (Ellis et al., 1993). Figure 39.a shows the cumulative annual streamflow simulated by the watershed model in the Río Salado when forced with rainfall data from the Socorro rain gauge. Recall that these model simulations should yield underestimations of runoff due to the use of uniform rainfall forcing from the Socorro rain gauge. The differences between wet and dry years are more apparent in the historical data due to the scale required to show the 1972 event. When examining the close-up view of the modeled time series in Figure 39.b, we

observe that there are obvious wet and dry periods in the model simulations, yet they differ from the historical flows in magnitude. The simulated mean runoff over the record is closer to the observed mean value because these values are less affected by the extreme streamflows that occur in 1972 in the historical dataset.

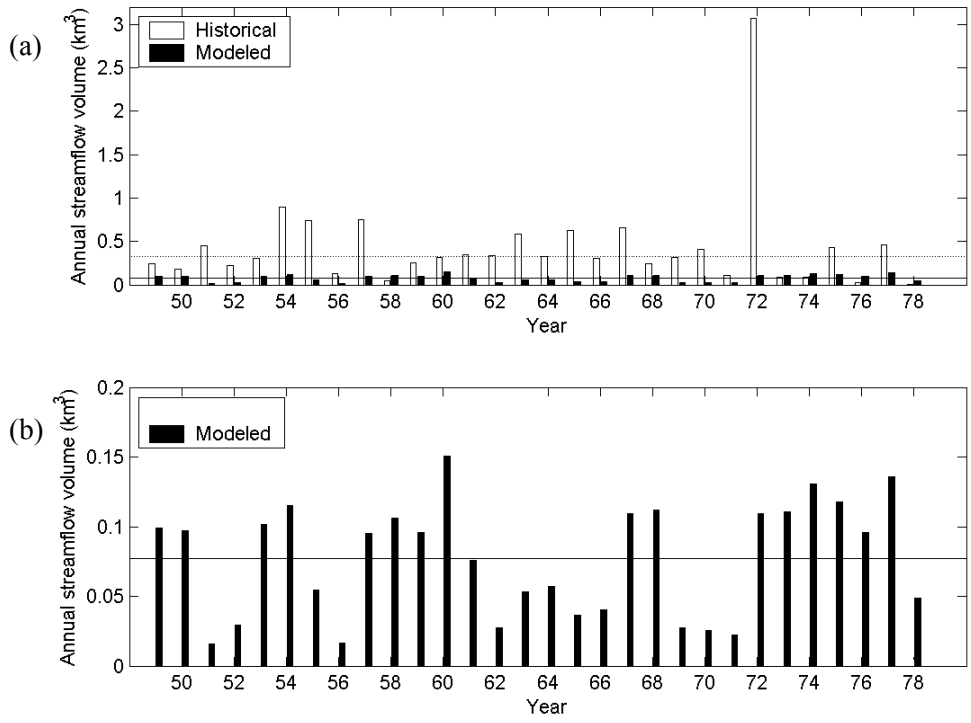

FIGURE 39: Annual streamflow volumes for Río Salado basin. (a) Comparing stream gauge to model results generated using rainfall forcing from the Socorro gauge, 1949-1978. Mean values: Historic = 0.432 km3 (blue dotted line), Model = 0.077 km3 (red solid line). (b) Close up view of model results to illustrate inter-annual variations.

In addition to the inter-annual variability of streamflows, we are also interested in the seasonal variations in runoff volumes at the basin outlet. Knowledge of the seasonality of tributary streamflows is beneficial in planning water use strategies. Figure 40 shows the strong seasonality present in historical monthly streamflows of the Río Salado. Notice the high flow volumes from July to September, indicating the flood pulses during the summer monsoon season. While the monsoon signal is not as distinct in the modeled results, it is still recognizable. The remaining

months in the modeled data have larger flows than were recorded historically. This suggests that the use of the Socorro rain gauge as uniform forcing to the watershed model primarily underestimates summer precipitation in the basin headwaters. The overestimation of winter streamflows may be a result of the streambed selected for this simulation (e.g. not enough transmission losses). The next section explores the effect of different parameterizations of channel losses in the long-term simulations of the Río Salado.

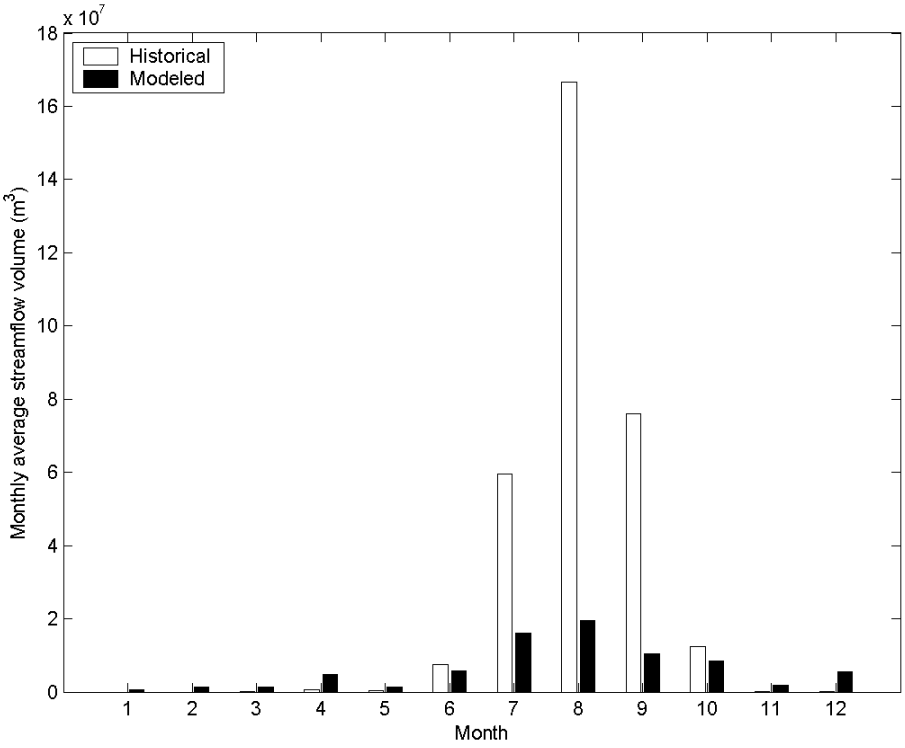

FIGURE 40: Monthly average streamflow volumes for Río Salado basin, comparing stream gauge to model results generated using rainfall forcing from the Socorro gauge, 1949-1978. The year 1972 is removed from historical data in order to limit the effect of the extreme year on the average values.

Long term simulation using synthetic climate forcing

In this section, we examine a synthetic run of the model over a 60-year period to provide insights into the capabilities of the model when using stochastic rainfall forcing. It should be noted that each HRU is forced with a precipitation dataset that is directly related to the nearest rain gauge

(e.g. Augustine, Brushy Mountain, Datil, Laguna, or Socorro). A representative model run (seed value of 25) for a 60-yr period resulted in a cumulative evapotranspiration ratio (ET/P) of 84.0% and a cumulative runoff ratio (R/P) of 11.0%, with the remaining 5.0% leading to drainage to the regional aquifer and changes in soil moisture levels. This is consistent with the semiarid nature of the Río Salado where evapotranspiration should be the primary loss mechanism. As a result, the overall water balance in the semiarid basin is considered to be comparable to observed conditions.

We start by examining the differences between precipitation and runoff time series for the 60-year simulation, allowing for model spin-up during the first 10 years (Figure 41, left column). The time series of the monthly total precipitation volumes, which are applied to the Río Salado basin, is shown in Figure 41.a. The interception and infiltration mechanisms capture much of the precipitation, resulting in runoff volumes that are greatly reduced and show greater monthly variability (Figure 41.b). The right column of Figure 41 shows the cumulative volumes for each of the time series. The cumulative runoff volume (7.86 km^3) is 11.0% of the total precipitation (71.62 km^3). Since runoff is produced by both saturation-excess and infiltration-excess mechanisms within the model, we explore how these two runoff types differ over the Río Salado basin in the following section.

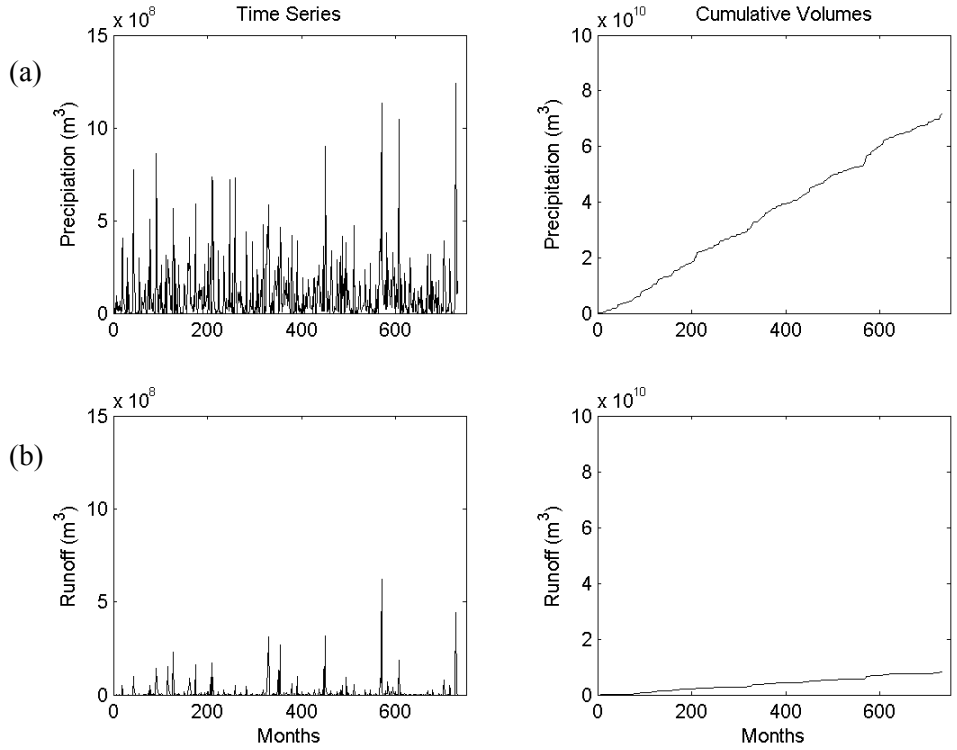

FIGURE 41: Synthetic 60-year simulation applied to all HRUs in the Río Salado. Monthly time series (left) and cumulative volumes (right) of (a) precipitation and (b) total runoff.

The majority of the runoff produced by the watershed model is in the form of infiltration-excess runoff. Due to the threshold behavior occurring when rainfall intensities exceed the saturated hydraulic conductivity of the soil, a large portion of the rainfall that reaches the ground surface during high intensity storms becomes infiltration-excess runoff. This leaves a smaller amount of water available to fill the soil column and subsequently result in saturation-excess runoff. The left column of Figure 42 shows the monthly time series of the two runoff types. Notice that infiltration-excess runoff occurs with greater frequency and magnitude than saturation-excess runoff. The right column of Figure 42 shows the accumulation of runoff volumes over the 60 years of the simulation. Infiltration-excess runoff (7.32 km^3) makes up 93.1% of the total runoff volume produced, whereas the remaining 6.9% (0.54 km^3) is in the form of saturation-excess runoff.

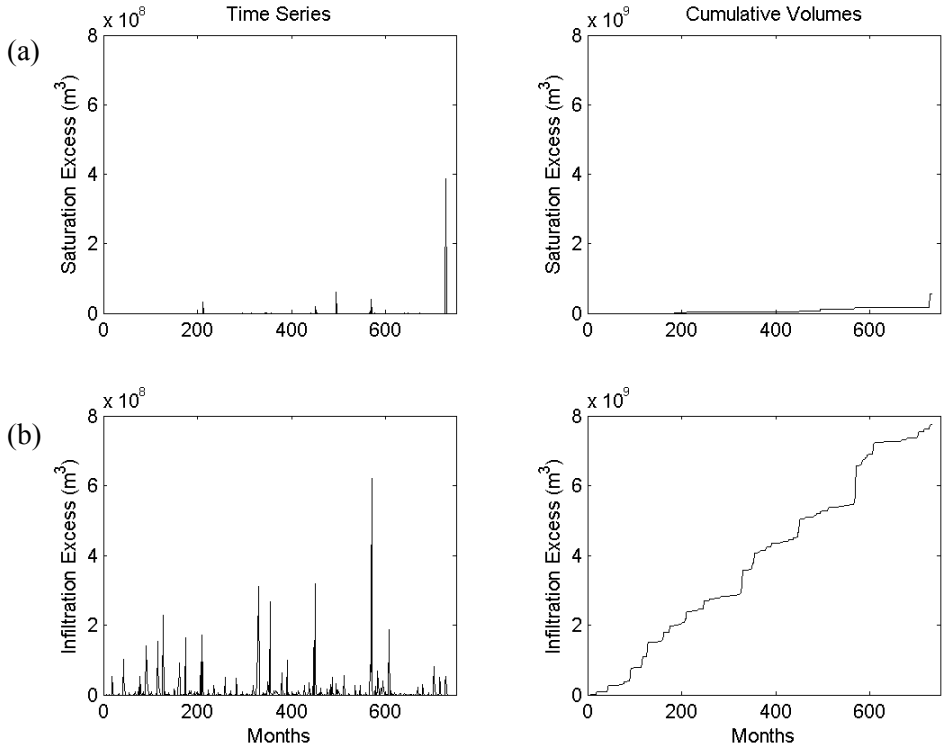

FIGURE 42: Synthetic 60-year simulation applied to all HRUs in the Río Salado. Monthly time series (left) and cumulative volumes (right) of runoff produced via (a) saturation-excess and (b) infiltration-excess mechanisms.

Our next comparison will be of the remaining terms in the water balance, evapotranspiration and drainage to the regional aquifer, using basin-averaged monthly values. The basin-averaged volumes are computed by multiplying the volume for each HRU by the area of the HRU, then summing these values over the entire basin. Finally, the summation is divided by the total basin area, which results in a basin-averaged volume. The basin averaging procedure results in less frequent rainfall events with lower monthly volumes (Figure 43.a), as compared to basin totals (see Figure 41.a). This may be a result of the large area HRUs, which are weighted more heavily, receiving less precipitation in this example run as compared to smaller HRUs. The basin-averaged evapotranspiration (ET) shown in Figure 43.b follows a similar temporal pattern as the precipitation, but with smaller volumes. The minimum values of ET (~$5x10^6$ m^3) are greater than the minimum precipitation, as evapotranspiration is a continuous process occurring over long

interstorm periods, in contrast to the more sporadic storm events. Drainage from the soil column (Figure 43.c) is less responsive to precipitation inputs than the ET, primarily due to the dampening affect caused by the soil (1.5 m depth) that the water must move through before draining to the regional aquifer. Nevertheless, drainage patterns increase when precipitation is high for consecutive periods, for example near months 200 and 600 in the model simulation. From Figure 43 (right column), the fraction of the water losses going into evapotranspiration and drainage can be easily identified. The total volume for the basin-averaged precipitation is 5.38 km^3, which is smaller than the total precipitation produced by simple summation. This supports the argument that some large-area HRUs do not receive high amounts of precipitation. The basin-averaged ET (4.57 km^3) accounts for 84.8% of the basin-averaged precipitation, while the basin-averaged drainage (0.14 km^3) accounts for only 2.6%. The remaining 12.6% leaves the basin primarily as runoff or becomes long-term (but small) increases in the soil moisture storage or snow pack volume.

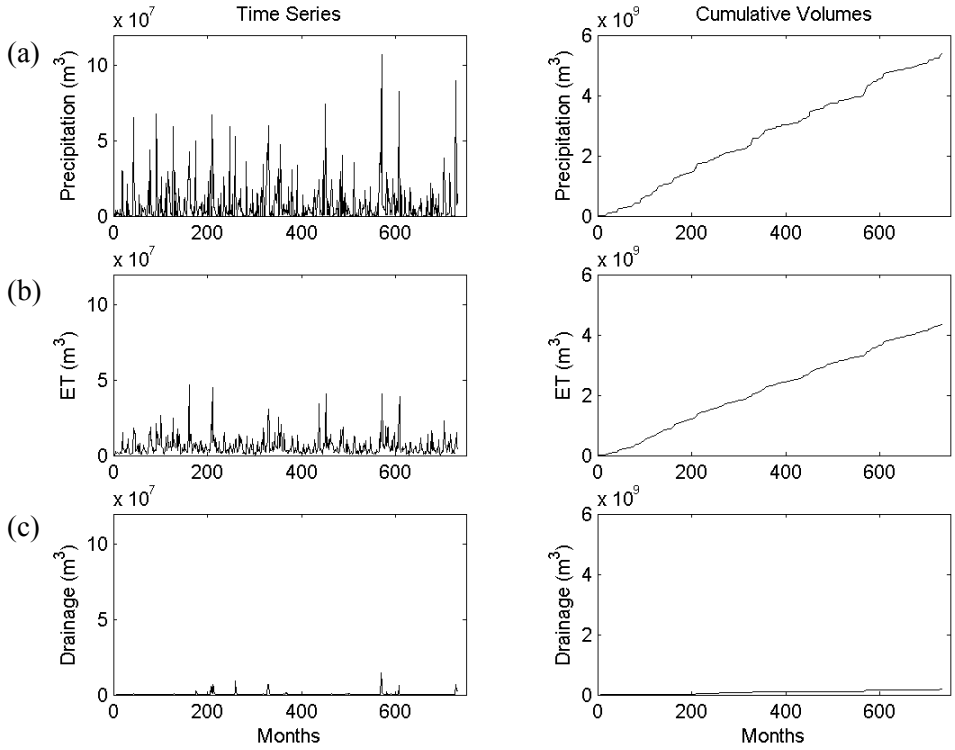

FIGURE 43: Synthetic 60-year simulation applied to all HRUs in the Río Salado. Monthly time series (left) and cumulative volumes (right) of (a) basin-averaged precipitation volume, (b) basin-averaged evapotranspiration volume, and (c) basin-averaged drainage volume.

We examine the basin-averaged soil moisture for each layer as a time series in Figure 44. Figure 44.a shows the basin-averaged soil moisture in the top 10 cm for the entire basin. Clearly, this layer is very responsive to atmospheric forcing, and remains fairly dry for the duration of the simulation. The observed variability in soil moisture is caused by the shallow nature of the top layer and its exposure to precipitation, evaporation and transpiration. The middle layer is equally responsive, but is able to maintain higher moisture levels throughout many of the long interstorm periods (Figure 44.b), due to its increased depth. The lower layer is affected to a smaller degree due to its increased separation from the atmosphere. Losses from the lower layer are limited to transpiration, drainage, and diffusion to the middle layer. This relative isolation allows the lower layer to retain moisture for extended periods of time encompassing multiple storm and interstorm

events. Note from these soil moisture time series that an effective spin-up period for the watershed model is approximately 100 months.

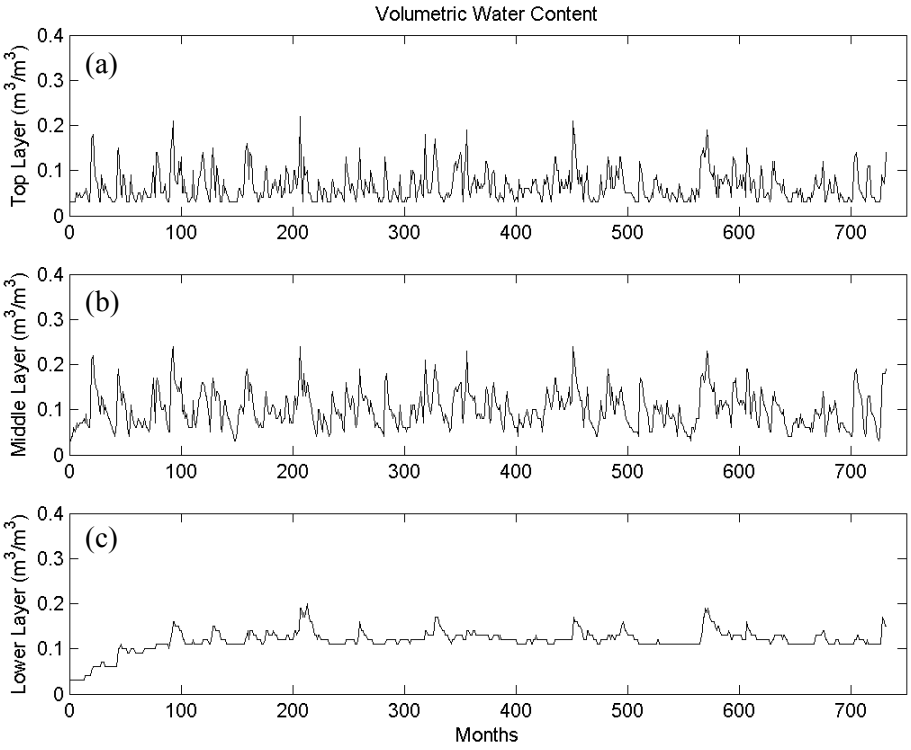

FIGURE 44: Synthetic 60-year simulation applied to all HRUs in the Río Salado. Monthly time series of volumetric water content for the (a) top layer, (b) middle layer, and (c) lower layer.

To examine the effects of channel losses on the volume of runoff measured at the outlet, we used three different soil classes for the stream channel bottom applied uniformly over the stream network. Figure 45 shows that as the hydraulic conductivity of the streambed increases the amount of water that reaches the outlet is greatly reduced. The channel losses are 8.3% of the total runoff for the sandy loam streambed, 17.5% for the loamy sand streambed and 40.3% for the sand streambed. Increasing the hydraulic conductivity of the channel reduces the runoff ratio (R/P) to 10.1%, 9.1%, and 6.6% for each stream bed type, respectively. The water lost in the channel is drained into the regional aquifer and not tracked further in the model.

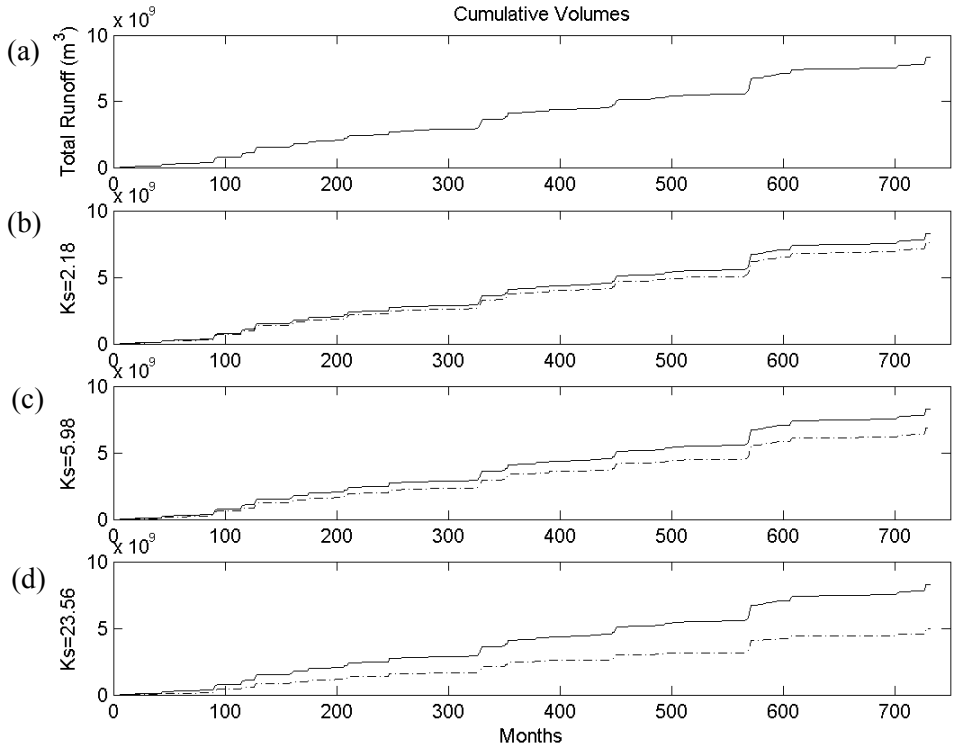

FIGURE 45: Comparison of (a) total runoff and routed runoff with channel transmission losses for stream channels with different saturated hydraulic conductivities, (b) sandy loam (2.18 cm/hr), (c) loamy sand (5.98 cm/hr), and (d) sand (23.56 cm/hr). Note that the total runoff from (a) is repeated in (b-d).

This concludes our examination of the model performance for a long-term synthetic case using stochastic forcing. These results have increased our confidence in the model's capability to simulate the water balance at the monthly scale, over the entire Río Salado. In particular, it is clear that long–term simulations are possible over the large Río Salado basin and can capture anticipated behavior in terms of water-balance metrics such as the runoff ratio and evapotranspiration ratio.

Comparison of ensemble simulations using stochastic climate forcing

Studies of the long-term impacts of climate trends require understanding of how variations in precipitation will affect the watershed model response. This section is an attempt to quantify the variability introduced into the model response through random sampling of the stochastic climate

forcing. We examine alternative scenarios in an ensemble approach to assess the response of the watershed model to the uncertainty in climate forcing. We attempt to capture this uncertainty by changing the seed value used in the random number generation of the precipitation and temperature time series. The forcing for the simulations are conditioned on the five rain gauges surrounding the Río Salado and preserve the spatial and seasonal variations in precipitation event intensity, duration and frequency, as well as the temperature seasonality. Twenty-five realizations are used, allowing us to examine how stochastic climate forcing influences the hydrologic response. We first examine the water balance (runoff generation, ET, and drainage), and then inspect the runoff partitioning for the ensemble of twenty-five long-term (60-yr) model runs.

Figures 46 and 47 show the ensemble of 25 simulations for each variable in the water balance as well as the ensemble mean. The ensemble mean is a more stable representation of the performance of the watershed model, because it averages over the variability that is possible within individual realizations. Notice that the differences among the ensemble members tend to grow in time as more randomness is introduced in the climate forcing. Clearly, differences occur in the propagation of the precipitation uncertainty into the various hydrological processes. However, it is somewhat difficult to precisely determine differences in the magnitude of the variability in Figure 46 and Figure 47, due to the variations in the scale of the y-axis. As a result, we will examine the difference in uncertainty for each variable by looking at the coefficient of variation ($CV = \sigma/\mu$) computed at the end of the long–term simulations. Smaller CV values for a particular variable indicate less uncertainty or difference among realizations (or ensemble members). Table 8 indicates that the runoff mechanisms have greater ensemble variability (CV) than the precipitation forcing, with the largest variability observed for saturation-excess runoff.

The drainage from the bottom soil layer is nearly five times as variable as the precipitation forcing and the modeled evapotranspiration. This analysis shows that the manner in which the precipitation uncertainty propagates through the watershed model differs depending on the processes involved. Threshold processes that are dependent on both precipitation and on the degree of saturation of the soil, which both vary with time (e.g. saturation-excess runoff and drainage), have greater variability in a semiarid region where the soils are usually dry. Processes such as infiltration-excess runoff and ET that respond to only one time-dependent variable (precipitation) have less variability. Furthermore, evapotranspiration exhibits ensemble variability close to the precipitation forcing, suggesting that temperature and soil moisture changes have a smaller effect on ET than on other processes. Clearly, this analysis reveals that the basin hydrologic response to precipitation uncertainty is complex and non-linear. Different hydrological processes can amplify precipitation variability by differing amounts. Thus, the HRU-based watershed model is capable of reproducing the nonlinear response anticipated in natural basins.

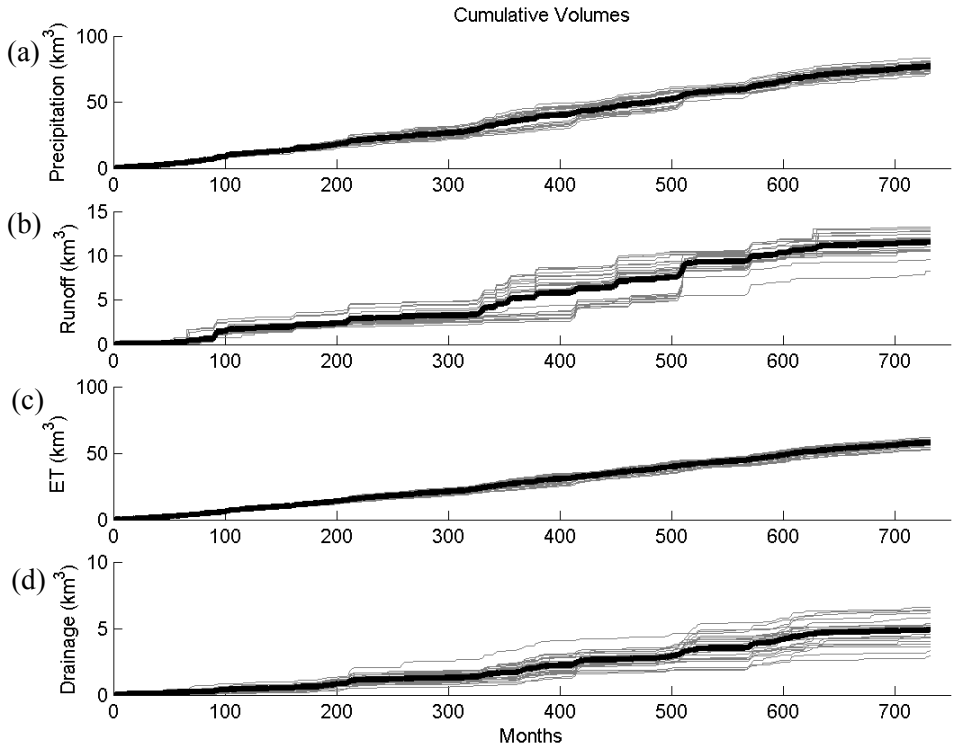

FIGURE 46: Ensemble of synthetic 60-year simulations (25 total) applied to all HRUs in the Río Salado. Cumulative volumes of (a) total precipitation, (b) total runoff, (c) ET, and (d) drainage. Note the different scales used to improve visualization. The thick lines denote the ensemble mean.

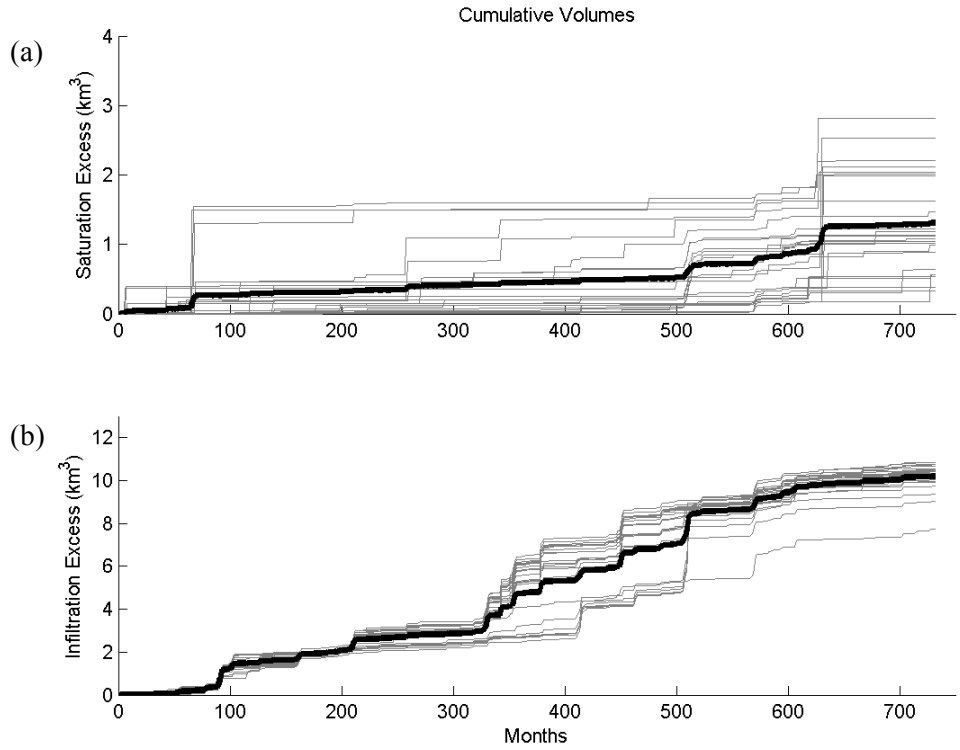

FIGURE 47: Ensemble of synthetic 60-year simulations (25 total) applied to all HRUs in the Río Salado. Cumulative volumes of runoff partitioning: (a) saturation-excess runoff and (b) infiltration-excess runoff. Note the different scales used to improve visualization. Thick lines denote the ensemble mean.

Variable	μ (m^3)	σ (m^3)	CV
Precipitation	77.02	3.22	0.04
Total Runoff	11.51	1.12	0.10
Infiltration-excess Runoff	10.19	0.68	0.07
Saturation-excess Runoff	1.31	0.69	0.53
ET	58.01	2.51	0.04
Drainage	4.90	0.93	0.19

TABLE 8: Statistical variables for each output variable, mean (μ), standard deviation (σ), and coefficient of variation (CV), showing differences in uncertainty among the 25 ensemble simulations.

Using stochastic precipitation forcing allowed us to better address the issue of runoff underestimation identified in basin scale results. Figure 48 compares the mean total runoff volume at the Río Salado outlet (over 30 yrs) for the ensemble of 25 runs using different seed values with the measured historical data. The maximum and minimum runoff volumes are also shown to emphasize that the realizations of the model vary greatly in terms of the

amount of runoff produced. Clearly, the stochastic nature of the precipitation forcing greatly improves the runoff comparison between the model simulations and the historical observations. This is primarily due to the inclusion of data from the Datil and Brushy Mountain sites, which have large mean annual precipitations (see Figure 17). Thus, while we do not explicitly account for the elevation effect on precipitation, by adding these two stations we significantly improve the performance of the model. In addition, summing the large volume of water measured in 1972 at the stream gauge (3 km^3) to the maximum volume from the ensemble (7.8 km^3) brings us within 20% of the measured historical volume (13 km^3). These results increase our confidence in the model formulation despite the limitations already discussed regarding precipitation forcing.

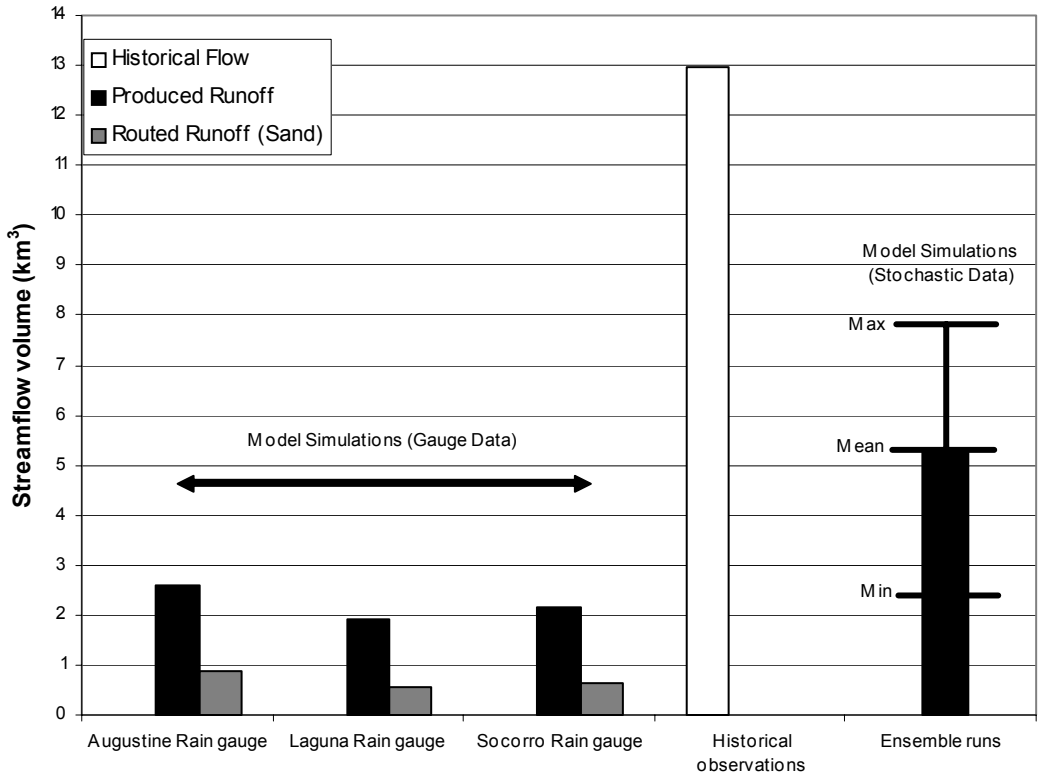

FIGURE 48: Cumulative stream flow volumes for the Río Salado basin from the historical stream gauge observations and model simulations generated using uniform rainfall forcing from the various rain gauges over the period 1949-1978. The ensemble model simulations using stochastic data result in less underestimation of total runoff. Note that adding the 3 km^3 of runoff generated by the extreme events in 1972 would further improve the estimation.

In the next section we will test the ability of the watershed model as a tool to explore the potential impacts of climate change. We will accomplish this by varying the precipitation forcing. In particular, we examine the effects of increasing and decreasing both summer and winter precipitation under conditions of both constant temperature and increasing temperature. This will allow us to simulate the effects of climate change on large semiarid basins such as the Río Salado.

Sensitivity to climate change scenarios

Knowledge of the effects of climate change on river basins will be important for future water resources management. However, there are differing ideas about how these changes will manifest themselves in terms of precipitation frequency and intensity. For example, Seager et al. (2007) state that southwestern North America will become generally more arid as the 21st century progresses. On the other hand, several studies indicate that increases in precipitation intensity (i.e. extreme events) may occur for certain regions of the southwestern United States (Diffenbaugh et al., 2007, McCabe and Hay, 1995, Nash and Gleick, 1991, Peterson et al., 2008). Additionally, climate models used to generate precipitation predictions can result in a wide range of scenarios that differ significantly (e.g. IPCC-AR3, 2001, IPCC-AR4, 2007, Serrat-Capdevila et al., 2007).

We will examine two cases where the total precipitation volume increases through different mechanisms. In the first case, we reduce the interstorm duration of the winter season (Dec. – Feb.), resulting in an increase in winter precipitation. This winter precipitation increase is consistent with on-going trends of increasing cold season precipitation observed by Hamlet and Lettenmaier (2007) and Molnar and Ramirez (2001) for the 20th century. In the second case, we increase the intensity of summer storms, to simulate an increase in the number of extreme events (Madsen and Figdor, 2007, Peterson et al., 2008). Figure 49.a shows that decreasing the mean interstorm duration of the winter months has a non-linear effect on the total precipitation volume produced by the model. This is because changing the length of interstorm events affects the number of storms that occur in a given month. This is different from the linear change in precipitation volume caused by increasing the storm intensity (Figure 49.c). The linear or non-linear trends in the precipitation forcing propagate into the other water balance variables at

different degrees (Figures 49.b and 49.d) as well as into the allocation of runoff (Figure 50). Clearly, the increase in winter precipitation induced by smaller interstorm lengths leads to an increase in the drainage (e.g. regional recharge), a decrease in the evapotranspiration and a small decrease in the runoff volume. This suggests that the additional light-intensity rainfall has primarily led to higher volumetric soil moisture contents (not shown). This is supported by the greater amount of saturation-excess runoff evident in the winter months. The responses in the summer scenario are quite different. Increases in summer precipitation induced by higher rainfall intensities lead to a large increase in runoff volumes, a small rise in drainage and a corresponding decrease in evapotranspiration. The runoff increase is a result of higher soil moistures levels generating greater amounts of saturation-excess runoff during smaller storms.

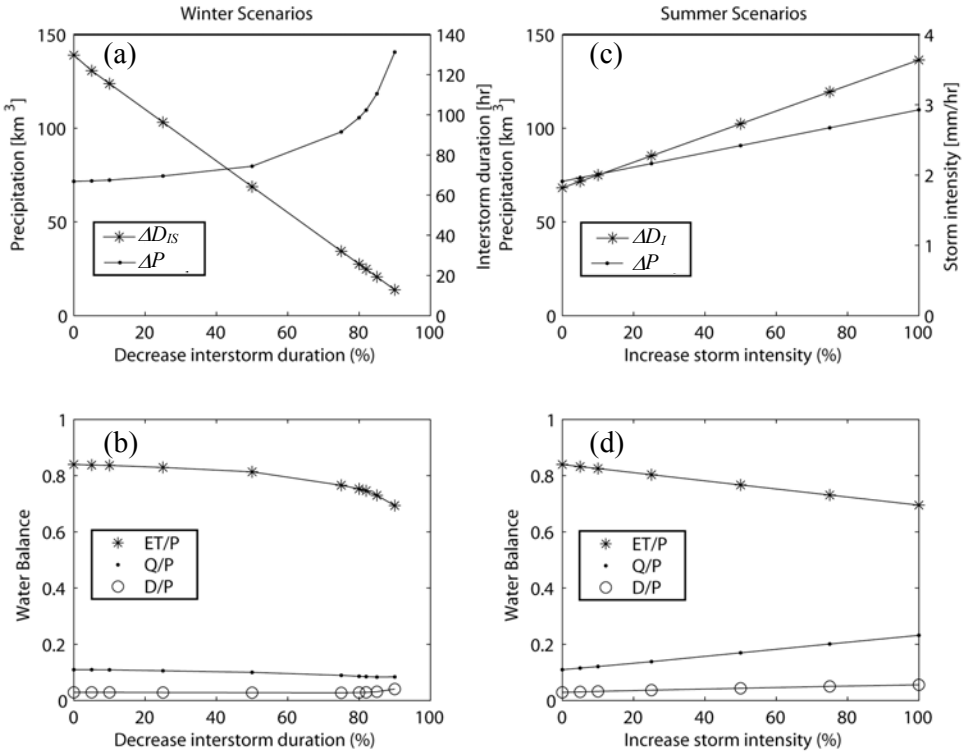

FIGURE 49: Change in precipitation volume and water balance ratios (ET/P, Q/P, D/P) as a result of (a and b) a decrease in winter (DJF) interstorm duration and (c and d) an increase in summer (JAS) storm intensity, both expressed as percentage changes from parameters of the base case. The change in interstorm duration (ΔD_{IS}) and storm intensity (ΔP) are also illustrated for the various scenarios.

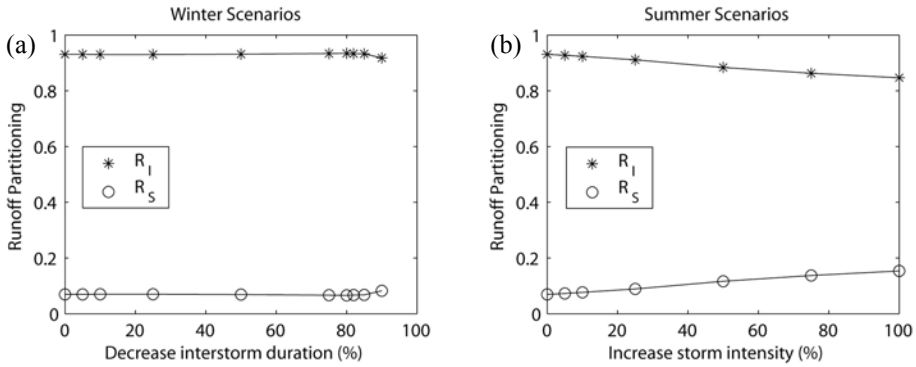

FIGURE 50: Change in runoff partitioning as a result of (a) a decrease in winter (DJF) interstorm duration and (b) an increase in summer (JAS) storm intensity, both expressed as percentage changes from parameters of the base case. R_I is the fraction of the total runoff that is in the form of infiltration-excess runoff and R_S is the fraction of the total runoff that is in the form of saturation-excess runoff.

For the winter and summer scenarios, we chose two cases that each had an equal increase in the total precipitation volume for the 60-yr simulation (-82% interstorm duration for winter scenarios and +100% rainfall intensity for summer scenarios, respectively) and then compared ensemble simulations (25 simulations) for each case (Figure 51). Note that the precipitation ensembles (Figure 51.a) are similar by design.

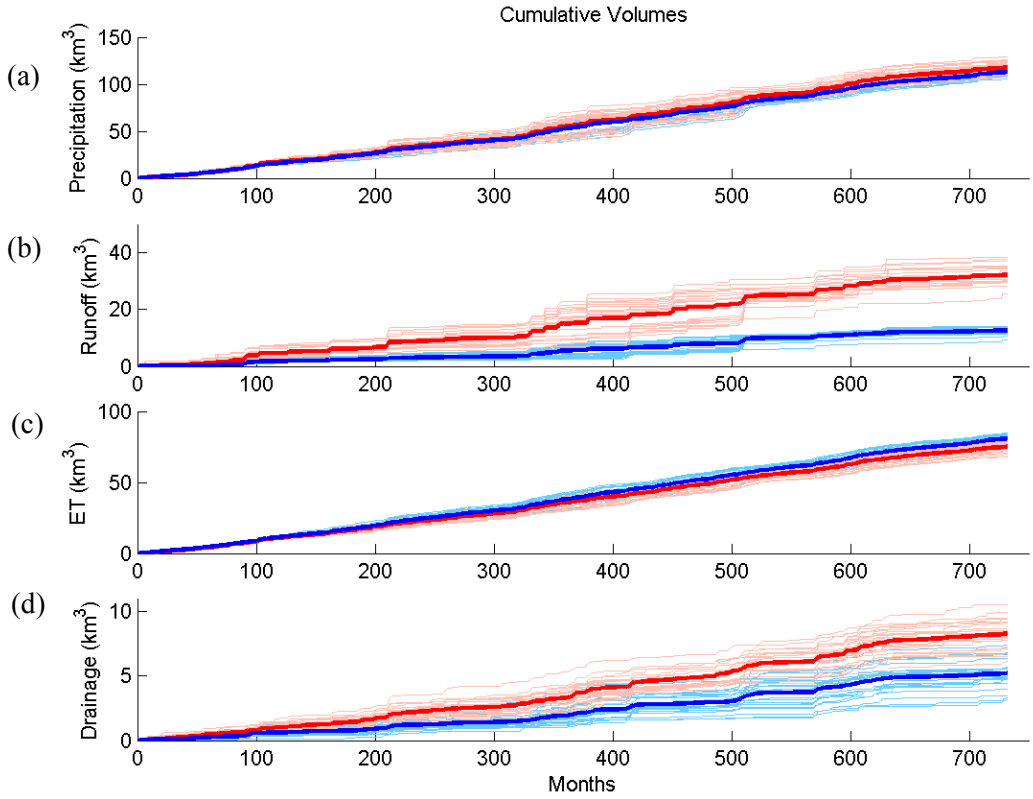

FIGURE 51: Comparison of ensemble simulations for a decrease in winter (DJF) interstorm duration (-82%, light blue) and an increase in summer (JAS) storm intensity (+100%, light red). Cumulative volumes of (a) total precipitation, (b) total runoff, (c) ET, and (d) drainage. Note the different scales used to improve visualization. The thick lines denote the ensemble mean (summer = dark red, winter = dark blue).

The effects of the different precipitation forcing scenarios are apparent in the runoff and drainage amounts (Figures 51.b and 51.d). Apparently, despite having nearly identical total precipitation amounts, the two scenarios lead to distinct runoff and drainage responses that do not overlap, even when accounting for climate forcing variability. When examining the ensembles of runoff generation, the variability associated with the saturation-excess runoff is less distinct between the winter and summer simulations, as compared to the infiltration-excess runoff (Figure 52). Table 9 displays the statistical information (mean, standard deviation, coefficient of variation) for the winter and summer simulations. Notice that in both cases the runoff is more than twice as variable as the precipitation forcing, while the drainage is over five times as variable as the

precipitation in the winter but just over twice as variable in the summer. It is also important to note that the statistical properties of the two ensembles are significantly different such that whether winter or summer precipitation changes occur affects the overall basin response. If both precipitation changes were to occur simultaneously, we should expect a superposition of the simulated hydrologic changes.

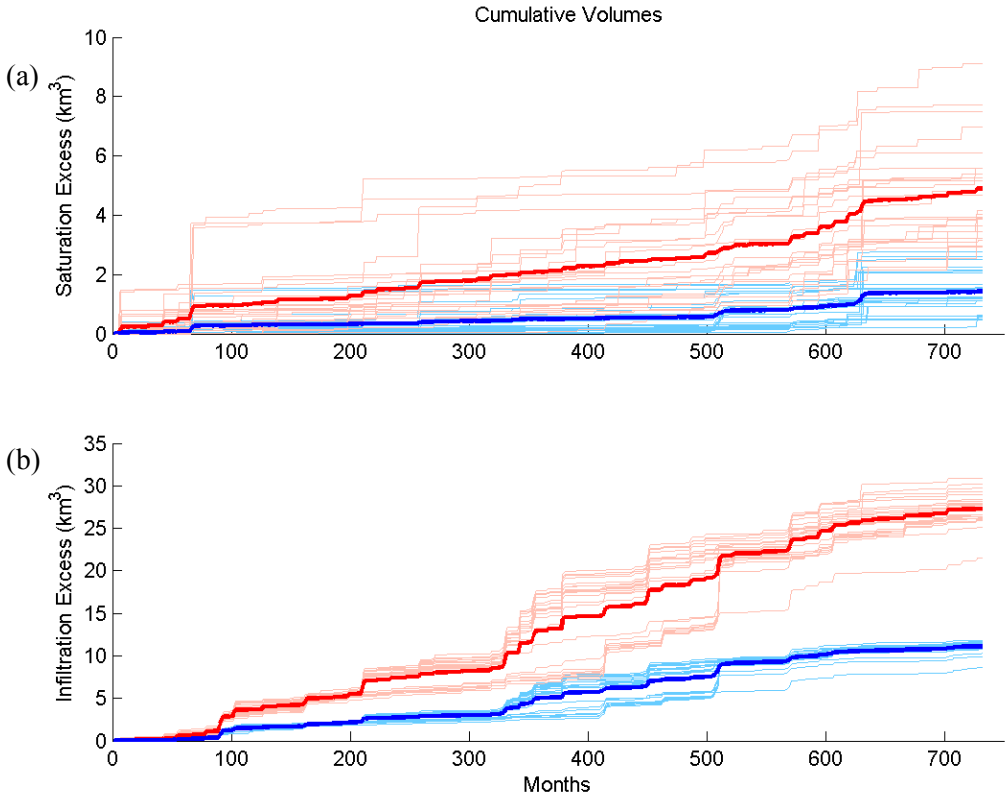

FIGURE 52: Comparison of ensemble simulations for a decrease in winter (DJF) interstorm duration (-82%, light blue) and an increase in summer (JAS) storm intensity (+100%, light red). Cumulative volumes of runoff partitioning: (a) saturation-excess runoff and (b) infiltration-excess runoff. Note the different scales used to improve visualization. The thick lines denote the ensemble mean (summer = dark red, winter = dark blue).

Season	Winter Scenarios			Summer Scenarios		
Variable	**μ (m^3)**	**σ (m^3)**	**CV**	**μ (m^3)**	**σ (m^3)**	**CV**
Precipitation	112.99	4.09	0.04	117.51	5.90	0.05
Total Runoff	12.54	1.11	0.09	32.19	2.99	0.09
Infiltration-excess Runoff	11.11	0.67	0.06	27.30	1.88	0.07
Saturation-excess Runoff	1.43	0.68	0.48	4.89	1.61	0.33
ET	80.78	3.31	0.04	75.05	3.42	0.05
Drainage	5.21	1.07	0.21	8.27	1.08	0.13

TABLE 9: Statistical variables for each output variable, mean (μ), standard deviation (σ), and coefficient of variation (CV), showing differences in uncertainty among the 25 ensemble simulations.

The final experiment performed in this study was to examine the effects of imposing increases on the temperature parameters (maximum, minimum and mean monthly values) for each scenario (winter and summer). In each case, we increased the parameters that are used in the stochastic temperature generator from 0 to 4 degrees C in 1-degree increments. As shown in Figure 53, these temperature increases have a limited but discernable effect on the model outputs at the end of the 60-yr simulations. There is a slight increase in the evapotranspiration ratio, with a 5% increase for the winter simulations and 2% increase for the summer scenarios. The ratios (Q/P, D/P) only change by 1% or less. We believe that this lack of response to temperature change is consistent with the limited propagation of uncertainty into the evapotranspiration response in the watershed model. Increases in air temperature only moderately affect the potential evapotranspiration, primarily in the winter, and seem to have minimal propagation to actual evapotranspiration given the water limited conditions in the basin. Figure 54 shows that the 4-degree increase in temperature results in a very small change in the soil moisture levels over time. In addition, the relatively minor snow packs in the Río Salado have a limited impact on the water balance changes induced by higher air temperatures. A lack of coupling between air temperature,

surface conditions and subsequent precipitation in the model also diminished the overall effects of the imposed temperature increases.

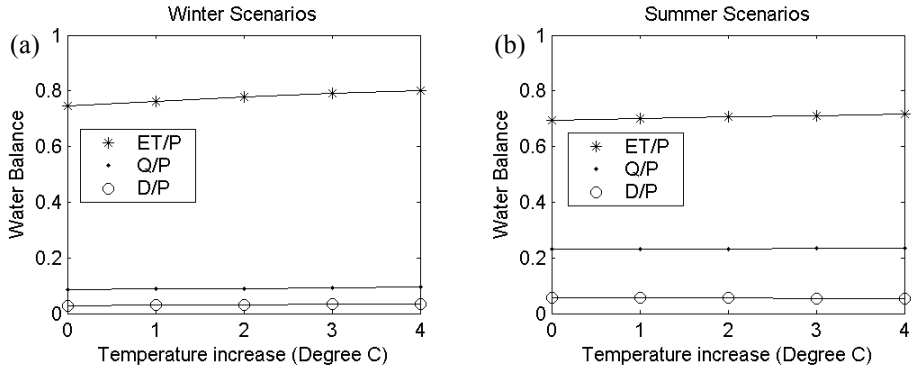

FIGURE 53: Change in precipitation volume and water balance ratios (ET/P, Q/P, D/P) as a result of temperature increases for (a) a decrease in winter (DJF) interstorm duration (82%) and (b) an increase in summer (JAS) storm intensity (100%).

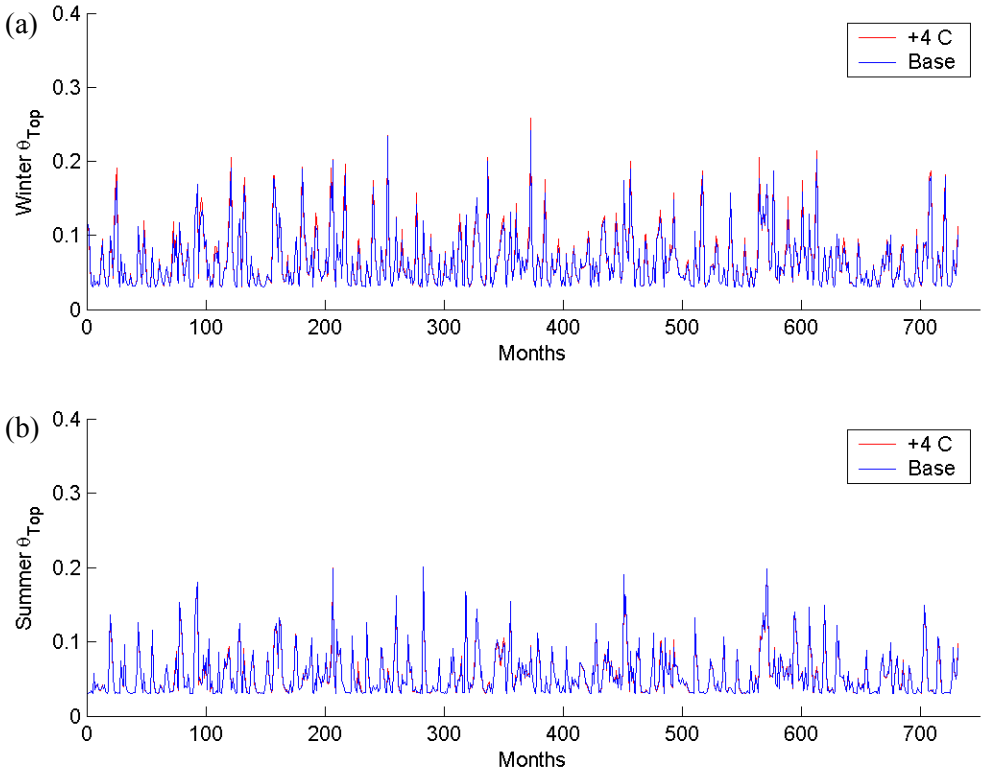

FIGURE 54: Difference in top layer soil moisture for temperature based climate change scenarios, base case (blue) and +4°C (red).

Summary

This concludes the presentation of the model application and testing section, which has included a detailed explanation of the capabilities of the watershed model. The model's performance at the point scale allowed for comparison with soil moisture data, and helped build confidence in the model physics. At the HRU scale, model output provided a view of the effects of vegetation and soil parameters on the water balance dynamics. Performance at the basin scale was evaluated in comparison to historical streamflow measurements at the basin outlet, and while the model underestimated the total volumes the results helped us gain insight into the need for accurate precipitation forcing parameters. The final set of results dealt with climate variability and imposed climate changes. The response of the watershed model to these climate scenarios reinforces the belief that we have a robust semi-distributed hydrological model that can aid decision makers in semiarid regions.

SUMMARY, CONCLUSIONS AND RECOMMENDATIONS

Summary

With populations across the globe continuing to increase, the risks of water related conflicts becoming violent also grow. Water policy makers attempt to diminish these conflicts by balancing the needs of all interested parties. A well-developed hydrologic model is a tool that can be useful in the water related decision-making processes.

The goal of this project was to create a semi-distributed watershed model that incorporated the following objectives. The model must be usable in semiarid areas and able to account for differences in vegetation and soil properties. The primary hydrological predictions of interest include tributary basin runoff, soil moisture, evapotranspiration and deep drainage. These variables allow understanding of the hydrological or water balance components and their variations to imposed changes or trends in climate forcing. It was also necessary that the model be capable of processing large basins quickly to provide "real time" results for decision-making purposes. To accomplish these objectives, we created a watershed model using the Powersim system dynamics software package and applied it to the Río Salado due to its semiarid nature and the availability of historical data for model testing purposes. The application in the Río Salado serves as a prototype for modeling ungauged and gauged tributaries in the entire Río Grande basin.

Major conclusions

This section describes the major conclusions reached upon completion of this study. These conclusions encompass the entirety of the project from the development of the watershed model

to testing at different scales and the analysis of model sensitivity to changes in atmospheric forcing.

(1) The model domain is discretized into Hydrologic Response Units (HRUs) allowing us to represent the watershed using physical equations applied to areas with relatively uniform soil and vegetation properties. The watershed model implements relativity simple equations to solve the water balance and account for hydrological states and fluxes. To simulate precipitation forcing, we implemented a Poisson rectangular pulse model. Hydrological processes such as snow, interception, evapotranspiration and runoff are accounted for. Runoff is generated via both infiltration-excess and saturation-excess mechanisms and routed through the channel network to the basin outlet.

(2) To reduce the model computational load, we have implemented an event based time scale that accounts for storm and interstorm periods within a monthly time step. The storm/interstorm event scheme was implemented as a sub-routine within the Powersim model framework. This event scheme allowed us to capture important processes in semiarid regions that would have been missed by performing calculations on a monthly time step.

(3) Powersim facilitates user interaction and thus decision-making through a graphical user interface by allowing users to change parameter values. These changes can be made using toggles and input fields, while the model provides real time visual displays of model output. As a result, the watershed model is fairly easy to use by non-experts.

(4) Point scale soil moisture tests at the Deep Well site in the Sevilleta National Wildlife Refuge reveal that the watershed model is capable of suitably simulating changes in soil moisture at the event scale. As seen in Figure 30 and Figure 31, the watershed model performs reasonably well at the point scale, especially with regard to the timing of soil moisture pulses. Some accuracy at the point scale was eventually sacrificed to improve performance at the basin scale, in particular for the deeper soil layers, which are consistently drier in the model as compared to the measured data.

(5) HRU scale tests were performed to test the watershed model response to changes in vegetation and soil parameters. The model was tested for a forest/sand HRU and a grass/clay loam HRU over a wet and dry year. Plausible model results helped build confidence in the capabilities of the model at the HRU scale and demonstrate the model sensitivity to soil and vegetation parameters.

(6) Basin-scale simulations from the watershed model were compared to historical stream gauge data (1949-1978) for the Río Salado at the monthly, yearly and decadal time scales. While the model underestimated the volume of water reaching the basin outlet, this is primarily a result of the scarcity of precipitation data for the upper elevations of the basin. At the basin scale, the watershed model was able to simulate both inter-annual and seasonal variability reasonably well. As shown in Figure 40, the model captures increases in summer month precipitation in a manner similar to the actual

data, albeit with lower volumes. This shows that the stochastic precipitation generator provides a reasonable estimate of possible precipitation scenarios.

(7) Climate variability was subsequently introduced into the model from the stochastic nature of the precipitation and temperature forcing. Soil- moisture levels in the top two soil layers closely mimic the precipitation patterns, while evapotranspiration, runoff and drainage each exhibit increasingly variable responses. Ensemble simulations were performed to analyze the effects of different realizations of the stochastic model. This test provides an example of model performance by accounting for the randomness in climate forcing encountered in nature.

(8) Climate-change scenarios in the form of increased precipitation and temperature were also evaluated. The watershed model was able to capture the non-linearity inherent in nature when simulating changes in precipitation forcing. The non-linear behaviors induced by the model can be seen in Figure 48 in the different path that can be taken to reach an almost identical increase in total precipitation. The distinct differences in the ensemble simulations with regard to runoff production and deep drainage further emphasize the unique behaviors induced by changes in the precipitation forcing. Increases in the temperature parameters in line with IPCC predictions had little influence on model performance, suggesting that the Río Salado may be less affected by temperature changes as compared to precipitation changes. This is a consequence of the fact that the bulk of the basin streamflow is in response to

extreme precipitation events, which are not as sensitive to the soil moisture state of the system.

Limitations of current study and future work

In this section we describe current limitations of this research project and the watershed model in particular and propose potential avenues for future work.

(1) Portability of the model to new regions is hindered by the large amount of preprocessing (ArcGIS, Matlab, EXCEL) required to setup the model. Preprocessing includes watershed delineation, creation of HRUs, conversion of precipitation data into forcing parameters, and construction of spreadsheet datasets for model input. To remedy this, an automated set of tools for basin, HRU and forcing preprocessing should be created. For example, the application of the model to the Río Grande will require pre-processing of 190 tributary basins. In addition, improved methods for model output visualization are needed.

(2) The application of the watershed model at the event timescale reduces the models ability to precisely replicate field measurements. While using finer resolution temporal data to force the model will improve results, the cost will be in increased processing time.

(3) The use of coarse soil/vegetation class maps in the HRUs and the application hydrological processes in a uniform manner within each HRU reduce the reality of the model representation of the natural landscape. While higher

resolution data is available, a model with finer spatial discretization will require additional computing resources.

(4) Connectivity of the stream channel to the shallow aquifer or regional groundwater system in the form of base flow is not included in the model at this time. The lack of connection between the stream network and groundwater affects both the timing and magnitude of streamflow measured at the basin outlet. To remedy this, the watershed model needs to be fully integrated to the Sandia system dynamics toolbox, which contains a groundwater module. In addition, a more sophisticated channel routing may improve the basin scale results by more properly treating HRU flow paths.

(5) Areas with limited availability of input data in the form of precipitation measurements will experience diminished ability of the model to produce accurate results. Additionally, locations with limited historical data (streamflow, evapotranspiration, and soil moisture) will have difficulties associated with model verification. A possible approach for future studies is to apply the model to a more instrumented watershed with long-term historical data.

(6) The employment of simple climate change scenarios in this study only provide preliminary assessments which should be further investigated by tying the model simulations to more accurate climate change predictions for the southwestern United States.

(7) An improved snow model, which accounts for a multiple-layer snow pack and canopy interception of snow, is necessary to properly capture snow dynamics.

REFERENCES

Alfieri, J., personal communication, September 27, 2007

Aragón, C.A. 2008. Development and testing of a semi-distributed waterhed model: Case studies exploring the impact of climate variability and change in the Río Salado. Master of Science Thesis, New Mexico Institute of Mining and Technology, 158 pp.

Archibold, 2008. Los Angeles Eyes Sewage as a Source of Water. *New York Times*

Arnold J.G., Srinivasan R, Muttiah R.S., and Williams J.R., 1998. Large area hydrologic modeling and assessment Part I: model development. *Journal of the American Water Resources Association.* 34(1): 73–89.

Arnold, J.G. and N. Fohrer. 2005. SWAT2000: Current capabilities and research opportunities in applied watershed modeling. *Hydrological Processes.* 19(3): 563-572.

Band, L. E., 1986. Topographic partition of watersheds with digital elevation models. *Water Resources Research.* 22(1): l5-24.

Bras, R.L. 1990. *Hydrology: An introduction to hydrologic science*. Addison-Wesley, Reading, MA. 643 pp.

Beven, K.J. 2000. *Rainfall-Runoff Modelling, A Primer*. John Wiley, Hoboken, NJ. 360 pp.

Breuer, L., Eckhardt, K., Frede, H-G., 2003. Plant parameter values for models in temperate climates. *Ecological Modeling.* 169: 237-293.

Burnash, R.J.C., R.L. Ferral, and R.A. McGuire. 1973. A generalized streamflow simulation system: Conceptual modeling for digital computers, Technical Report. *National Weather Service*, Sacramento, CA. 204 pp.

Byers, E., and Stephens, D.B., 1983. Statistical and stochastic analysis of hydraulic conductivity and particle size in a fluvial sand. *Soil Science Society of America Journal.* 47(6): 1702-1081.

Cox, W., 2004. Water Supply vs. the Environment: Finding the Appropriate Balance. *World Water Congress 2004.* (138):365.

Diffenbaugh, N.S., Pal, J.S. Trapp, R.J., and Giorgi, F., 2005. Fine-scale processes regulate the response of extreme events to global climate change. *Proceedings of the National Academy of Sciences of the United States of America.* 102(44): 15774-15778.

Eagleson, P.S., 1978. Climate, soil, and vegetation, 2, The distribution of annual precipitation derived from observed storm sequences. *Water Resources Research.* (14): 713–721.

El-Nasr, A.A, Arnold, J.G., Feyen, J., and Berlamont, J., 2005. Modelling the hydrology of a catchment using a distributed and semi-distributed model. *Hydrological*

Processes. 19: 573-587.

Falkenmark, M. and Rockstrom, J., 2004. *Balancing Water and Human Nature.* Earthscan, 8-12 Camden High Street, London. 239 pp.

Federer, C.A., Vörösmarty, C. and Fekete, B. 2003. Sensitivity of annual evaporation to soil and root properties in two models of contrasting complexity. *Journal of Hydrometeorology.* 4: 1276-1290.

Federer, C.A. 1996. Intercomparison of methods for calculating potential evaporation in regional and global water balance models. *Water Resources Research*. 32(7): 2315- 2321.

Grimm, N.B., Chacon, A., Dahm, C.N., Hostetler, S.W., Lind, O.T., Starkweather, P.L., Wurtsbaugh, W.W., 1997. Sensitivity of Aquatic Ecosystems to Climatic and Anthropogenic Changes: The Basin and Range, American Southwest and Mexico. *Hydrological Processes.* 11: 1023-1041.

Gurtz, J., Baltenzweiler, A., and Lang, H., 1999. Spatially distributed hydrotope-based modeling of evopotranspiriation and runoff in mountainous basins. *Hydrological Processes.* 13: 2751-2768.

Gutierrez-Jurado, H.A., Vivoni, E.R., Harrison, J.B.J., Guan, H. 2006. Ecohydrology of root zone water fluxes and soil development in complex semiarid rangelands. *Hydrological Processes.* 20: 3289-3316.

Haan, C.T., 1977. *Statistical methods in hydrology*. The Iowa State University Press. 378 pp.

Hamlet, A.F. and Lettenmaier, D.P., 2007. Effects of 20th century warming and climate variability on flood risk in the western U.S. *Water Resources Research.* 43, W06427: 1-17.

Hargreaves, G. H. 1975. Moisture availability and crop production. *Transportation-ASAE.* 18(5): 980–984.

Hargreaves, G.L., Hargreaves, G.H., and Riley, J.P., 1985. Irrigation Water Requirements for Senegal River Basin. *Journal of Irrigation and Drainage Engineering-ASCE.* 111(3): 265-275.

Hargreaves, G.H., and Allen, R.G., 2003. History and evaluation of Hargreaves evapotranspiration equation. *Journal of Irrigation and Drainage Engineering-ASCE.* 129(1): 53-63.

Hay, L.E., Clark, M.P., Pagowski, M., Leavesley, G.H., and Gutowski Jr., W.J., 2006. One-way coupling of an atmospheric and a hydrologic model in Colorado. *Journal of Hydrometeorology.* 7: 569-589.

Houghton, J. T. and Ding, Y., (Eds.), 2001. *IPCC: 2001: Climate Change 2001: The Scientific Bias*, Cambridge, Cambridge University Press. 873 pp.

Jenson, S.K., and Domingue, J.O., 1988. Extracting Topographic Structure from Digital

Elevation Data for Geographic Information System Analysis. *Photogrammetric Engineering and Remote Sensing.* 54(11): 1593-1600.

Jenson, S.K., 1991. Applications of Hydrologic Information Automatically Extracted From Digital Elevation Models. *Hydrological Processes.* 5(1): 31-44.

Liang, X., Lettenmaier, D.P., Wood, E.F., and Burges, S.J., 1994. A simple hydrologically based model of land surface water and energy fluxes for general circulation models. *Journal of Geophysical Research.* 99(D7): 14,415-14,428.

Liang, X., Wood, E.F., and Lettenmaier, D.P., 1996. Surface soil moisture parameterization of the VIC-2L model: Evaluation and modification. *Global and Planetary Change.* 13: 195-206.

Liang, X., and Xie,Z.H., 2001. A new surface runoff parameterization with subgrid-scale soil heterogeneity for land surface models. *Advances in Water Resources.* 24(9-10):1173–1193.

Madsen, T., and Figdor, E., 2007. *When it Rains it Pours: Global Warming and the Rising Frequency of Extreme Precipitation in the United States.* Environment America – Research & Policy Center: 1-48.

Marks, D. M., Dozier, J., and Frew, J., 1984. Automated Basin Delineation From Digital Elevation Data. *Geoprocessing.* 2: 299-311.

Martinec, J., A. Rango, and E. Major. 1983. *The Snowmelt-Runoff Model (SRM) User's Manual*. NASA Reference Publication. 1100, Washington, D.C., USA. 118 pp.

McCabe, G. J. and Hay, L. E.: 1995, Hydrological Effects of Hypothetical Climate Change in the East River Basin, Colorado, U.S.A., *Hydrological Sciences.* 40: 303–317.

Molles, Jr., M.C., Dahm, C.N., and Crocker, M.T., 1992. *Climatic Variability and Streams and Rivers in Semi-arid Regions*. N.H.R.I. Symposium Series 7, Environment Canada: 197-202.

Molnar, P. and Ramierez, J.A., 2001. Recent Trends in Precipitation and Steramflow in the Rio Puerco Basin. *Journal of Climate.* 14(10): 2317-2328.

Moore, D.,1996-2001. Meteorological data and Time Domain Reflectometery data. Sevilleta Long Term Ecological Research program website. http://sev.lternet.edu/.

Morris, D.G., and Heerdegen, R.G., 1988. Automatically Drained Catchment Boundries and Channel Netowrks and their Hydrological Applications. *Geomorphology.* 1: 131-141.

Nash, J.E. and Sutcliffe, J.V., 1970. River flow forecasting through conceptual models part I- A discussion of principles. *Journal of Hydrology.* 10: 282-290.

Nash, L. L. and Gleick, P. 1991, The Sensitivity of Streamflow in the Colorado Basin to Climatic Changes, *Journal of Hydrology.* 125: 221–241.

Nijssen, B., and D. P. Lettenmaier 1997. Streamflow simulation for continental-scale river basins. *Water Resources Research.* 33(4): 711–724.

O'Callaghan, J.F., and Mark, D.M., 1984. The Extraction of Drainage Networks From Digital Elevation Data. *Computer Vision, Graphics and Image Processing* 28: 328-344.

Peterson, T. C., Zhang, X., Brunet-India, M., and. Vazquez-Aguirre, J. L., 2008. Changes in North American extremes derived from daily weather data. *Journal of Geophysical Research.* 113: 1-9.

POST, 2006. *Balancing Water Supply and the Environment*. The Parliamentary Office of Science and Technology, 7 Millbank, London. 1-4

Rawls, W.J., Ahuja, L.R., Brakensiek, D.L., Shirmohammadi, A., 1993. *Handbook of Hydrology, Chapter 5: Infiltration and soil water movement*. McGraw-Hill, Inc. p 5.14.

Rodriguez-Iturbe, I., and Eagleson, P.S., 1987. Mathematical models of rainstorm events in space and time. *Water Resources Research.* 23(1): 181-190.

Rutter, A.J., Kershaw, K.A., Robins, P.C., and Morton, A.J., 1971. A predictive model of rainfall interception in forests. I. Derivation of the model from observations in a plantation of Corsican pine. *Journal of Agricultural Meteorology*. 9: 367-384.

Salvucci, G.D., 1997. Soil and moisture independent estimation of stage-to evaporation from potential evaporation and albedo or surface temperature. *Water Resources Research.* 33: 111-122.

Seager, R., Ting, M., Held, I., Kushinr, Y., Lu, J., Vecchi, G., Huang, H-P. , Harnik, N., Leetmaa, A., Lau, N-C., Li, C., Velez, J., and Naik, N., 2007. Model Projections of an Imminent Transition to a More Arid Climate in Southwestern North America. *Science Express.* 316(5828): 1181-1184.

Serrat-Capdevila, A., Valde's, J.B., Gonzalez Perez, J., Baird, K., Mata, L.J., and Maddock III, T., 2007. Modeling climate change impacts and uncertanity on the hydrology of a riparian system: The San Pedro Basin (Arizona/Sonora). *Journal of Hydrology.* 347(1-2): 48-66.

Shuttleworth, W.J., 1993. *Handbook of Hydrology, Chapter 4: Evaporation*. McGraw -Hill, Inc. P 4.18.

Singer, M.B., and Dunne, T., 2004. An empirical-stochastic, event-based program for simulating inflow from a tributary network: Framework and application to the Sacramento River basin, California, *Water Resources Research*. 40(W07506): 1-19.

Singh, V.P., 1995. *Computer Models of Watershed Hydrology*. Chapter 1, Watershed Modeling. Water Resources Publications, Highlands Ranch, Colorado: 1-22.

Simcox, A.C., 1983, The Rio Salado at flood, *New Mexico Geological Society*

Guidebook, 34th Field Conference, Socorro region II.325-327.

Stephens, D.B. and Knowlton, R.K., 1986. Soil water movement and recharge through sand at a semiarid site in New Mexico. *Water Resources Research.* 22(6): 881-889.

Stephens, D.B., Cox, W., and Havlena, J., 1988. *Field study of ephemeral stream infiltration and recharge* – Technical completion report. New Mexico Water Resources Research Institute 228: 188 pp.

Tarboton, D.G., Bras, R.L., and Rodriguez-Iturbe, I., 1988. The Fractal Nature of River Networks. *Water Resources Research.* 24(8): l3l7-l322.

Tarboton, D.G.,1997. A New Method for the Determination of Flow Directions and Upslope Areas in Grid Digital Elevation Models. *Water Resources Research.* 33(2): 309-319.

Tarboton, D.G., Bras, R.L., and Rodriguez-Iturbe, I.,1991. On the Extraction of Channel Networks from Digital Elevation Data. *Hydrological Processes.* 5(1): 81-100.

Tarboton, D.G., Bras, R.L., and Rodriguez-Iturbe, I.,1992. A Physical Basis for Drainage Density. *Geomorphology.* 5(1/2): 59-76.

Toepfer, K. Interview, 1999. UNEP Helmsman Toepfer Addresses Environmental Challenges. *Environmental Science and Technology.* 33(1): 18-23.

Tucker, G.E., and Bras, R.L., 2000. A stochastic approach to modeling the role of rainfall variability in drainage basin evolution. *Water Resources Research.* 36(7): 1953-1964.

USACE. 1994. *Multi-sub-basin modeling*. Report EM 1110-2-1417: 10.1-10.5.

Ward, F.A., B.H. Hurd, T. Rahmani, and N. Gollehon. 2006. Economic impacts of federal policy responses to drought in the Río Grande Basin. *Water Resources Research.* 42(W03420): 1-13.

Watson, R.T. et al. (Eds.), 2007. *IPCC: 2007: Climate Change 2007: AR4 Synthesis Report,* Cambridge, Cambridge University Press. 52 pp.

Wigmosta, M.S., Vail, L.W., and Lettenmaier, D.P., 1994. A distributed hydrology-vegetation model for complex terrain. *Water Resources Research*. 30(6): 1665-1679.

Yardley, 2007. Beneath Booming Cities, China's Future Is Drying Up. *New York Times*

YDP/Cienega Workgroup, 2005. *Balancing Water Needs on the Lower Colorado River: Recommendations of the Yuma Desalting Plant/Cienega de Santa Clara Workgroup*. YDP/Cienega Workgroup, Arizona. 29 pp.

APPENDIX 1 – VARIABLE INFILTRATION CAPACITY CURVE

Calculation of infiltration capacity using *b*-curve begins with Equation A.1.1

$$\left(1-\frac{i_o}{i_m}\right)=\left(1-A_{sf}\right)^{\frac{1}{b}}. \tag{A.1.1}$$

Rearranging Equation A.1.1 allows us to find the fraction of the area that is saturated (A_{sf}) in terms of the maximum infiltration capacity of the soil, i_m, and the consumed infiltration capacity, i_o, as:

$$A_{sf}=1-\left(1-\frac{i_o}{i_m}\right)^b. \tag{A.1.2}$$

We can also rearrange Equation A.1.1 in order to solve for the consumed infiltration capacity:

$$i_o=i_m\left[1-\left(1-A_{sf}\right)^{\frac{1}{b}}\right]. \tag{A.1.3}$$

In order to find i_m, we use the following expression:

$$V_m=\int_0^{i_m}\left(1-\frac{i_o}{i_m}\right)^b di\ , \tag{A.1.4}$$

where V_m is the maximum volume of storage space for the soil. Equation A.1.4 represents the area under the infiltration capacity curve when integrating with respect to the y-axis.

Using the following *u* substitution:

$$u=1-\frac{i_o}{i_m} \tag{A.1.5}$$

$$du=-\frac{i_o}{i_m}di_o \tag{A.1.6}$$

and changing the limits of integration:

$$\begin{aligned} i&=0 & u&=1\\ i&=i_m, & u&=0 \end{aligned} \tag{A.1.7}$$

we arrive at the integral below:

$$V_m = i_m \int_0^1 (u)^b du \,. \tag{A.1.8}$$

Integrating the right side and evaluating with the new limits results in Equation A.1.10 which expresses V_m in terms of i_m and b, and can be rearranged to solve for the maximum infiltration capacity of the soil i_m.

$$V_m = i_m \left[\frac{u^{(1+b)}}{(1+b)} \Big|_0^1 \right] \tag{A.1.9}$$

$$V_m = \frac{i_m}{(1+b)} \tag{A.1.10}$$

$$i_m = V_m (1+b) \,. \tag{A.1.11}$$

Finding the consumed infiltration capacity i_o requires the same integration described in Equations A.1.4 – A.1.6, using the volume consumed (V_o) in place of V_m. The limits of integration change as follows:

$$\begin{array}{ll} i = 0 & u = 1 \\ i = i_o\,, & u = 1 - \dfrac{i_o}{i_m}\,, \end{array} \tag{A.1.12}$$

which gives us the following integral:

$$V_o = i_m \int_{1-\frac{i_o}{i_m}}^1 (u)^b du \,. \tag{A.1.13}$$

Integrating the right side and evaluating with the new limits results in Equation A.1.15, which expresses V_o in terms of i_m and b, and can be rearranged to solve for the maximum infiltration capacity of the soil i_m.

$$V_o = i_m \left[\frac{u^{(1+b)}}{(1+b)} \Bigg|_{1-\frac{i_o}{i_m}}^{1} \right] \tag{A.1.14}$$

$$V_o = i_m \left[\frac{1}{(1+b)} - \frac{\left(1-\frac{i_o}{i_m}\right)^{1+b}}{(1+b)} \right]. \tag{A.1.15}$$

Equations A.1.16 – A.1.22 show algebraic manipulation necessary to arrive at Equation A.1.23 which describes the consumed infiltration capacity i_o in terms of the maximum and consumed volumes (V_m and V_o).

$$\frac{V_o}{i_m} = \frac{1}{(1+b)} - \frac{\left(1-\frac{i_o}{i_m}\right)^{1+b}}{(1+b)} \tag{A.1.16}$$

$$\frac{V_o}{i_m}(1+b) = 1 - \left(1-\frac{i_o}{i_m}\right)^{1+b} \tag{A.1.17}$$

$$\frac{V_o}{V_m} = 1 - \left(1-\frac{i_o}{i_m}\right)^{1+b} \tag{A.1.18}$$

$$\left(1-\frac{i_o}{i_m}\right)^{1+b} = 1 - \frac{V_o}{V_m} \tag{A.1.19}$$

$$1-\frac{i_o}{i_m} = \left(1-\frac{V_o}{V_m}\right)^{\frac{1}{1+b}} \tag{A.1.20}$$

$$\frac{i_o}{i_m} = 1 - \left(1-\frac{V_o}{V_m}\right)^{\frac{1}{1+b}} \tag{A.1.21}$$

$$i_o = i_m \left[1 - \left(1-\frac{V_o}{V_m}\right)^{\frac{1}{1+b}} \right] \tag{A.1.22}$$

$$i_o = V_m\left(1+b\right)\left[1-\left(1-\frac{V_o}{V_m}\right)^{\frac{1}{1+b}}\right] \tag{A.1.23}$$

To find the consumed infiltration capacity as a function of the volumetric water content (Equation A.1.26), we simply put the volumes in terms of soil moisture.

$$V_o = \theta_i - \theta_r$$
$$V_m = \phi - \theta_r \tag{A.1.24, A.1.25}$$

$$i_o = \left(\phi-\theta_r\right)\left(1+b\right)\left\{1-\left[1-\frac{\left(\theta_i-\theta_r\right)}{\left(\phi-\theta_r\right)}\right]^{\frac{1}{1+b}}\right\} \tag{A.1.26}$$

APPENDIX 2 – EFFECTIVE HYDRAULIC CONDUCTIVITY

This appendix describes a modification of the Brooks-Corey equation to calculate drainage using an effective hydraulic conductivity. We begin with the original Brooks- Corey equation:

$$Q_{out} = -K_s A\left(\frac{\theta_i - \theta_r}{\phi - \theta_r}\right)^{(m)} \tag{A.2.1}$$

where K_S is the saturated hydraulic conductivity (cm/hr), A is the area, θ_i is the current volumetric water content (m^3/m^3), ϕ is the porosity of the soil, θ_r is the residual water content (m^3/m^3), and m is defined as:

$$m = \left(\frac{2}{B_P} + 3\right). \tag{A.2.2}$$

The volumetric flow rate out of the soil can also be described as a change in volume of water over time:

$$Q_{out} = \frac{dV}{dt}, \tag{A.2.3}$$

With:

$$V = Az_i\theta_i, \tag{A.2.4}$$

where z_i is the depth of the soil layer. Substituting Equation A.2.4 in to Equation A.2.3 gives us Equation A.2.5, which relates the flow rate to the change in volumetric water content with time.

$$Q_{out} = Az_i \frac{d\theta_i}{dt}. \tag{A.2.5}$$

Setting Equation A.2.5 equal to Equation A.2.1 gives us the following:

$$Az_i \frac{d\theta_i}{dt} = -K_s A\left(\frac{\theta_i - \theta_r}{n - \theta_r}\right)^m. \tag{A.2.6}$$

Rearranging Equation A.2.5 we arrive at:

$$\frac{d\theta_i}{dt} = -B\left(\theta_i - \theta_r\right)^m, \tag{A.2.7}$$

where:

$$B = \frac{K_s}{z_i\left(n - \theta_r\right)^m} \ . \tag{A.2.8}$$

To solve Equation A.2.7, we must perform a series of integrations beginning with:

$$\int_{\theta_i}^{\theta_{final}} \frac{d\theta}{dt} = -\int_{t_1}^{t_2} B\left(\theta_i - \theta_r\right)^m \tag{A.2.9}$$

By combining like terms, we get Equation A.2.10

$$\int_{\theta_i}^{\theta_{final}} \frac{d\theta}{\left(\theta - \theta_r\right)^m} = -\int_{t_1}^{t_2} B dt \ , \tag{A.2.10}$$

which we can integrate and evaluate the right side easily because B is constant. Using a u substitution of $u = \left(\theta - \theta_r\right)$ and $du = d\theta$, and changing the limits of integration on the left side we get:

$$\int_{\theta_i - \theta_r}^{\theta_{final} - \theta_r} \frac{du}{u^m} = -B\left(t_2 - t_1\right). \tag{A.2.11}$$

By integrating the left side, evaluating for the new limits gives us Equation A.2.12, which can be rearranged to Equation A.2.13.

$$\left(\frac{1}{1-m}\right) u^{1-m} \Bigg|_{\theta_i - \theta_r}^{\theta_f - \theta_r} = -B\left(t_2 - t_1\right) \tag{A.2.12}$$

$$\left(\theta_{final} - \theta_r\right)^{1-m} = -\left(1-m\right) B\left(t_2 - t_1\right) + \left(\theta_i - \theta_r\right)^{1-m} \tag{A.2.13}$$

A final algebraic manipulation provides us with a saturation adjusted water content in the form of equation A.2.14.

$$\theta_{final} = \left[-(1-m) B (t_2 - t_1) + (\theta_i - \theta_r)^{1-m} \right]^{\frac{1}{1-m}} + \theta_r \qquad \text{(A.2.14)}$$

This new water content is used to calculate the effective hydraulic conductivity of the soil using the Brooks Corey definition:

$$\frac{K(\theta)}{K_s} = \left(\frac{\theta_{final} - \theta_r}{n - \theta_r} \right)^m \qquad \text{(A.2.15)}$$

or

$$k(\theta) = Bz \left(\theta_{final} - \theta_r \right)^m \qquad \text{(A.2.16)}$$

APPENDIX 3 – POWERSIM IMPLEMENTATION

This appendix will guide a user through the Powersim model. We will first describe the input requirements, and then show model screen shots. Next we will discuss computational efficiency.

Input requirements

After the watershed in a study area is delineated using GIS and the HRUs have been created, the soil and vegetation parameter data from each HRU must be input into an EXCEL spreadsheet (rain.xls). This spreadsheet contains all input and output files used by the model. HRU parameters are inserted into the "JUNK" sheet in the rain.xls file. Stochastic rainfall forcing parameters can be derived by running the (GAUGE)eventrain.m file for each gauge in Matlab, (GAUGE) is a keyword that is replaced by the name of the rain gauge to be used, and inserted into the "RainGauges" sheet. Stochastic temperature forcing parameters can be derived by running the (GAUGE)Temp.m file for each gauge in Matlab, and inserted into the Temperatures sheet. Actual precipitation data used for model testing is inserted into the "Socorro Raingauge" sheet. Precipitation data from the Deep Well site is located in the "Deep Well Rainfall" sheet. Each of these input sheets is used by Powersim to deliver data to the watershed model.

Model screenshots

This section provides the reader with screenshots from Powersim showing the components of the model.

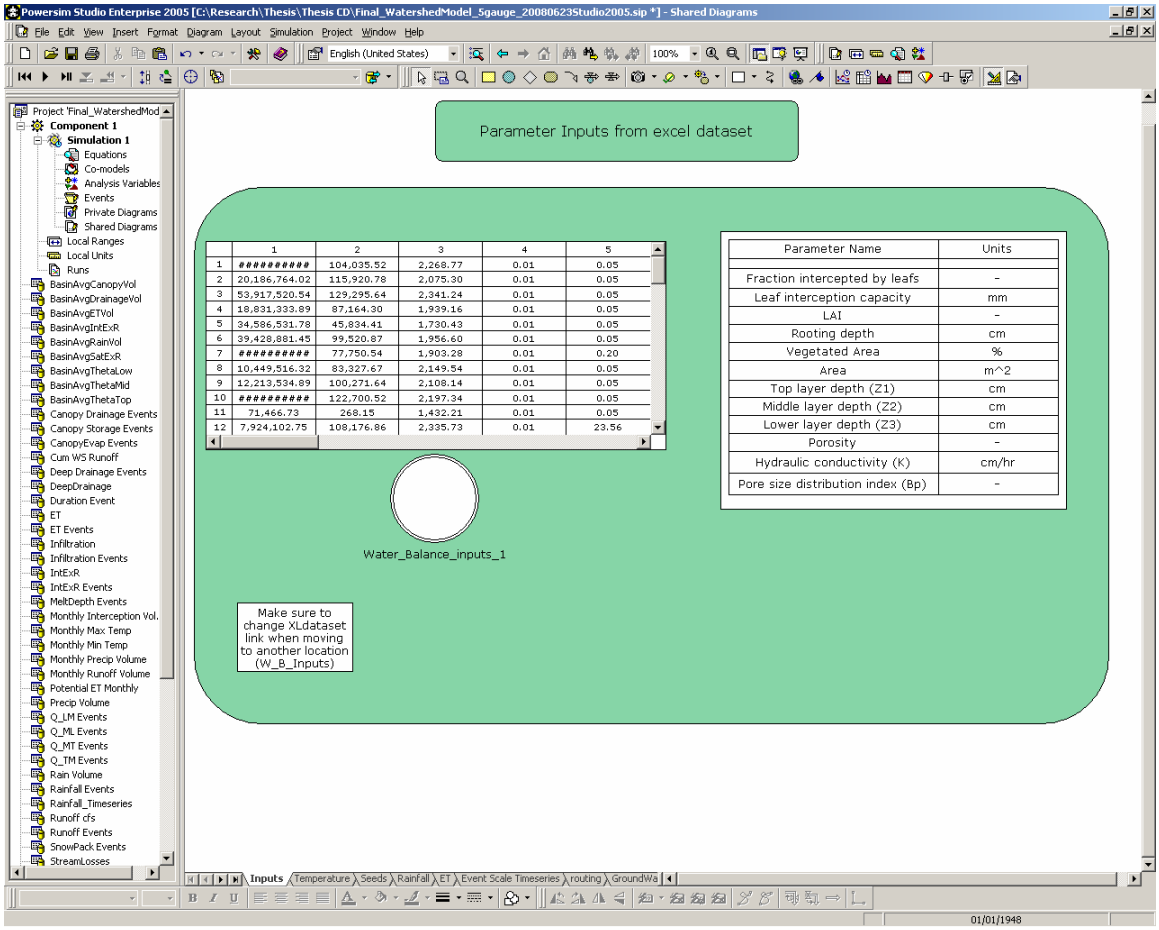

FIGURE 55**:** Parameter inputs for HRUs linked to rain.xls

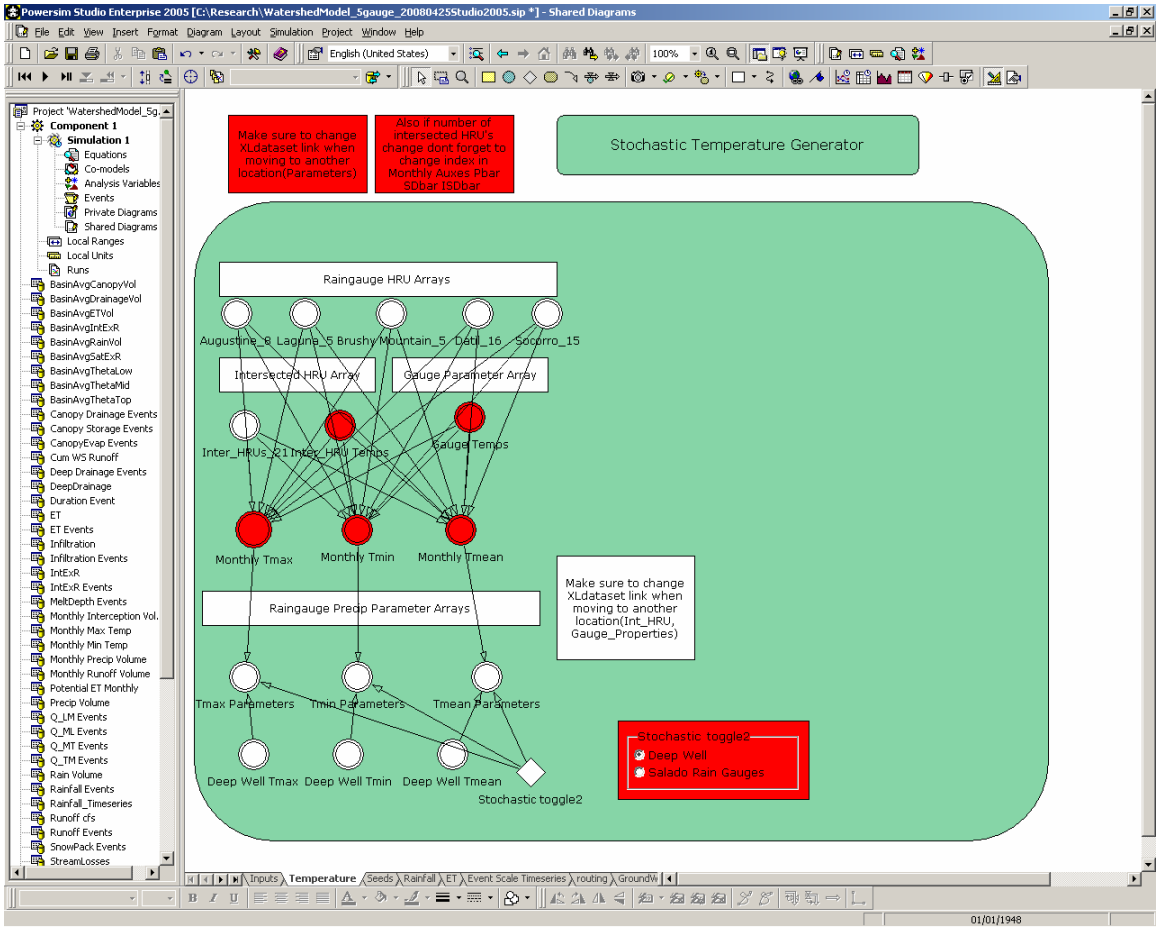

FIGURE 56: Stochastic temperature generator, which uses parameters from the five surrounding gauges.

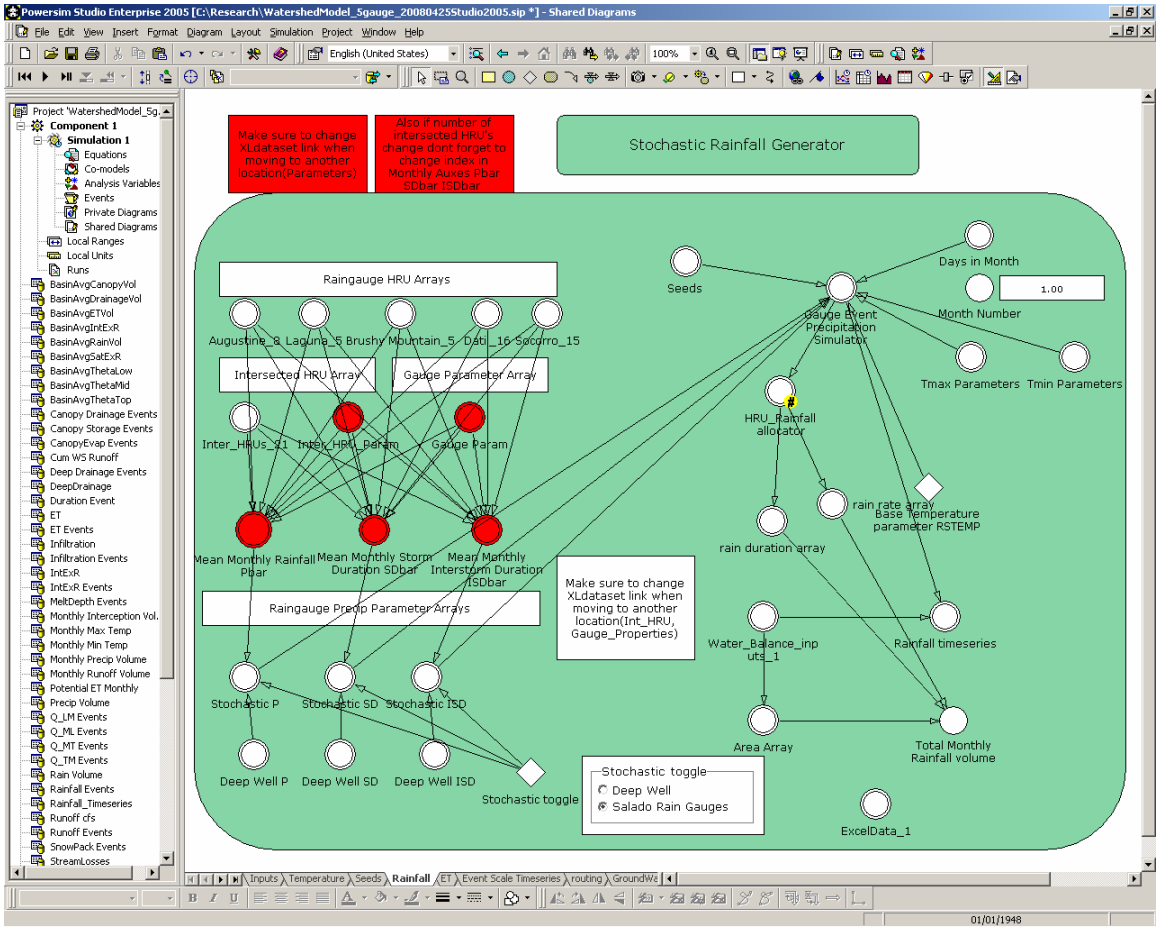

FIGURE 57: Stochastic precipitation generator, which uses parameters from the five surrounding gauges.

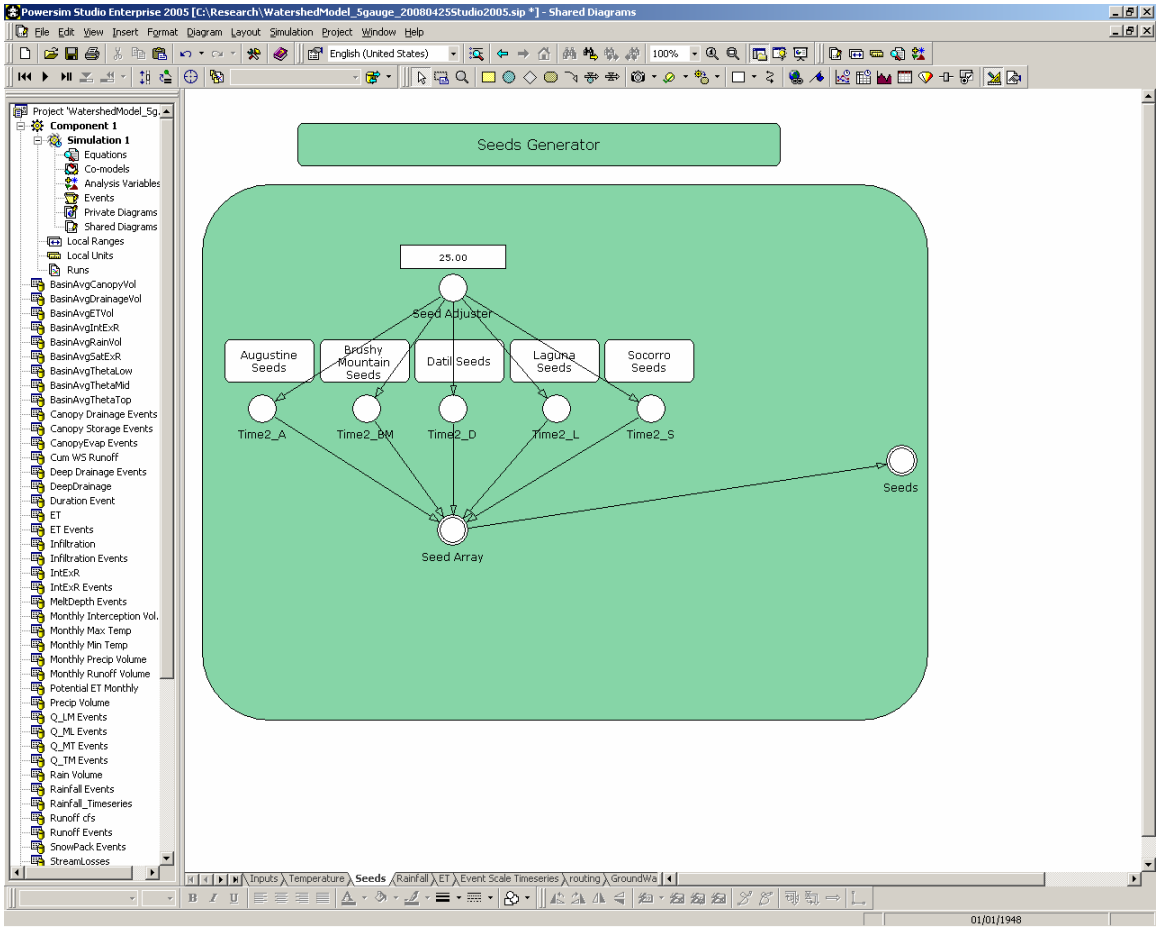

FIGURE 58: Seed generator used for stochastic simulations.

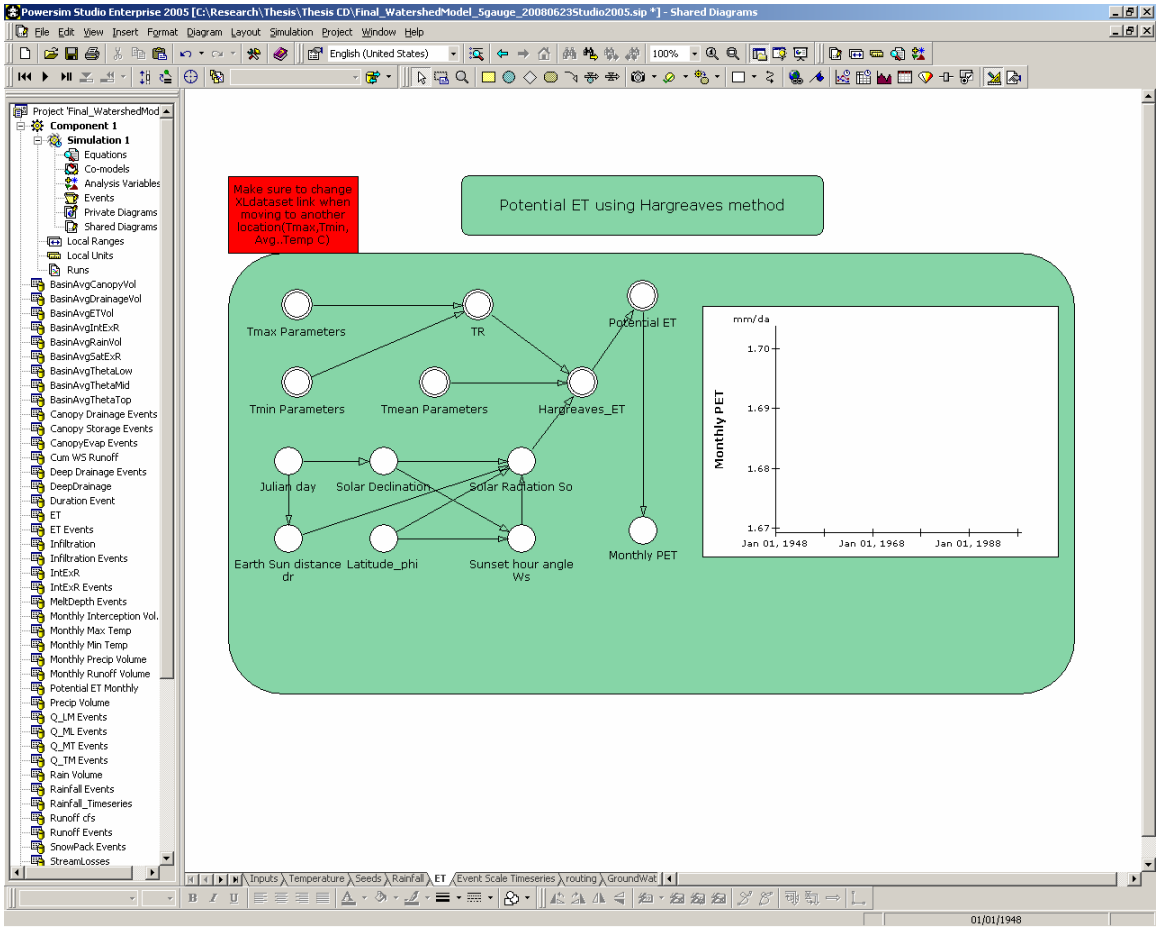

FIGURE 59: Calculates potential ET using Hargreaves method.

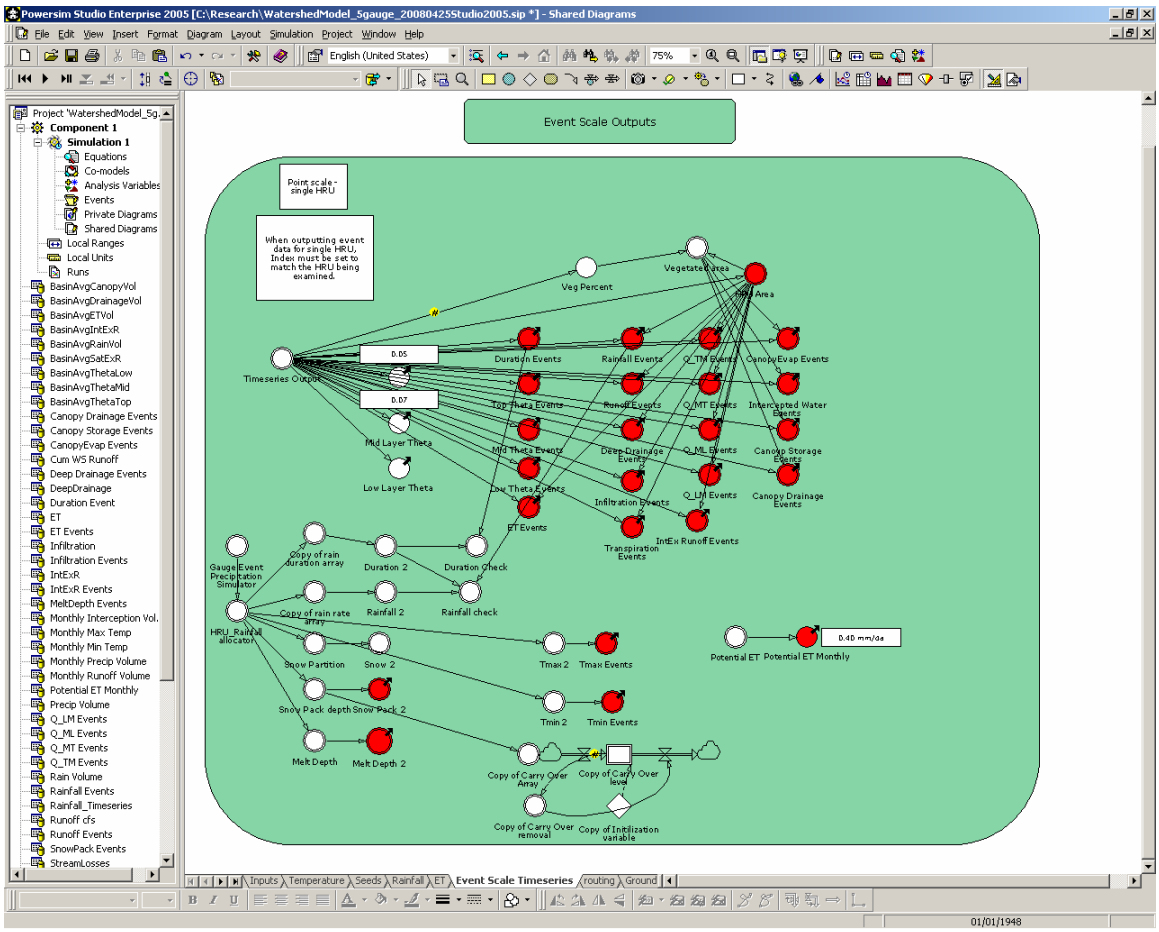

FIGURE 60: Links to send event scale output to rain.xls

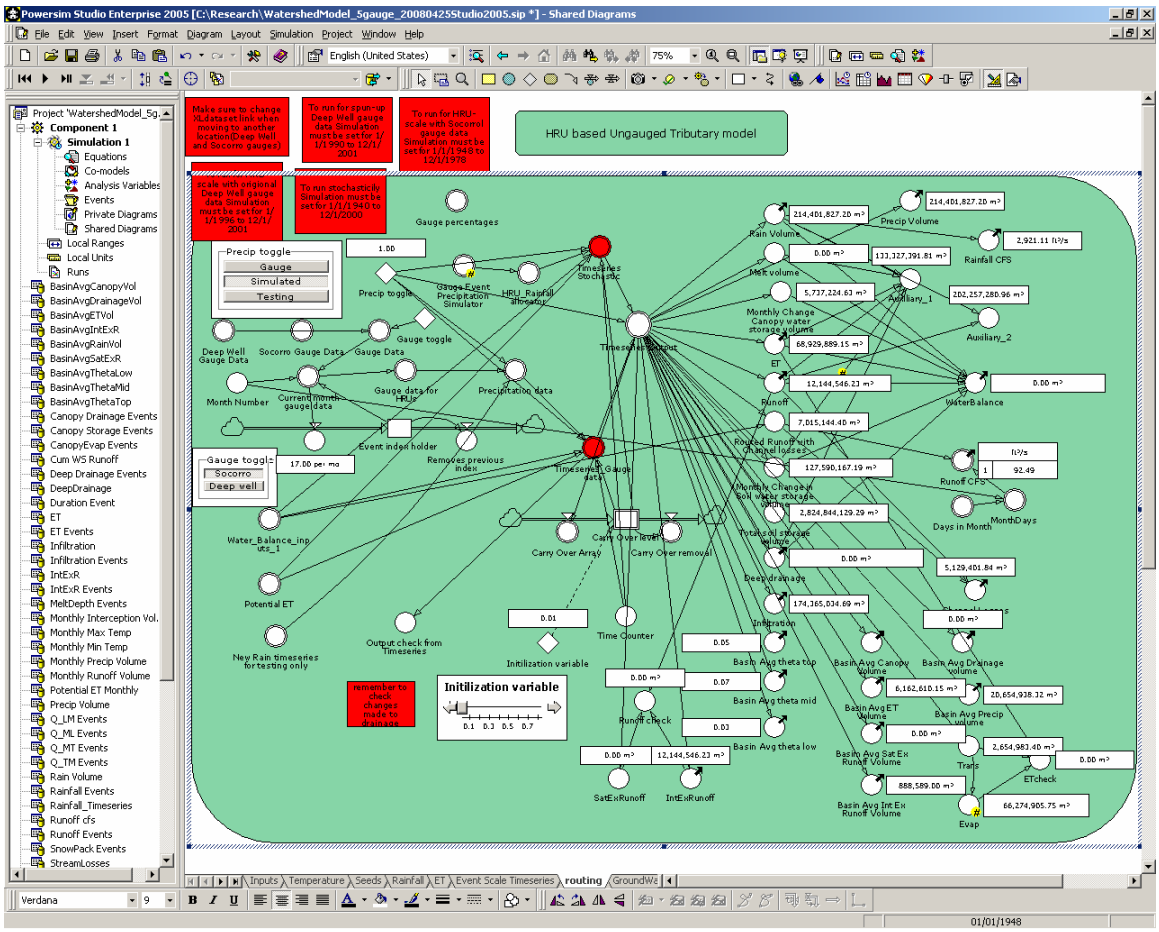

FIGURE 61: Main module for the watershed model. The shaded circles contain VB-script code to run the model using either stochastic or gauge forcing data.

Computational efficiency

The watershed model requires a great amount of preprocessing both with HRU generation and calculation of parameter values for vegetation, soil, and atmospheric forcing. However, in contrast to the long set-up time, the model is currently capable of performing a 50yr run using stochastically generated precipitation data in 11min. This makes it possible to test the models response to changes in atmospheric forcing quickly, which is ideal for decision-making settings. All output data is put into either the “Event Theta" tab or the “Runoff” tab in the rain.xls spreadsheet.

VB-script code

The following are the contents of the main VB-script code used in the model.

```
VBFUNCTION( "result" = HRU,1..102,1..24|
        "WBArray"= Water_Balance_inputs_1,
        "Rain" = 'HRU_Rainfall allocator',
              "Timecounter" = 'Time Counter',
        "ET" ='Potential ET'*1<<da/mm>>,
              "CoArray"='Carry Over level',
              "toggle" = 'Precip toggle'
              |

"if toggle = 1 then"
// Initialize output arrays

"For m = 0 to 69 "
          "For j = 0 to 99"
          "For h = 0 to 4"
            "result(m,j,0) = -1" //A (-1) in the ST column indicates the end of data series
          "Next"
          "Next"
"Next"

// Initialize watershed cumulative variables

"WsRunoff = 0"
"WsPrecip = 0"
"WsET = 0"
"WsMelt = 0"
"WsSoilStorage_change = 0"
"WsCanopyW_Change = 0"
"WsInfil = 0"
"Ws_count = 0"
"WsDrainage = 0"
"WsSatExR = 0"
"WsIntExR = 0"
"WsSnow = 0"
"WsA = 0"
"Ws_Trans = 0"
"WSE = 0"
"WsRain = 0"
"WsWVmax = 0"

"Ws_theta_top_avg =0"
"Ws_theta_mid_avg = 0"
"Ws_theta_low_avg = 0"
"Ws_CanopyW_avg = 0"
"Ws_ET_avg = 0"
"Ws_SatExR_avg = 0"
"Ws_IntExR_avg = 0"
"Ws_Drainage_avg = 0"
"Ws_Rain_avg = 0"
```

```
"TLWV = 0 "//Top layer m^3
"MLWV = 0"//Middle layer m^3
"LLWV = 0"//Lower layer m^3
"ULWV = 0"//Upper two layers water volume m^3

//Begining of loop over HRU's imputs
"For m = 0 to 67"//when using simulated rainfall change to (0 to HRU-2)

//Fill variables for each HRU based on data from WBArray
"A = WBArray(m,0)" //Area <<m^2>>
"FrintL = WBArray(m,14)" // Fraction of precip intercepted by leafs
"Ks = WBArray(m,19)/(100)" // Hydraulic conductivity of soil <<m/hr>> 4 orig, 19 new, 20 effective
"LAI = WBArray(m,10)"// Leaf Area Index
"IntcapL = WBArray(m,13)" // Interception capacity of leafs <<mm>>
"z1 = WBArray(m,7)/100" // Top layer soil depth <<m>>
"z2 = WBArray(m,8)/100" // Upper Layer soul depth <<m>>
"z3 = WBArray(m,9)/100" // Lower Layer soil depth <<m>>
"Bp = WBArray(m,5)" // Pore size distribution Index
"n = WBArray(m,6)" // Porosity of soil
"RootingDepth = WBArray(m,12)/100" //Rooting depth of plant cm
"VegPercent = WBArray(m,11)"// Percent of HRU that is covered by vegetation
"HRUnumber = m" // number of HRU
"Pack_A = A" // area of snow pack, when =A, snow is evenly distributed over HRU
"Duration = 0"// Length of storm or interstorm period

"cumRain=0"
"CumCanopyW_change = 0"
"CumSoilStorage_change = 0"
"CumDrainage = 0"
"CumRunoff = 0"
"CumPrecip = 0"
"CumET = 0"
"CumMelt = 0"
"CumInfil = 0"
"CumSatExR = 0"
"CumIntExR = 0"
"CumSnow = 0"
"CumE = 0"
"CumTrans =0"
"CumCanopyW = 0"
"cumtime = 0"

"Theta_top = 0"
"Theta_mid = 0"
"Theta_low = 0"
"Theta_Final = 0"
"Theta_Final_Top =0"
"Theta_mt = 0"
"Theta_lm = 0"
"Area_unsat = 0"
"Aras_sat = 0"

"ntop=n"
"Kstop = ks"// set to Sand for Deep well simulations
"Bptop = bp"
```

```
//Soil Water

//Maximum water volume
"TLWVmax = A*n*z1"//Top layer m^3 limits evaporation
"MLWVmax = A*n*z2"//Middle layer m^3
"LLWVmax = A*n*z3"//Lower layer m^3
"ULWVmax = TLWVmax+MLWVmax+LLWVmax"// The top and middle layers are combined and
treated as single (upper) layer to prevent over estimation of runoff

"WVmax = TLWVmax+MLWVmax+LLWVmax"//maximum volume of water in entire soil column

//Soil column volume
"TLV = A*z1"//Top layer m^3
"MLV = A*z2"//Upper layer m^3
"LLV = A*z3"//Lower layer m^3
"ULV = TLV+MLV+LLV"//Upper layer top + mid used in saturatation excess runoff m^3

//need for each HRU
"theta_s_star = WBArray(m,17)"// star soil moisture replaces theta f
"theta_r = WBArray(m,15)" // hydroscopic soil moisture content
"theta_s = theta_s_star"// threshold soil moisture content
"theta_w = WBArray(m,16)" // wilting point soil moisture content
"theta_f = theta_s_star"// field capacity soil moisture content
"theta_sat = n "//saturated  soil moisture contentWBArray(m,18)

//for deep well test
"theta_s_startop = theta_s_star"// star soil moisture replaces theta f
"theta_rtop = theta_r" // hydroscopic soil moisture content
"theta_stop = theta_s_startop"// threshold soil moisture content
"theta_wtop = theta_w" // wilting point soil moisture content
"theta_ftop = theta_s_startop"// field capacity soil moisture content
"theta_sattop = Theta_sat "//saturated  soil moisture contentWBArray(m,18)
"rainpercent = CoArray(m,0)"

"if theta_r> CoArray(m,1) then"
"theta_topP = theta_r"
"else"
"theta_topP = CoArray(m,1)"
"end if"

"if  theta_r> CoArray(m,2) then"
"theta_midP = theta_r"
"else"
"theta_midP = CoArray(m,2)"
"end if "

"if theta_r > CoArray(m,3) then"
"theta_lowP = theta_r"
"else"
"theta_lowP = CoArray(m,3)"
"end if "

"CanopyWP = CoArray(m,4)"

"if theta_topP<theta_r then"
```

```
            "theta_topP = theta_r"
"end if"

"if theta_midP<theta_r then"
            "theta_midP = theta_r"
"end if"

"if theta_lowP<theta_r then"
            "theta_lowP = theta_r"
"end if"


"TLWVP = theta_topP*TLV" //Top layer m^3
"MLWVP = theta_midP*MLV"//Middle layer m^3
"LLWVP = theta_lowP*LLV"//Lower layer m^3
"ULWVP = TLWVP+MLWVP+LLWVP"//Upper two layers water volume m^3

//////////infamous b parameter
"bi = 1.4" // shape parameter for VIC model ??shape of hillslope??

//Initial Soil water volume  reset soil to residual at end of each month
//need to use previous months theta for each HRU this will require output of theta
//for each layer

//Initalization from previous month
"CanopyW = CanopyWP"
"CanopyWI = CanopyWP"
"TLWV = TLWVP "//Top layer m^3
"MLWV = MLWVP"//Middle layer m^3
"LLWV = LLWVP"//Lower layer m^3
"ULWV = ULWVP"//Upper two layers water volume m^3
"TLWVI = TLWVP "//Top layer m^3
"MLWVI = MLWVP"//Middle layer m^3
"LLWVI = LLWVP"//Lower layer m^3
"ULWVI = ULWVP"//Upper two layers water volume m^3
"theta_top = theta_topP" //Top layer m^3
"theta_mid = theta_midP"//Middle layer m^3
"theta_low = theta_lowP"//Lower layer m^3


"potentialET = ET(m)/24000 "//<<m/hr> converted from mm/da
"RhoW = 1000"//density of water


//Initalization of variables

"Available_water = 0"
"theta_top_avg = 0"
"theta_mid_avg = 0"
"theta_low_avg = 0"
"count = 0"
"Rain_avg = 0"

" "
//event loop
"FOR i = 0 to 99"
```

```
  "IF Rain(m,i,0) < 0 then"
          "IF i = 0 then"
          "result(m,0,0) = rainpercent"
          "result(m,0,1) = theta_mid"
          "result(m,0,2) = theta_low"
          "result(m,0,3) = CanopyW"
          "result(m,0,6) = theta_top"
          "End IF"

      "exit FOR"

   "else"
          "IF Rain(m,i,0) > 0 then"
                  "potentialET = 0"//ET is turned off during storm events
          "else"
                  "potentialET = ET(m)/24000"// EvapTrans rate m/hr
          "end IF"
   "End IF"

//more initalization
"P=0"
"A_veg = 0"
"Throughfall = 0"
"Available_water = 0"
"Available_space = 0"
"SatEx_Runoff = 0"
"IntEx_Runoff = 0"
"RainPercent = 0"
"UnIntVol = 0"
"IntVol = 0"
"IntC = 0"
"IntR = 0"
"K_theta = 0"
"Runoff = 0"
"rainfall = 0"
"rainvol = 0"
"precipvol = 0"
"meltrate = 0"
"meltvol = 0"
"Q_TM = 0"
"Q_MT = 0"
"Q_ML = 0"
"Q_LM = 0"
"Q_deep = 0"
"Q_base = 0"
"DeepDrainage = 0"
"CanopyIN = 0"
"CanopyEvap = 0"
"Impervious_vol = 0"
"InfiltrationRate = 0"
"Infil = 0"
"Inflow_vol = 0"
"EvapTop = 0"
"EvapMid = 0"
"TransTop = 0"
```

```
"TransMid = 0"
"TransLow = 0"
"Transpiration = 0"
"ActualET = 0"
"ET2 =0"
"B = 0"
"m2 = 0"
"ic = 0"
"ic_max = 0"

//input of precipitation timeseries
"Rainfall = Rain(m,i,0)/1000"//Rainfall rate in m/hr
"Duration = 24*Rain(m,i,1)"//length of storm in hours
"Snow = Rain(m,i,2)/1000" // snowfall rate in m/hr
"Snowpack = Rain(m,i,3)/1000" // snowpack depth in mm
"Meltrate = Rain(m,i,4)/1000"// melt rate in m/hr
"Precip = Rain(m,i,5)/1000"// melt rate in m/hr
"P = Rainfall+Snow"//  precip rate m/hr
"Rainvol = Rainfall*A*Duration"
"Precipvol = Precip*A*Duration"//m^3
"Meltvol = Meltrate*A*Duration"//m^3 ??need value for area covered by snow pack???
"cumtime = cumtime + Duration"//cumulative time in hrs

"if Timecounter > 2005 then"
"Rainfall = 0"
"Rainvol = 0"
"Precipvol =0"//m^3
"Meltvol =0"
"End IF"


//Interception by vegetated area
"A_veg = A*VegPercent"

"IntC = (LAI*IntcapL*.001)*A_veg"

//Interception rate
//??only rainfall is intercepted what happens to snow that falls on canopy??
"IntR = (FrintL*LAI)*Rainfall"
        "If Rainfall <= 0 then"
                "IntR=0"
        "end IF"

        "IF IntR>=Rainfall then"
                "IntR = Rainfall"
        "else"
                "IntR = (FrintL*LAI)*Rainfall"// m/hr
        "end IF"

//////////////////
//"IntR = 0" test for increasing soilmoisture by removing interception
//////////////////

//Potential Interception volume
"Intvol = IntR*A_veg*Duration"//m^3 ??portion of vegetated area doesnt recieve rainfall???
```

```
//Un-intercepted volume automatically gets to ground
"UnIntvol = Rainvol-Intvol"//this is rain only

//input of water to the canopy
        "IF (IntR*Duration*A_veg+CanopyW)>=IntC then"
                "CanopyIN = (IntC - CanopyW)"
                "Throughfall = (IntR*Duration*A_veg-CanopyIn)" //m^3
                "CanopyW = IntC"  //m^3
                "IntVol = CanopyIN"
        "else"
                "CanopyIN = IntR*Duration*A_veg" //m^3 check this it doesnt look right????
                "CanopyW = CanopyW+Intvol" //m^3
                "Throughfall = 0"
        "end IF"

//Canopy Evap
        "IF potentialET*A_veg*duration =< CanopyW then"
                "CanopyEvap = potentialET*A_veg*duration" //m^3/hr
        "else"
                "CanopyEvap = CanopyW" //m^3/hr
        "end IF"

"CanopyW = CanopyW - CanopyEvap"

        "IF CanopyW <= 0 then"
                "CanopyW = 0" //m^3
        "end IF"

//Start new structure for VIC: throughfall reaching soil -> calculate runoff -> infiltration
//-> fill upper layer -> ET -> drainage -> diffusion/reallocation of water -> loop
" "

//Add melt water from snowpack to throughfall
"Available_water = Throughfall + UnIntVol+ MeltVol"//m^3  water is now distributed evenly over area

"Area_unsat = A-Area_sat"

"IF Area_unsat = 0 then"
"Area_unsat = 0.00001"
"end IF"

//infiltration excess runoff is calculated by comparing throughfall
//rate to hydraulic conductivity for soil
"if Duration>0 then"
"InfiltrationRate = Available_water/((Area_unsat)*Duration)"//m/hr
"else"
"InfiltrationRate = 0"
"end if"

//"InfiltrationRate =0" testing remove later
        "IF InfiltrationRate<=Ks then"
                "IntEx_Runoff = 0"
        "else"
                "IntEx_Runoff = Available_water-Ks*(Area_unsat)*Duration"//m^3
                "Available_water = Ks*(Area_unsat)*Duration"
        "end IF"
```

```
//Volume of void space in soil column that can be filled
"Available_space = ULV*theta_sat - ULWV"

//Saturation excess runoff
        "IF Available_water>=Available_space then"
                "SatEx_Runoff = Available_water - Available_space"//m^3
                "Available_water=Available_space"
                "ULWV = ULWVmax"
        "else"
                "SatEx_Runoff = 0"
        "end IF"

// compare infiltration capacity (ic) from previous time step to icmax
"ic = ULWVmax*(1+bi)*(1-(1-(ULWV/ULWVmax))^(1/(1+bi)))"
"ic_max = (ULWVmax)*(1+bi)" // maximum infiltration capacity
"Area_sat = (1-(1 - (ic/ic_max))^bi)*A"//new saturated area based on VIC moisture re-distribution
"Area_unsat = A-Area_sat"

//Total runoff
"Runoff = IntEx_Runoff + SatEx_Runoff"//m^3
"Inflow_vol =  Available_water"
"Available_water = 0"
"Infil = Inflow_vol"//needed for output dont remove

        "IF Inflow_vol >=0 then"
                "if Inflow_vol > (TLWVmax - TLWV)+ (MLWVmax - MLWV) then"

                        "LLWV = LLWV + (Inflow_vol-((TLWVmax - TLWV)+ (MLWVmax -
MLWV)))"
                        "TLWV = TLWVmax"
                        "MLWV = MLWVmax"
                        "Inflow_vol = 0"
                "else"
                        "if Inflow_vol > (TLWVmax - TLWV) then"
                        "MLWV = MLWV + (Inflow_vol-(TLWVmax - TLWV))"
                        "TLWV = TLWVmax"
                        "Inflow_vol = 0"
                        "else"

                        "TLWV = TLWV + Inflow_vol" // Top layer m^3
                        "Inflow_vol = 0"
                        "end IF"
                "end IF"
        "end IF"


//Soil moisture
"theta_top = TLWV/(TLV)" //Top layer
"theta_mid = MLWV/(MLV)" //Upper layer
"theta_low = LLWV/(LLV)" //Lower layer

//Top layer evap
        "IF theta_top <= theta_rtop then"
                "EvapTop = 0"
        "else"
```

```
                "EvapTop = (potentialET*Area_sat +potentialET*(A-Area_sat)*(theta_top -
theta_rtop)/(ntop - theta_rtop)) *duration "

                "IF Duration > 48 then"
                "ET2 = 0.811*Evaptop*(48/Duration)"
                "Evaptop = 0.5*(Evaptop+ET2)"
                "end if"

                "IF TLWV < EvapTop then"
                        "EvapTop = TLWV - A*z1*theta_rtop"

                "End IF"

                "if TLWV < A*z1*theta_rtop then"
                        "EvapTop = 0"
                "end IF"
        "End IF"

"TLWV = TLWV - EvapTop"

"theta_top = TLWV/(TLV)" //Top layer

//Mid layer evap
        "IF theta_mid <= theta_r then"
                "EvapMid = 0"
        "else"
                "EvapMid = (potentialET*Area_sat +potentialET*(A-Area_sat)*(theta_mid - theta_r)/(n
- theta_r)) *duration "//)*duration"

                "IF Duration > 48 then"
                "ET2 = 0.811*EvapMid*(48/Duration)"
                "EvapMid = 0.5*(EvapMid+ET2)"
                "end if"

                "IF MLWV< EvapMid then"
                        "EvapMid = MLWV - A*z2*theta_r"

                "End IF"
                "if MLWV < A*z2*theta_r then"
                        "EvapMid = 0"
                "end IF"

        "End IF"

"MLWV = MLWV - EvapMid"
"theta_mid = MLWV/(MLV)" //Mid layer

//percentage of root depth in each soil layer
        "IF RootingDepth < z1 then"
                "r1 = 1"
                "r2 = 0"
                "r3 = 0"
        "else"
                "r1=z1/RootingDepth"

                "IF RootingDepth < z2+z1 then"
```

```
                    "r2 = (RootingDepth - z1)/RootingDepth"
                    "r3 = 0"
                "else"
                    "r2 = z2/RootingDepth"
                    "r3 = (RootingDepth - (z2+z1))/RootingDepth"

                "end IF"
        "end IF"

//Top layer trans Add seasonal component turn off transpiration in winter. Decide which
//of ET components should be applied first.
        "IF theta_top< theta_rtop then"
            "TransTop = 0"
        "End IF"

        "IF theta_top > theta_ftop then"
            "TransTop = potentialET*r1*A_veg*duration" //m^3

            "IF Duration > 48 then"
            "ET2 = 0.811*TransTop*(48/Duration)"
            "Transtop = 0.5*(TransTop+ET2)"
            "end if"
        "else"
            "IF theta_top < theta_wtop then"
                "TransTop = 0"
            "else"
                "TransTop = (potentialET*A_veg*r1*duration*(theta_top -
theta_wtop)/(theta_ftop - theta_wtop))"


                "IF Duration > 48 then"
                "ET2 = 0.811*Transtop*(48/Duration)"
                "Transtop = 0.5*(Transtop+ET2)"
                "end if"

            "end IF"
        "End IF"

        "IF TLWV-A*z1*theta_rtop < TransTop then"
            "IF TLWV > A*z1*theta_rtop then"
                "TransTop = TLWV - A*z1*theta_rtop"
            "else"
                "TransTop = 0"
            "End IF"
        "End IF"

        "TLWV = TLWV - TransTop"

        "theta_top = TLWV/(TLV)" //Top layer

//Middle layer trans
        "IF theta_mid< theta_w then"
            "TransMid = 0"
        "End IF"

        "IF theta_mid > theta_f then"
```

```
                "TransMid = potentialET*r2*A_veg*duration"//m^3/hr

                "IF Duration > 48 then"
                "ET2 = 0.811*TransMid*(48/Duration)"
                "TransMid = 0.5*(TransMid+ET2)"
                "end if"

        "else"
                "IF theta_mid < theta_w then"
                        "TransMid = 0"
                "else"
                        "TransMid=(potentialET*A_veg*r2*duration*(theta_mid - theta_w)/(theta_f -
theta_w))"//)"

                        "IF Duration > 48 then"
                        "ET2 = 0.811*TransMid*(48/Duration)"
                        "TransMid = 0.5*(TransMid+ET2)"
                        "end if"

                "end IF"
        "End IF"

        "IF MLWV-A*z2*theta_w < TransMid then"
                "IF MLWV > A*z2*theta_w then"
                        "TransMid = MLWV - A*z2*theta_w"

                "else"
                        "TransMid = 0"
                "End IF"
        "End IF"

 "Output_test= theta_mid"
                "MLWV = MLWV - TransMid"
                "theta_mid = MLWV/(MLV)"


//Lower layer trans
        "IF theta_low< theta_r then"
                "TransLow = 0"
        "End IF"

        "IF theta_low > theta_f then"
                "TransLow = potentialET*r3*A_veg*duration"//m^3/hr

                "IF Duration > 48 then"
                "ET2 = 0.811*TransLow*(48/Duration)"
                "TransLow = 0.5*(TransLow+ET2)"
                "end if"


        "else"
                "IF theta_low < theta_w then"
                        "TransLow = 0"
                "else"
                        "TransLow = (potentialET*A_veg*r3*duration*(theta_low - theta_w)/(theta_f -
theta_w))"
```

```
                        "IF Duration > 48 then"
                        "ET2 = 0.811*TransLow*(48/Duration)"
                        "TransLow = 0.5*(TransLow+ET2)"
                        "end if"

                "end IF"
        "End IF"

        "IF LLWV- A*z3*theta_w < TransLow then"
                "IF LLWV > A*z3*theta_w then"
                        "TransLow = LLWV - A*z3*theta_w"

                "else"
                        "TransLow = 0"
                "End IF"
        "End IF"

"LLWV = LLWV - TransLow"
"theta_Low = LLWV/(LLV)"


"IF Theta_top-Theta_rtop<0.001 then"
        "theta_top = Theta_rtop"
"end IF"

"IF Theta_mid-Theta_r<0.001 then"
        "theta_mid = Theta_r"
"end IF"

"IF Theta_low-Theta_r<0.001 then"
        "theta_low = Theta_r"
"end IF"

"IF abs(Theta_top-Theta_mid)<0.001 then"
        "theta_top = Theta_mid"
"end IF"

"IF abs(Theta_mid-Theta_low)<0.001 then"
        "theta_mid = Theta_low"
"end IF"

// Flows between layers
//Q_TM downward flow from top layer to middle
"IF theta_top > theta_mid then"
        "m2 = (2/Bptop)+3"
        "B = Ks/(z1*((n-theta_r)^m2))"
        "Theta_Final_top = Theta_r +((((Theta_top-Theta_r)^(1-m2))-(1-m2)*B*duration)^(1/(1-m2)))"
        "K_theta = B*z1*(Theta_final_top - Theta_r)^m2" //new effective hydraulic conductivity
        "Q_TM = Ks*A*duration"

        "IF Q_TM> TLWV - A*z1*theta_mid  then"
                "Q_TM = TLWV - A*z1*theta_mid"

        "End IF"
        "If TLWV<A*z1*theta_rtop then"
```

```
                "Q_TM = 0"
        "End IF"


        "MLWV = MLWV + Q_TM"
        "TLWV = TLWV - Q_TM"
"else"
        "Q_TM = 0"
"end IF"

"theta_top = TLWV/(TLV)" //Top layer
"theta_mid = MLWV/(MLV)" //Upper layer

"IF abs(Theta_mid-Theta_low)<0.001 then"
        "theta_mid = Theta_low"
"end IF"

"IF Theta_mid-Theta_r<0.001 then"
        "theta_mid = Theta_r"
"end IF"

//Q_mid2low  downward flow from middle to lower
"IF theta_mid > theta_low then"

        "m2 = (2/Bp)+3"
        "B = Ks/(z2*((n-theta_r)^m2))"
        "Theta_Final_mid = Theta_r+((((Theta_mid-Theta_r)^(1-m2))-(1-m2)*B*duration)^(1/(1-m2)))"
        "K_theta = B*z2*(Theta_final_mid - Theta_r)^m2"    // new effective hydraulic conductivity
        "Q_ML = K_theta*A*duration"  //m^3

        "IF Q_ML> MLWV - A*z2*theta_low  then"
                "Q_ML = MLWV - A*z2*theta_low"
        "End IF"
        "IF MLWV<A*z2*theta_r then"
                "Q_ML = 0"
        "End IF"


        "MLWV = MLWV - Q_ML"
        "LLWV = LLWV + Q_ML"
"else"
        "Q_ML = 0"
"end IF"

"theta_mid = MLWV/(MLV)" //Upper layer
"theta_low = LLWV/(LLV)" //Lower layer

"IF Theta_top-Theta_r<0.001 then"
        "theta_top = Theta_r"
"end IF"

"IF ABS(Theta_mid-Theta_top)<0.001 then"
        "theta_mid = Theta_top"
"end IF"

"IF Theta_mid-Theta_r<0.001 then"
```

```
        "theta_mid = Theta_r"
"end IF"

//Upward diffusion from Middle layer to Top layer
"IF theta_mid > theta_top then"
        "m2 = (2/Bp)+3"
        "theta_mt = (theta_top+theta_mid)/2"
        "B = Ks/(z2*((n-theta_mt)^m2))"
        "Theta_Final= Theta_mt+((((Theta_mid-Theta_mt)^(1-m2))-(1-m2)*B*duration)^(1/(1-m2)))"
        "K_theta = B*z2*(Theta_Final - Theta_mt)^m2"// new effective hydraulic conductivity
        "Q_MT =K_theta*A*duration"

        "IF Q_MT> MLWV - A*z2*theta_top  then"
                "Q_MT = MLWV - A*z2*theta_top"
        "End IF"
        "If MLWV<A*z2*theta_r then"
                "Q_MT = 0"
        "End IF"

        "TLWV = TLWV + Q_MT"
        "MLWV = MLWV - Q_MT"
"end IF"

"theta_top = TLWV/(TLV)" //Top layer
"theta_mid = MLWV/(MLV)" //Upper layer


"IF Theta_low-Theta_r<0.001 then"
        "theta_low = Theta_r"
"end IF"

//Deep Drainage and Base flow
"IF theta_low > theta_r then"
        "d_fract = 1"// fraction of volume leaving layer 3 as drainage
        "b_fract = 1-d_fract"// fraction of volume leaving layer 3 as base flow to stream network
        "m2 = (2/Bp)+3"
        "B = Ks/(z3*((n-theta_r)^m2))"
        "Theta_Final = Theta_r+((((Theta_low-Theta_r)^(1-m2))-(1-m2)*B*duration)^(1/(1-m2)))"
        "K_theta = B*z3*(Theta_final - Theta_r)^m2"// new effective hydraulic conductivity
        "Q_deep = d_fract*K_theta*A*duration" // m^3
        "Q_base = b_fract*K_theta*A*duration"

        "IF (Q_deep + Q_base) > LLWV - A*z3*theta_r  then"

                "IF Q_deep > 0 then"
                "Q_deep = d_fract*LLWV - A*z3*theta_r/2" // m^3
                "end IF"
                "IF Q_base > 0 then"
                "Q_base = b_fract*LLWV - A*z3*theta_r/2"
                "end IF"

        "End IF"

"else"
        "Q_deep = 0" // m^3
        "Q_base = 0"
```

```
"end IF"

"IF Theta_low-Theta_r<0.001 then"
        "theta_low = Theta_r"
"end IF"
"IF LLWV>A*z3*theta_r then"
        "IF LLWV-A*z3*theta_r<Q_deep + Q_base then"
                "Q_deep = d_fract*(LLWV-A*z3*theta_r)" // m^3 drainage to aquifer
                "Q_base = b_fract*(LLWV-A*z3*theta_r)"
                "LLWV = A*z3*theta_r"
        "else"
        "LLWV = LLWV - (Q_deep+Q_base)" //Lower layer m^3
        "end IF"
"else"
        "Q_deep = 0"
        "Q_base = 0"
"End IF"

"theta_low = LLWV/(LLV)" //Lower layer

"Runoff = Runoff + Q_base"

"IF Theta_mid-Theta_r<0.001 then"
        "theta_mid = Theta_r"
"end IF"

"IF abs(Theta_low-Theta_mid)<0.001 then"
        "theta_low = Theta_mid"
"end IF"

"IF Theta_low-Theta_r<0.001 then"
        "theta_low = Theta_r"
"end IF"

//Upward diffusion from lower layer to middle layer
"IF theta_low > theta_mid then "
        "m2 = (2/Bp)+3"
        "theta_lm = (theta_low+theta_mid)/2"
        "B= Ks/(z3*((n-theta_r)^m2))"
        "Theta_Final = theta_r+((((theta_low-Theta_r)^(1-m2))-(1-m2)*B*duration)^(1/(1-m2)))"
        "K_theta = B*z3*(Theta_Final - Theta_r)^m2" //new effective hydraulic conductivity
        "Q_LM = K_theta*A*duration"// 0" m^3

        "IF Q_LM> LLWV - A*z3*theta_mid  then"
                "Q_LM = LLWV - A*z3*theta_mid"
        "End IF"

        "If LLWV<A*z3*theta_r then"
                "Q_Lm = 0"
        "End IF"

        "MLWV = MLWV + Q_LM"
        "LLWV = LLWV - Q_LM"
"end IF"

"ULWV = TLWV + MLWV + LLWV"
```

```
//Water volume

//recalculate thetas based on new water volumes
"theta_top = TLWV/TLV" //Top layer
"theta_mid = MLWV/MLV" //Upper layer
"theta_low = LLWV/LLV" //Lower layer

"if theta_top<theta_r then"
"theta_top = theta_r"
"End If"

"if theta_mid<theta_r then"
"theta_mid = theta_r"
"End If"

"if theta_low<theta_r then"
"theta_low = theta_r"
"End If"

//HRU theta summation
"theta_top_avg = theta_top_avg + theta_top"
"theta_mid_avg = theta_mid_avg + theta_mid"
"theta_low_avg = theta_low_avg + theta_low"


"ActualET =(EvapTop+EvapMid+TransTop+TransMid+CanopyEvap+TransLow)"
//potentialET*A*Duration"
"Transpiration = (TransTop+TransMid+TransLow)"
"Esc = (CanopyEvap+ EvapTop+EvapMid)"
" "

// to output results set “result (m,i) = desired output variable”
"result(m,i,0) = rainpercent"
"result(m,i,1) = theta_mid"
"result(m,i,2) = theta_low"
"result(m,i,3) = CanopyW"
"result(m,i,4) = A"
"result(m,i,5) = Runoff"
"result(m,i,6) = theta_top"
"result(m,i,7) = Q_TM"
"result(m,i,8) = Q_MT"
"result(m,i,9) = Q_ML"
"result(m,i,10) = Duration"
"result(m,i,11) = ActualET"
"result(m,i,12) = Rainvol"
"result(m,i,13) = Infil"
"result(m,i,16) = Q_deep"
"result(m,i,15) = Q_LM"
"result(m,i,14) = Intvol"
"result(m,i,17) = Transpiration"
"result(m,i,18) = CanopyEvap"
"result(m,i,19) = Throughfall"
"result(m,i,20) = TransMid"
"result(m,i,21) = Precipvol"
"result(m,i,22) =IntEx_Runoff"
"result(m,i,23) =SatEx_Runoff"
```

```
//cululative volumes for events
"CumMelt = CumMelt + Meltvol"
"CumCanopyW_Change = CanopyW - CanopyWI"
"CumSoilStorage_Change =(TLWV + MLWV+ LLWV) -(TLWVI+MLWVI+LLWVI) "//"
"CumDrainage = CumDrainage + Q_deep"
"CumRunoff = CumRunoff+Runoff"//m^3
"CumRain = CumRain + Rainvol"//m^3
"CumPrecip = CumPrecip + Precipvol"
"CumET = CumET + ActualET"//m^3
"CumInfil = CumInfil + Infil"
"CumSatExR = CumSatExR + SatEx_Runoff"
"CumIntExR = CumIntExR + IntEx_Runoff"

"CumCanopyW = CumCanopyW + CanopyW"
"CumTrans = CumTrans + Transpiration"
"CumE = CumE + Esc"

//Carry over values
"result(m,101,0) = rainpercent"
"result(m,101,1) = theta_mid"
"result(m,101,2) = theta_low"
"result(m,101,3) = CanopyW"
"result(m,101,6) = theta_top"
"count = count+1"
"next"


"theta_top_avg = theta_top_avg/count"
"theta_mid_avg = theta_mid_avg/count"
"theta_low_avg = theta_low_avg/count"

//HRU Monthly times HRU areas for basin averaging
"theta_top_avg = theta_top_avg*A"
"theta_mid_avg = theta_mid_avg*A"
"theta_low_avg = theta_low_avg*A"
"CanopyW_avg = CumCanopyW*A"
"ET_avg = CumET*A"
"SatExR_avg = CumSatExR*A"
"IntExR_avg = CumIntExR*A"
"Drainage_avg = CumDrainage*A"
"Rain_avg = CumRain*A"
"Precip_avg = CumPrecip*A"


"Ws_theta_top_avg = Ws_theta_top_avg + theta_top_avg"
"Ws_theta_mid_avg = Ws_theta_mid_avg + theta_mid_avg"
"Ws_theta_low_avg = Ws_theta_low_avg + theta_low_avg"
"Ws_CanopyW_avg = Ws_CanopyW_avg + CanopyW_avg"
"Ws_ET_avg = Ws_ET_avg + ET_avg"
"Ws_Precip_avg = Ws_Precip_avg + Precip_avg"
"Ws_SatExR_avg = Ws_SatExR_avg + SatExR_avg"
"Ws_IntExR_avg = Ws_IntExR_avg + IntExR_avg"
"Ws_Drainage_avg = Ws_Drainage_avg + Drainage_avg"
"Ws_count = Ws_count + 1"
"Ws_Rain_avg = Ws_Rain_avg + Rain_avg"
```

```
//Initial values stored to check change in storage volume for water balance
"TLWVI = TLWV" //Top layer m^3
"MLWVI = MLWV"//Middle layer m^3
"LLWVI = LLWV"//Lower layer m^3
"ULWVI = ULWV"//Upper two layers water volume m^3

//cumulative volumes for watershed
"WsDrainage = WsDrainage + CumDrainage"
"WsRain =WsRain + CumRain"
"WsPrecip = WsPrecip + CumPrecip"
"WsET = WsET + CumET"
"WsRunoff = WsRunoff + CumRunoff"
"WsCanopyW_Change = WsCanopyW_Change + CumCanopyW_Change"
"WsSoilStorage_Change = WsSoilStorage_Change + CumSoilStorage_Change"
"WsWVmax = WsWVmax + WVmax"
"WsMelt = WsMelt + CumMelt"
"WsInfil = WsInfil + CumInfil"
"WsA = WsA + A"
"WsSatExR = WsSatExR + CumSatExR"
"WsIntExR = WsIntExR + CumIntExR"

"Ws_Trans = Ws_Trans + CumTrans"
"WSE = WSE + CumE"
"next"

//Basin averaged results theta
"Ws_theta_top_avg = Ws_theta_top_avg/WsA"
"Ws_theta_mid_avg = Ws_theta_mid_avg/WsA"
"Ws_theta_low_avg = Ws_theta_low_avg/WsA"
"Ws_CanopyW_avg = Ws_CanopyW_avg/WsA"
"Ws_ET_avg = Ws_ET_avg/WsA"
"Ws_SatExR_avg = Ws_SatExR_avg/WsA"
"Ws_IntExR_avg = Ws_IntExR_avg/WsA"
"Ws_Drainage_avg = Ws_Drainage_avg/WsA"
"Ws_Rain_avg = Ws_Rain_avg/WsA"
"Ws_Precip_avg = Ws_Precip_avg/WsA"

//watershed scale outputs
"result(0,0,0) = output_test"//change to match others0 remove
"result(68,100,0) = RainPercent"
"result(68,100,1) = Ws_theta_mid_avg"
"result(68,100,2) = Ws_theta_low_avg"
"result(68,100,3) = Ws_CanopyW_avg"
"result(68,100,4) = WsA"
"result(68,100,5) = WsRunoff"
"result(68,100,6) = Ws_theta_top_avg"
"result(68,100,7) = WsMelt"
"result(68,100,8) = WsWVmax"
"result(68,100,9) = WsCanopyW_Change"
"result(68,100,10) = WsSoilStorage_change"
"result(68,100,11) = WsDrainage"
"result(68,100,12) = WsRain"
"result(68,100,13) = WsInfil"
"result(68,100,14) = WsET"
"result(68,100,15) = Ws_SatExR_avg"
```

```
"result(68,100,16) = WsPrecip"
"result(68,100,17) = Ws_ET_avg"
"result(68,100,18) = Ws_Drainage_avg"
"result(68,100,19) = Ws_IntExR_avg"
"result(68,100,20) = Ws_Precip_avg"
"result(68,100,21) = Ws_Trans"
"result(68,100,22) = WsIntExR"
"result(68,100,23) = WsSatExR"

"end if"
)
```

The following are the contents of the VB-script code used to calculate potential evapotranspiration.

```
VBFUNCTION("Storm" = HRU|
        "Seed"=Seeds,
        "Month" = 'Days in Month',
              "Tmeanb" = 'Tmean Parameters',
        "So" = 'Solar Radiation So'*1<<da/mm>>,
              "TrArray" = TR
              |

"Tempseed = Seed(0,0)"
"t=Seed(4,4)"

"rnd(-1)"
"randomize(t)"

"For k = 0 to 69" // initialize variables Set K, when using simulated rainfall change to (0 to HRU-2)
            "Tr = TrArray(k,0)"
            "Tmean = TrArray(k,1)"

            "Trand = rnd(Tempseed)" // set random temp value

            "ET_H = (0.0023*So*(Tmean+17.8)*(Tr)^(0.5)) "//Hargreaves ET equation mm/da

            "Storm(k) = ET_H"

  "next" // HRU loop
)*1<<mm/da>>
```

The following are the contents of the VB-script code used to calculate the stochastic precipitation forcing

```
VBFUNCTION("Storm" = 1..5,1..100,1..9|
        "Pbar"='Stochastic P',//mm/hr
        "SDbar"='Stochastic SD',
        "ISDbar"='Stochastic ISD',
        "Seed"=Seeds,
        "Month" = 'Days in Month',
              "Tmaxb" = 'Tmax Parameters',
              "Tminb" = 'Tmin Parameters',
```

```
            "Tb" = 'Base Temperature parameter RSTEMP'*1<<1/C>>|

"For k = 0 to 4" // initialize variables Set K K, when using simulated rainfall change to (0 to HRU-2)

   "for j = 0 to 99"
     "Storm(k,j,0) = -1"
     "Storm(k,j,1) = -1"
     "Storm(k,j,2) = -1"
     "Storm(k,j,3) = -1"
     "Storm(k,j,4) = -1"
     "Storm(k,j,5) = -1"
     "Storm(k,j,6) = -1"
     "Storm(k,j,7) = -1"
     "Storm(k,j,8) = -1"
   "next"
"next"

"Snowpack = 0"
"Snow = Snowpack"
"Mf = 0.0011 * 100"  //should not be > 1 update snow density (100)

"m2 = Month(0)"

"For k = 0 to 4 " // initialize variables

"Tempseed = Seed(0,k)"
"SDseed = Seed(1,k)"
"Rseed = Seed(2,k)"
"ISDseed = Seed(3,k)"
"t=Seed(4,k)"
//"t = (250207) "

"rnd(-1)"
"randomize(t)"

  "rain = 0"
  "precip = 0"
  "timesum = 0"
  "Prand = 0"
  "SDrand = 0"
  "ISDrand = 0"
  "Trand = 0"
  "P = 0"
  "SnowFrac = 0"
  "SD = 0"
  "ISD = 0"
  "i = 0"
  "MeltFrac = 0"
  "MeltVol = 0"
  "Melt=0"
  "SnowpackP = 0"

// begin loop for storms
  "For i = 0 to 99"

     "Prand = rnd(Rseed)" // set random precipitation value
```

```
"SDrand = rnd(SDseed)" // set random storm duration value
"ISDrand = rnd(ISDseed)" // set random interstorm duration value
"Trand = rnd(Tempseed)" // set random temp value
"Snowpack = SnowpackP" // previous snow pack level
        "P=0"
        "TrandI = rnd(Tempseed)"// set random temp value for interstorm period
        "ISD = -ISDbar(k,Month(0))*LOG(ISDrand)" // calculate new interstorm duration (days)

        "timesum = timesum+ISD" // calculate current elapsed time

        "Tmax = -Tmaxb(k,Month(0))*LOG(TrandI)"
        "Tmin = -Tminb(k,Month(0))*LOG(TrandI)"
        "Tavg = (Tmax+Tmin)/2"//2

"If Tmin>= Tb then"
                "SnowFrac = 0"
"else"
         "if Tmax<= Tb then"
                "SnowFrac = 1"
         "else"
        "if Tmax > Tmin then"
                "SnowFrac = (Tb-Tmin)/(Tmax-Tmin)"
        "else"
                "SnowFrac = (Tb-Tmax)/(Tmin-Tmax)"
        "end if"
   "end if"
"end if"

"If Tavg>= Tb then"
        "MeltFrac = Mf*(Tavg-Tb)"
        "else"
        "MeltFrac = 0"
"end if"

        "Rain = P*(1-SnowFrac)" //mm/hr
        "Snow = P*SnowFrac"      //mm/hr
        "Snowpack = SnowPack+Snow*ISD*24"//mm

        "MeltVol = Snowpack*MeltFrac"// Maximum volume that could melt given temperatures mm
        "Precip = p"//mm/hr

  "if Snowpack >= MeltVol then"
     "Snowpack = Snowpack - MeltVol"//mm
     "Melt =  MeltVol/(ISD*24)"//mm/hr
  "else"

          "Melt = Snowpack/(ISD*24)"
          "Snowpack = 0"
  "end if"

"If timesum > month(m2) then"     // check that total time does not exceed 30 days in a month

        "Tr =  Month(m2) - (timesum-ISD)"
        "Storm(k,i,0) = Rain" //mm/hr
        "Storm(k,i,1) = Tr"//days
        "Storm(k,i,2) =Snow"
```

```
        "Storm(k,i,3) =Snowpack"
        "Storm(k,i,4) = Melt/(Tr*24)"
        "Storm(k,i,5) = Precip"
        "Storm(k,i,6) = Tmax"
        "Storm(k,i,7) = Tmin"
        "Storm(k,i,8) = MeltVol"
        "SnowpackP = Snowpack"
        "exit for"
"end if"

  "Storm(k,i,0) = Rain"//mm/hr
  "Storm(k,i,1) = ISD"//days
  "Storm(k,i,2) =Snow"
  "Storm(k,i,3) =Snowpack"
  "Storm(k,i,4) = Melt"
  "Storm(k,i,5) = Precip"
  "Storm(k,i,6) = Tmax"
        "Storm(k,i,7) = Tmin"
        "Storm(k,i,8) = MeltVol"
        "SnowpackP = Snowpack"
"i=i+1"

"P = -Pbar(k,Month(0))*LOG(Prand)" // calculate new rainfall intensity mm/hr
"SD = -SDbar(k,Month(0))*LOG(SDrand)" // calculate new storm duration (days)

"timesum = timesum+SD" // calculate current elapsed time in days

"if Tmaxb(k,Month(0))<= -Tmaxb(k,Month(0))*LOG(Trand) then"
   "Tmax = Tmaxb(k,Month(0))"
"else"
   "Tmax =-Tmaxb(k,Month(0))*LOG(Trand)"
"end if"

"if Tminb(k,Month(0)) >= -Tminb(k,Month(0))*LOG(Trand) then"
   "Tmin = Tminb(k,Month(0))"
"else"
   "Tmin = -Tminb(k,Month(0))*LOG(Trand)"
"end if"

"Tavg = (Tmax+Tmin)/2"

"If Tmin > Tb then"
                "SnowFrac = 0"
"else"
         "if Tmax <= Tb then"
                "SnowFrac = 1"
         "else"
        "if Tmax > Tmin then"
                "SnowFrac = (Tb-Tmin)/(Tmax-Tmin)"
        "else"
                "SnowFrac = (Tb-Tmax)/(Tmin-Tmax)"
        "end if"
   "end if"
"end if"

"If Tavg>= Tb then"
```

```
            "MeltFrac = Mf*(Tavg-Tb)"
            "else"
            "MeltFrac = 0"
    "end if"

            "Rain = P*(1-SnowFrac)" //mm/hr
            "Snow = P*SnowFrac"      //mm/hr
            "Snowpack = Snowpack+Snow*SD*24" //mm

            "MeltVol = Snowpack*MeltFrac"// Maximum volume that could melt given temperatures mm
     "Precip = p" //mm/hr

     "if Snowpack >= MeltVol then"
       "Snowpack = Snowpack - MeltVol"//mm
       "Melt = MeltVol/(SD*24)" //mm/hr
     "else"
       "Melt = SnowPack/(SD*24)"
            "Snowpack = 0"

     "end if"

    "If timesum > month(m2) then"  // check that total time does not exceed 30 days in a mont h
            "Tr =  Month(m2) - (timesum-SD)"// time remaining in days
            // Output to storm array
            "Storm(k,i,0) = Rain"//mm/hr
            "Storm(k,i,1) = Tr" //days
            "Storm(k,i,2) = Snow"
            "Storm(k,i,3) = Snowpack"
            "Storm(k,i,4) = Melt/(Tr*24)"
            "Storm(k,i,5) = Precip"
            "Storm(k,i,6) = Tmax"
            "Storm(k,i,7) = Tmin"
            "Storm(k,i,8) = MeltVol"
            "SnowpackP = Snowpack"
            "exit for"
    "end if"

// Output to storm array
    "Storm(k,i,0) = Rain"//mm/hr
    "Storm(k,i,1) = SD" //days
    "Storm(k,i,2) = Snow"
    "Storm(k,i,3) = Snowpack"
    "Storm(k,i,4) = Melt"
    "Storm(k,i,5) = Precip"
    "Storm(k,i,6) = Tmax"
    "Storm(k,i,7) = Tmin"
    "Storm(k,i,8) = MeltVol"
    "SnowpackP = Snowpack"

  "next" // end of loop
"next" // HRU loop

)
```